Coherent control of charge and heat transport in semiconductor nanostructures

Miguel Rey Mazón

Junio de 2006

Memoria presentada para optar al grado de Doctor en Ciencias Físicas por la Universidad Autónoma de Madrid

Director: Fernando Sols Lucia
Tutor: Enrique Velasco Caravaca

A mis padres

ALTO JORNAL

Dichoso el que un buen día sale humilde
y se va por la calle, como tantos
días más de su vida, y no lo espera
y, de pronto, ¿qué es esto?, mira a lo alto
y ve, pone el oído al mundo y oye,
anda, y siente subirle entre los pasos
el amor de la tierra, y sigue, y abre
su taller verdadero, y en sus manos
brilla limpio su oficio, y nos lo entrega
de corazón porque ama, y va al trabajo
temblando como un niño que comulga
mas sin caber en el pellejo, y cuando
se ha dado cuenta al fin de lo sencillo
que ha sido todo, ya el jornal ganado,
vuelve a su casa alegre y siente que alguien
empuña su aldabón, y no es en vano.

Claudio Rodríguez, *Conjuros* (1958)

In my periods of weakness and spiritual emptiness and lethargy, I reach out to Bach's music to revive and fire my desire for creativity.

M. C. Escher

Contents

Agradecimientos

Degno d'eterna gloria fia sol
colui ch'avrà di sè vittoria.[1]

(Monteverdi, L'Orfeo)

La presente memoria es fruto de algunos años de trabajo. Si en ellos he aprendido algo, y si he sido capaz de realizar la investigación cuyos resultados aquí se detallan, se debe a una cierta conjunción de decisiones y esfuerzos, pero también de circunstancias y casualidades, de los que uno no siempre es el único responsable. Por ello quiero dar las gracias a las personas cuya contribución, científica o no, me ha ayudado a llegar hasta el final.

Debo agradecer en primer lugar a mi director de tesis, Fernando Sols, la oportunidad de trabajar con él en problemas relevantes en el interesante campo de la física de sistemas mesoscópicos. Además, a través de él he trabado contacto con otros grupos en cuya colaboración se ha desarrollado la mayor parte de la labor aquí presentada.

Durante todos estos años he podido continuar mi labor investigadora gracias a que he disfrutado de una plaza de profesor asociado a tiempo parcial (LRU) en el Departamento de Física Teórica de la Materia Condensada de la Universidad Autónoma de Madrid (UAM). La docencia me ha dado no pocos quebraderos de cabeza y ha contribuido a prolongar la duración de esta tesis, pero no es menos cierto que a través de ella he ganado una excelente experiencia como profesor. A Enrique Velasco le agradezco su colaboración como tutor.

Debo a Mathias Wagner la parte fundamental del código en FORTRAN, que *heredé* como parte de una colaboración científica, frustrada por su abandono de la ciencia básica. Los cálculos numéricos han sido realizados en su práctica totalidad en el Centro de Computación Científica (CCC) de la UAM. Quiero agradecer

[1] *Sólo será digno de gloria eterna aquel que consiga la victoria sobre sí mismo.*

su asistencia técnica en las etapas iniciales de la tesis.

La colaboración con el grupo de Michael Strass, Sigmund Kohler y Peter Hänggi, de la Universidad de Augsburgo (Alemania), a través del programa Hispano-Alemán de Acciones Integradas (proyecto HA2003-0091), ha sido fundamental para llevar esta tesis a buen puerto. Estoy muy agradecido a Michael por una lectura atenta de este documento, por haberme enseñado los secretos de PyX y de la teoría de Floquet, y por los buenos ratos pasados durante este tiempo de contacto científico. Sigmund ha logrado transmitirme parte de sus amplios conocimientos sobre transporte cuántico y ha respondido con paciencia a todas las preguntas sobre física y política alemana. Junto con ellos, del resto del grupo de *Theorie I* he aprendido a distinguir un *Biergarten* auténtico de una imitación.

Asimismo, me he beneficiado del intercambio de ideas con muchos colegas de profesión científica, tanto investigadores como estudiantes de doctorado, en Madrid y en los congresos, cursos y conferencias a los que he tenido la oportunidad asistir gracias a varios proyectos de investigación. Agradezco en especial a Gloria Platero algunas discusiones científicas y un cierto apoyo moral.

En mi estancia en el despacho C-V-505 he tenido la oportunidad de conocer a muchas personas que han hecho esta experiencia más llevadera. Quisiera agradecer a mis sucesivos compañeros de despacho —Elsa, Elena, Heiner, Sigmund, Pablo y Dani— haber compartido las alegrías y penas de la vida de un doctorando. Elsa y Elena me han infundido más ánimos de los que probablemente ellas se imaginen.

Con el resto de doctorandos del C-V me unen menos lazos científicos que de amistad en mayor o menor grado. El *grupo de las 13.45h* merece especial atención porque hemos compartido grandes momentos en la UAM y, sobre todo, fuera de ella. Guardo especial aprecio a Fernando, compañero además de grandes expediciones pirenaicas; a Yannick, Héctor, Diego, César, Sebastián, Pavel, Míriam, Ramiro, Blanca, Juan; y de los primeros años, David y Manuel.

Mi vida fuera de la ciencia no ha sido menos importante que mi actividad como físico. Parafraseando a Les Luthiers debería decir que ha sido, en general, *más* importante. A Jano y Juan, antiguos compañeros de la carrera, les agradezco haber tenido más fe en mi tesis que yo mismo. Creo que María J., Fernando, Nacho, Guille, Marta y demás siempre me han visto como un bicho raro por hacer investigación (y supongo que tienen razón), pero no por ello han dejado de apoyarme. Entre mi gente del baloncesto, sin embargo, ser doctor deja casi

de ser una novedad (al menos en el ICD). A Ana le agradezco los ánimos en momentos de baja motivación. Rodrigo y Rodrigo estuvieron ahí para hablar de ciencia, de música, y aprender a poner gintónics, entre otras muchas cosas.

Dejo para el final mis más emotivos agradecimientos a Miguel y a Miguel. Los ratos en la UAM de los *años heroicos* han sido fundamentales para nuestra profunda amistad y creo que también para el desarrollo de esta tesis.

Por último, mi familia "en sentido amplio" ha apoyado mi decisión de hacer una tesis desde el principio. A mis padres y hermanos les agradezco su paciencia y sus ánimos en los momentos difíciles a lo largo del camino.

Miguel
Madrid, junio 2006

Resumen

El interés en la construcción de dispositivos de menor coste y mayores prestaciones ha llevado, prácticamente desde los inicios de la electrónica, a la búsqueda y desarrollo de estructuras cada vez más pequeñas. En la actualidad nos encontramos muy cerca de alcanzar el límite físico impuesto por la naturaleza a este proceso de miniaturización. Para poder diseñar nuevos elementos electrónicos y comprender su funcionamiento se ha hecho necesario estudiar las propiedades de sistemas cuyas características principales están determinadas por las leyes de la mecánica cuántica.

La teoría cuántica de los sólidos también es necesaria para comprender cómo funciona el paradigma de la electrónica convencional, la unión p-n entre semiconductores. Sin embargo, cuando la relación entre el tamaño del dispositivo y la temperatura a la que se encuentra es la adecuada, se manifiestan nuevos fenómenos cuánticos incluso en sistemas compuestos por muchos átomos. Uno de ellos es la *cuantización* de los niveles energéticos en los que los electrones, principales responsables del transporte de carga, pueden situarse. El otro es el mantenimiento de la *coherencia de fase* a lo largo del proceso de transporte. Por ambos motivos se ha acuñado el término de *sistemas mesoscópicos* para designar a este tipo de estructuras en los que, estando a medio camino entre el tamaño de los átomos y el de los sistemas macroscópicos, tienen lugar fenómenos de transporte cuántico.

Los semiconductores son, una vez más, protagonistas de esta nueva etapa. Las técnicas de manipulación de materiales (crecimiento de capas con precisión atómica, bajas temperaturas, microscopías atómicas) han permitido la fabricación de los llamados *pozos* y *puntos cuánticos*. Este nombre designa estructuras en las que los electrones quedan confinados en una región del espacio. El confinamiento se consigue (en los puntos cuánticos *verticales*) combinando semiconductores con diferente separación entre las bandas de conducción y valencia, o (en puntos cuánticos *planos*) mediante el uso de voltajes aplicados a electrodos metálicos.

En ambos casos los electrones encuentran barreras energéticas más o menos elevadas a su alrededor que impiden su paso a otras zonas.

Esta tesis considera algunos problemas relacionados con el transporte de carga y de calor en pozos o puntos cuánticos dobles, en presencia de voltajes externos con dependencia temporal periódica. Cuando el transporte tiene lugar de forma coherente, la interacción con potenciales o campos dependientes del tiempo modifica sustancialmente las propiedades de transmisión a través de nanoestructuras semiconductoras. Por esta razón, hemos estudiado el comportamiento de la componente continua de la corriente en diferentes situaciones de interés.

En primer lugar se trata el efecto de *control coherente de la corriente eléctrica*. Escogiendo los parámetros del voltaje ac aplicado, la interacción entre los dos pozos cuánticos puede modificarse, llegando a anularse para determinados valores de la amplitud de voltaje y la frecuencia de la oscilación. El estudio de la *supresión coherente de la transmisión por efecto túnel* era conocida en sistemas aislados, pero su consideración en problemas de transporte, donde el contacto con los electrodos debe incluirse explícitamente, ha sido tenido en cuenta solo recientemente. Los resultados numéricos han sido obtenidos mediante el formalismo de dispersión (*scattering*) de Landauer (1957), con las modificiaciones adecuadas para tratar el caso de sistemas dependientes del tiempo. Para el cálculo de las transmisiones se han utilizado los formalismos de matrices de transferencia (Wagner, 1995) y de Floquet-Green (Kohler *et al.*, 2005). Las matrices de transferencia son una versión particular de la teoría de Floquet cuando los estados asintóticos de los electrones se toman como ondas planas. Los cálculos realizados reproducen en el límite de alta frecuencia los resultados de una aproximación analítica en el modelo de enlaces fuertes (*tight-binding*). Esta aproximación ofrece interesantes resultados analíticos más fáciles de interpretar cualitativamente, puesto que transforman el problema inicial dependiente del tiempo en un problema independiente del tiempo. La dependencia temporal queda incluida renormalizando los parámetros (acoplamiento entre pozos y distribución de electrones en los contactos) que determinan la corriente eléctrica.

La producción de una corriente eléctrica en ausencia de un voltaje (continuo) externo es el otro asunto tratado en esta tesis. La aplicación de una señal alterna a una heteroestructura asimétrica causa que la probabilidad de transmisión dependa del lado (izquierdo o derecho) por el que incidan los electrones. De este modo, la corriente eléctrica puede *bombearse* a través de la heteroestructura. Este

efecto de *bombeo de electrones* es también de origen cuántico y puede entenderse con las herramientas de análisis de sistemas dependientes del tiempo utilizados para el problema anterior. En este caso, estamos interesados en demostrar que en dobles pozos cuánticos este transporte es *no adiabático* y tiene lugar gracias a la *transmisión túnel ayudada por fotones*, es decir, por la interacción con el campo o potencial eléctrico. Por otro lado, otro de nuestros objetivos ha sido estudiar si puede caracterizarse el comportamiento de un dispositivo de bombeo de electrones mediante las propiedades de transmisión y reflexión cuando es utilizado dentro de un circuito.

Por último, consideramos en esta tesis la producción de calor debido a la corriente de electrones en un dispositivo de bombeo. El formalismo de Landauer puede generalizarse una vez más para calcular cómo es el intercambio de energía de los electrones cuando atraviesan el doble pozo cuántico. Nos ha parecido especialmente relevante investigar las condiciones en las que una corriente de electrones puede contribuir a enfriar uno de los electrodos. Esto puede conseguirse con una elección de la estructura de niveles energéticos en los pozos y un ajuste de la frecuencia del potencial alterno aplicado. El fundamento de nuestro modelo para el enfriamiento se basa en el *intercambio* de electrones *calientes*, situados por encima del potencial químico del electrodo, por electrones *fríos* provenientes de estados situados del otro lado de la heteroestructura. Los resultados numéricos presentados en el último capítulo confirman nuestras hipótesis. Para comprobar nuestras predicciones cualitativas, hemos estudiado cómo depende la producción de calor de unas cuantas variables. De entre los casos de posible importancia experimental, la producción de calor en ausencia de corriente eléctrica es quizá el más interesante. Según nuestros cálculos, esto es posible para un amplio rango de temperaturas (entre unos 5 y ~ 40 K) de los electrodos.

1 Introduction

The unstoppable progress in the understanding of the physics, and the development of technological applications of solid state structures down to sizes of the atomic scale, was foreseen by the late Richard P. Feynman nearly 50 years ago. In his 1959 talk to the American Physical Society (Feynman, 1960) he made the scientific community aware of the wide prospects of the then emerging field of microscopic systems. *The principles of physics, as far as I can see*, he said, *do not speak against the possibility of maneuvering things atom by atom*, and by now it is quite clear that he was perfectly right.

Since those days, the interest in solid state devices has moved towards smaller and smaller sizes at increasing speed, so much that in a few years the quantum effects will dominate their working principles. This may sound a little too ambitious for anybody who has in mind the basic building block of today's electronics, the p-n transistor, whose most important properties are derived from the quantum theory of solids.

There are nevertheless reasons to think that the forthcoming generation of devices can be fundamentally new. As an example, one can consider the impact that the discovery of the *Giant Magnetoresistance Effect* has had in the evolution of the storage capacity of hard-disks (Baibich *et al.*, 1988), based ultimately on the properties of the spin, a magnitude with no classical counterpart. Thus, the fundamental limits imposed by Nature in the *downsizing* process of the building blocks of electronics are also understood by scientists and industry alike as an opportunity to enter a new era in the manipulation of matter at the nanometer scale.

Semiconductors have been of particular importance to the progress of both science and technology in the past century, principally but not exclusively by the invention of the transistor, and are also to take part in the next revolution. Extremely accurate growing and patterning techniques have brought semiconductor layers to be just a few atoms wide. As we will see below, this has intro-

duced quantum tunneling effects in the process of electron transfer across the layers and, moreover, makes it necessary to treat the charge carriers as quantum entities.

Many questions raised in the study of nanometer-sized systems have been answered by the exploration of their transport characteristics. Theories for transport aimed at the correct description of the empirical facts were one of the goals that instigated the application of the then-new quantum mechanics to the full microscopic description of solids, in the early 1930s. The advent of truly microscopic structures has motivated the study of electrical current, or the transport of heat through these systems, and the quantum mechanical fluctuations of these quantities, to gain further insight into the physical properties of such a system. To address these features new theoretical as well as experimental tools have been needed. A landmark in the history of solid state theory was the formulation of a quantum theory of transport for independent electrons in the form of a scattering formalism, achieved by the idea of Landauer (Landauer, 1957) soon before the above mentioned talk of Feynman.

Among the many interesting properties of transport at the nanoscale, this thesis considers in detail a number of problems posed by the production and control of charge and heat current in semiconductor heterostructures. Under the assumption of no electron–electron interactions, we study the action of external ac voltages on systems formed by two quantum wells or quantum dots. We carry out numerical calculations and prove that it is possible to control the dc component of the current in an externally biased system by means of an ac driving. This is shown to be a consequence of the coherent properties of quantum mechanical transmission. This effect had been predicted for isolated systems, but to our knowledge it has been investigated here for the first time.

Another remarkable feature of driven semiconductor quantum systems is the possibility of creating a dc current *without* the action of an external bias. This electron pump effect is also of quantum mechanical origin, too. We approach this issue from two different perspectives: first, a numerical analysis confirms the theory of *photon assisted tunneling* (see Platero and Aguado, 2004, for a review) for quantum pumps (Stafford and Wingreen, 1996). Second, we take into consideration the possibility of using one of these devices as a part of a bigger circuit. In this regime, it is interesting to study what is the behaviour of the *electron pump* as an element of such a circuit.

Electrical current is generally accompanied by the transfer of heat. Through inelastic scattering processes, this is also the case in quantum transport. As nanostructures offer the possibility of tailoring almost most of their physical properties, one may hope to control the direction of heat flow. Such is the main theme in this thesis, that in semiconductor heterostructures heat flow can be manipulated by the action of ac driving, and derive the conditions for such a device to work as a *heat pump*, i.e. to transfer heat from a colder to a hotter reservoir.

Outline of this work

This thesis is organized as follows. An overview of the physical systems for which we build our theory is given in this chapter as a general introduction. The scattering theory we need to treat quantum transport at the mesoscopic scale is presented then in chapter 2. We describe the static Landauer formalism, and subsequently explain how this theory has to be extended to treat systems with a periodic time dependence. The methods of transfer matrices and tight-binding description of quantum systems are also described. We defer to an Appendix a brief explanation of the details pertaining to the structure of transfer matrices and some useful results in the manipulation of Bessel functions.

Results are presented in three separate chapters: chapter 3 addresses the problem of coherent control of the current. This serves also as a comparison of the two methods mentioned above (transfer matrices and tight-binding), since there are some assumptions in the tight-binding model which can be treated exactly within a transfer matrix approach. Next, in chapter 4 we consider the subject of nonadiabatic electron pumping. We first present numerical results for the pump current and test the physical model by an exploration of the parameter space. This chapter ends with a characterization of an electron pump in a circuit in terms of its electromotive force and internal resistance. Finally, we discuss in chapter 5 heat production in heterostructures in ac driven systems. Our interest here is centered in the search for negative total heat production in one of the leads. After the derivation of the correct formula for heat production in the leads and the introduction of the model and main physical assumptions, we present numerical results that confirm our hypothesis. An exploration of some of the parameters allows for a critical assessment of the physical model.

1.1 A brief overview of mesoscopic systems

Quantum wells and quantum dots, the structures which are the subject of this thesis, represent the last step in the miniaturization process of electronic devices. In the beginning, single-electron effects were studied in granular metals and metallic tunnel junctions. Charge quantization was first observed in these systems (Zeller and Giaever, 1969). Later on, the precursors of quantum dots, in the form of small isolated islands by the effect of random impurities in silicon or GaAs wires, were the subject of experiments. Quantized energy levels were observed here for the first time (Field *et al.*, 1990; Staring *et al.*, 1992). The theory known as *Coulomb blockade* of Likharev and Zorin (1985) had already been proposed and came to explain the experimental features in terms of charging effects: the addition of a single electron is not possible if the charging energy is big enough so that this transfer process is energetically unfavourable.

The fact that it was the quantum properties of the samples which were being revealed ignited the rapid development of transport at the quantum scale. There are at least two ways in which it can be said that a system displays quantum behaviour. One is the quantization effects like those of Coulomb blockade referred to above. The other is the maintenance of quantum coherence, i.e. of the wave nature of the particles, over distances comparable to or greater than the extension of the system itself. Quantum coherence can be observed if all inelastic phase-breaking events have been *turned off*, and this implies highly clean samples free of impurities and usually very low temperatures. But this so-called *dephasing length* is also determined by the Fermi wavelength and degree of disorder (Stone, 1995), so it is not just the size of the system, but an interplay of all these quantities, what determines whether quantum phenomena are observable at all. They have been reported, usually in transport experiments, in systems ranging from down to nanometer-sized structures to samples as big as ~ 100 μm for low (i.e. miliKelvin) temperatures. The term *mesoscopic* was invented to refer to this class of devices or regime of transport lying somewhere between the dimensions of the atoms and those of macroscopic structures, where quantum properties can be observed (Imry, 1997; Beenakker and van Houten, 1991).

The advances in the manipulation of materials and fabrication techniques that have made possible the construction of these systems are not less astonishing than the theoretical discoveries they have either forecasted or confirmed. In fact,

it is fair to say that, at least from a theorist's point of view, they have been more astonishing and have many times been ahead of the theory. Among these incredibly precise techniques we must mention *Molecular-Beam Epitaxy* (MBE) for growing semiconductor layers, nanolithography for patterning, the advances in cryogenics, and the analysis of system structures by means of the various microscopies relying on quantum tunneling.

1.1.1 Semiconductor heterostructures

The most common experimental device in the research of quantum transport is probably the semiconductor heterostructure. This expression refers to the combination of two or more semiconductors, or semiconductor alloys (generally between elements of the groups III-V and II-VI of the periodic table), in a layered structure. Among these, the combination of gallium arsenide (GaAs) and its alloy with aluminium, $Al_xGa_{1-x}As$, where x denotes the Al fraction (typically 0.3), is the most popular (Beenakker and van Houten, 1991), replacing more traditional MOSFETs (Metal-Oxide Semiconductor Field-Effect Transistors). There are several reasons for this: the low electron effective mass ($m^* = 0.067m_e$), the high mobility (up to $\sim 10^6$ cm^2/V s) allowed by very clean samples, the possibility of modulating the separation of the conduction bands (around 0.3 V) by choosing the Al fraction, or the almost perfect match of the two lattices, which reduces scattering at the interfaces.

A nanometer-sized region of such a GaAs/AlGaAs combination defines a low-dimensional structure named *quantum dot* (QD) where electrons can be confined. In these nanometric samples, the allowed states for the electrons in the band structure become increasingly separated in energy, and for very strong confinement they are reduced to only a few. The position of the levels in the energy axis resembles that of electronic states in atoms, which justifies the name of *artificial atoms* (Ashoori, 1996; Kouwenhoven *et al.*, 2001).

The development of QDs has by far exceeded the most optimistic visions of Feynman. QDs are not only used as a tool for the study of quantum properties of the solid state, but also of interest in practical applications as metrology, transistors and quantum interference devices. In addition to this, QDs are promising candidates for a solid state implementation of quantum computation (Loss and DiVincenzo, 1998).

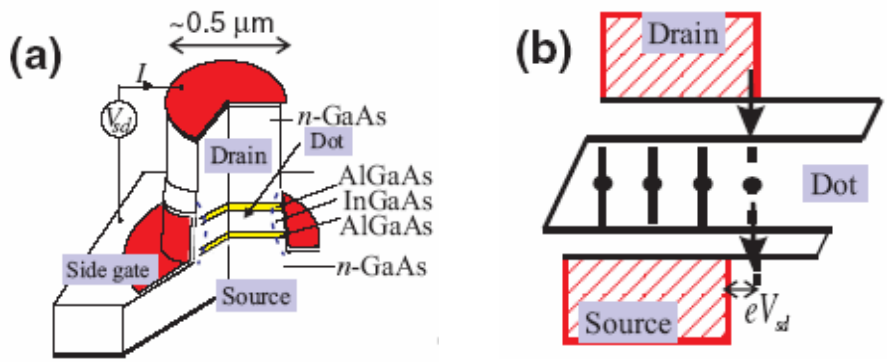

FIGURE 1.1: (a) Schematic representation of a vertical QD: an indium-doped GaAs layer is placed between two AlGaAs external layers, acting as tunnel barriers. The contacting electrodes are made of n-doped GaAs. (b) shows an energy diagram of the dot. Adapted from Kouwenhoven *et al.* (2001).

One can in principle design structures for transport (Kastner, 1993) to take place either perpendicularly to the direction in which the semiconductor layers were grown or to remain in the plane of one of the layers. This defines *vertical* and *planar* or *lateral* quantum dots (QDs).

Vertical quantum dots

Taking advantage of the mismatch of the conduction bands of GaAs and AlGaAs (where the separation between valence and conduction band is bigger), which acts as a tunnel barrier between both semiconductors, electrons can be confined in a thin GaAs layer between two external AlGaAs layers; further lateral confinement is achieved by etching off the surrounding material. Connecting this quantum well to two electrodes allows electrons to flow across the tunnel barriers and therefore create a current. A schematic diagram, together with an energy diagram of a vertical QD, is shown in Fig. 1.1. A spectroscopy of the levels inside the well is performed when measuring the $I - V$ curve, since electrons can tunnel into and out of the well when the Fermi energy of the external leads aligns with one of the levels. Typical sizes are a few tens of nanometers for either the barriers or the well itself. Barriers are of the order of 100 meV high and are well modelled by square barriers (Meirav and Foxman, 1995).

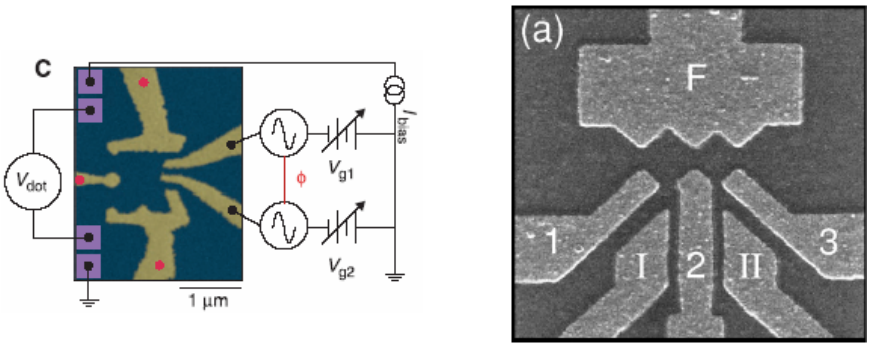

FIGURE 1.2: Scanning-electron microscopy (SEM) micrographs of single- and double QDs, taken from the original articles of Switkes *et al.* (1999) (left) and van der Wiel *et al.* (2003). Metallic gates are placed over a 2DEG (of darker color), to confine electrons in a zero-dimensional region, or to or introduce e.g. ac modulations of the dots. Left figure shows also the typical measurement configuration.

Lateral or planar quantum dots

The layering technique can be used to confine some of the electrons of a GaAs/ AlGaAs structure to a two-dimensional region to form a bidimensional electron gas (2DEG) (see Fig. 1.2, left). By attaching metallic gates one can further create tunable tunnel barriers and separate a small dot region from the rest of the 2DEG. Planar QDs are the actual heirs of the semiconductor islands in which quantum effects were first observed. The interest of these QDs is presently very high for a large number of reasons: electron–electron interactions can be studied in systems where the number of confined electrons (generally controllable by external gates) goes from zero to anything up to several thousands (Ashoori, 1996). The movement of the electron ranges from purely *ballistic* to *diffusive* regimes by means of scattering by impurities, suggesting research on the transition from coherent to incoherent transport and of the fluctuation properties of the current due to disorder (Beenakker and van Houten, 1991). When the electron dynamics is chaotic, transport has interesting statistical properties that affect the coherence and the electron–electron interactions (Alhassid, 2000).

In both (vertical and planar) cases, the interest on single QDs has moved into the next step in complexity, namely systems composed of two (or more) QDs. An example of this is shown on the right of Fig. 1.2. These have been given the name of *artificial molecules*, as single QDs were considered to be *artificial atoms*.

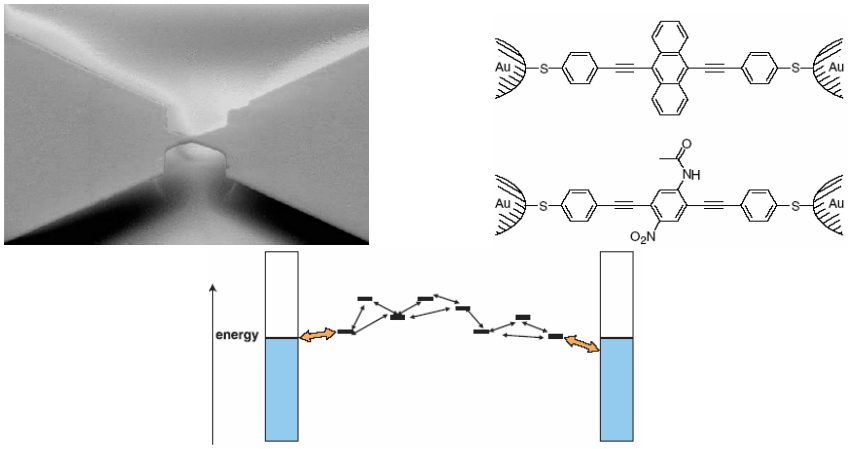

FIGURE 1.3: SEM graph of a break junction for measurements of molecular electronic devices. Two setups of an symmetric and an asymmetric organic molecule connected to metallic contacts are displayed on the right-top diagram, whereas an energy diagram of a generic molecule is shown in the lower part of the figure. Adapted from Reichert *et al.* (2002) and Nitzan and Ratner (2003)

Single-electron effects (Blick *et al.*, 1996) and various kinds of spectroscopic measurements (van der Wiel *et al.*, 2003) have been performed on these systems to gain a deeper understanding on the level structure and the interplay of various physical parameters.

1.1.2 Molecular wires

Semiconductor quantum dots have had to share their popularity among researchers with the emerging field of molecular electronics, the other nanometer-sized systems of interest. More than 30 years ago, Aviram and Ratner (1974) demonstrated the feasibility of building molecular devices and, in particular, the rectification properties of asymmetric organic molecules that could be of interest for the eventual construction of e.g. nanoscale transistors. This initial investigations have led to the experimental search for molecular rectifiers, single-molecule diodes and three-terminal transistors, to name only a few possible applications. The study of such systems and their transport properties has been greatly improved with the tools of scanning tunnel microscopy, available since the mid 1980s. They present some advantages over semiconductor quantum dots: since their length scale is of a few angstroms, the energy scale is higher and the quan-

tum effects more robust.

In Fig. 1.3 a typical scanning tunnel microscopy image of a break junction (taken from Reichert *et al.*, 2002) is shown, together with the scheme of the experimental setup of an organic molecule between two metallic contacts, and the energy diagram of a many site molecule (from Nitzan and Ratner, 2003), where the arrows indicate molecule–electrode and intersite coupling.

While having very different microscopic details, molecular wires fit also into the category of mesoscopic systems. They can also be described by the same scattering picture put forward in this thesis. The essential ingredients in the tight-binding formalism of section 2.3.3 (e.g. energy levels, coupling of the structure to the external leads, and coupling between its different parts) are directly translatable into the picture of molecular wires. Many results contained in this thesis —with the appropriate modifications— describe correctly the effect of external, time dependent driving on transport in molecular wires. This similarity is exploited, for example, in the article of Camalet *et al.* (2003). We refer the reader to the reviews of Nitzan and Ratner (2003) and Agraït *et al.* (2003) for more information on this subject.

2 Quantum transport in time-dependent systems

In this chapter the necessary tools to work with quantum systems, which shall be of use for the results of later chapters, are presented. First, we state in section 2.1 the scattering theory of Landauer for the calculation of electrical current in coherent structures, starting with the static picture. Then, the following sections address the necessary generalization to study time-dependent situations. Two similar and sometimes complementary approaches, transfer-matrices and tight-binding modelling of nanoscale conductors, are described next. They will be used to obtain numerically (and sometimes analytically) the transmission probability for electrons entering the system, the basic quantity that determines the current in the scattering formalism.

2.1 Scattering theory of transport in mesoscopic systems

In the decade of the 1950s, electron transport theories were based on either the application of Bloch's theorem in a semiclassical context, to calculate the acceleration of electrons in a Fermi gas by uniform electric fields, or on Kubo's linear response theory, in which the laws of time evolution were applied to closed conservative Hamiltonians (Landauer, 1987). By considering the fields to be the cause of the electrical currents, both methods were anchored to the classic view from which other areas, as e.g. circuit theory, had already departed putting currents and fields on equal grounds. It was then when Landauer (1957) introduced his ground-breaking idea of considering the coherent transmission of electron in solids as a quantum scattering problem. For over twenty years little attention was paid to this approach. The interest in the development of a scaling theory

for transport (Anderson *et al.*, 1980), and the achievement of the first truly nanometric samples, revived the interest in the formulation of Landauer. [1]

The Landauer picture of quantum transport might have been at first conceived and used rather *ad hoc*. It has nevertheless been both proven theoretically on solid physical grounds (Stone and Szafer, 1988) and experimentally tested (de Picciotto *et al.*, 2001), and provides a satisfactory formalism to address many problems in transport for independent electrons.

2.1.1 The Landauer approach

The central idea of the Landauer formula can be stated as follows (Landauer, 1957)[2]: a scattering center with reflection probability $R(E)$ is placed inside a perfectly conducting region between two leads. These hold equilibrium distributions of electron Fermi gases characterized by chemical potentials. If a current flows (say) left to right through this region, an excess of charge carriers accumulates to the left of the scatterer, so that the density there becomes $1 + R$. Accordingly, to the right this density will be $1 - R$, building up a difference (proportional to the voltage difference) equal to $2R$. The current flow is proportional to the transmission $T = 1 - R$, so that aside from numerical factors the conductance $G = I/V$ must be proportional to T/R. The complete derivation leads to the by now famous result

$$G = \frac{2e^2}{h}\frac{1-R}{R}\,, \tag{2.1}$$

where R is to be evaluated at the Fermi energy. The implicit assumptions made in this calculation amount to saying that the current and the voltage are measured in different sets of probes. This must be the case, as otherwise —i.e. if current and voltage were measured in the same pair of electrodes— the current through the contacts would drive the population of electrons in the leads out of equilibrium, and the chemical potential would be ill-defined.

Transmission and reflection probabilities are magnitudes one can compute if it is possible to know (or guess) the initial and final form of the scattering states.

[1] The original article, Landauer (1957), was cited five times until 1974 (in three cases by Landauer himself), and around 20 until 1977. The number of citations it has received by now —not counting later reprints and revised versions of the 1957 article— is over 1000.

[2] The reader is referred to the review of Stone and Szafer (1988) or to Landauer (1987) for a complete account of the history of the Landauer formula.

Thus conduction is in fact formulated as a scattering problem and, therefore, the knowledge of the transmission probability or probability amplitude is everything one needs to solve transport problems. As it is often said, for independent electrons *transmission is all* (Das and Green, 2003a,b).

In the other relevant experimental setup, current is driven and voltage is measured through the same pair of electrodes. Eq. (2.1) becomes[3]

$$G = \frac{2e^2}{h} T(E_{\mathrm{F}}) \,, \tag{2.2}$$

where E_{F} is the Fermi energy. In this case the dc current measured in the leads is calculated as

$$I = \frac{2e}{h} \int \mathrm{d}E [f_{\mathrm{L}}(E) - f_{\mathrm{R}}(E)] T(E) \,, \tag{2.3}$$

for a finite dc voltage between reservoirs $eV = \mu_{\mathrm{L}} - \mu_{\mathrm{R}}$, where

$$f_{\mathrm{L,R}}(E) = f(E - \mu_{\mathrm{L,R}}) = \frac{1}{1 + \exp[(E - \mu_{\mathrm{L,R}})/k_{\mathrm{B}}T]} \tag{2.4}$$

are the electron Fermi distributions. In this thesis we will use the generalization of this formula to the case of ac driven systems to obtain dc currents numerically.

Note that with Eqs. (2.1) and (2.2) one calculates the resistance *of the sample itself* and, respectively, the resistance of the sample together with the contacts. This issue will be of relevance in the discussion of the results of section 4.3.

Before considering the case of driven systems, we note two results related to the Landauer formula. They are both intended to generalize the above equations to more realistic situations. On the one hand, there is the issue of the leads. As they emit and receive electrons, they are in strict sense systems out of equilibrium. Büttiker *et al.* (1985) found that one can however find a new pair of *effective chemical potentials* to describe *fictious*, equilibrium-like electron distributions, which give the experimentally observed *effective potential difference*. To determine these new chemical potentials, one counts the piled up charges to the left and right of the sample, in the spirit of the original derivation of Landauer. This yields

$$G \equiv \frac{I}{V} = \frac{2e^2}{h} \left[\int \mathrm{d}E \frac{-\mathrm{d}f}{\mathrm{d}E} T(E) \right] \frac{\int \mathrm{d}E (-\mathrm{d}f/\mathrm{d}E)(\partial n/\partial E)}{\int \mathrm{d}E (-\mathrm{d}f/\mathrm{d}E) R(E) (\partial n/\partial E)} \,, \tag{2.5}$$

[3] To see further details of this *two- vs. four-terminal* controversy of the Landauer formula, see the review articles of Stone and Szafer (1988) and Imry and Landauer (1999), or Sols and Sánchez-Cañizares (1999).

where $-\mathrm{d}f/\mathrm{d}E \cong [f_\mathrm{L}(E) - f_\mathrm{R}(E)](\mu_\mathrm{L} - \mu_\mathrm{R})$ is the derivative of the equilibrium Fermi distribution and $\partial n/\partial E = 1/\pi\hbar v(E)$ stands for the one dimensional density of states. In this way the rather difficult task of finding the non-equilibrium electron distribution is avoided. A physical interpretation of the effect of transport over the system is gained in that one can see the reflected electrons as producing a certain screening that reduces the initial chemical potential difference.

By similar arguments, when there are N channels at the Fermi energy conductance becomes

$$G = \frac{2e^2}{h} \sum_i T_i \frac{2\sum_i v_i^{-1}}{\sum_i (1 + R_i - T_i) v_i^{-1}} \,, \tag{2.6}$$

where $R_i = \sum_j R_{ij}$ and $T_i = \sum_j T_{ij}$ represent the total reflection and transmission probabilities into the ith channel. The generalization for multi-terminal systems was provided by Büttiker (1986).

2.2 Scattering theory for driven systems

In order to use a scattering theory of quantum transport, we need to extend the Landauer picture to deal with the inelastic (though phase-conserving) processes induced by the ac driving. An *educated guess* which includes these non-conserving transitions, based on the Tsu-Esaki formulas for tunneling, leads to an expression for the dc current which is essentially correct. This deduction of a formula like Eq. (2.3) has been, however, rigorously proven. Wagner and Sols (1999) based their formula on the adiabatic time evolution of the scattering states. Kohler, Lehmann, and Hänggi (2005) used a formalism that combines the Floquet theory for time periodic systems and Green functions, which we review briefly for later reference.

In addition to this, even if a less formal way is taken to derive a correct scattering expression for the dc current in driven systems, one still faces the question of how to calculate now the inelastic transmission probabilities. For semiconductor heterostructures we have a method very well suited for a numerical accomplishment of this task. Partially based on the Floquet approach mentioned above, the method of *transfer matrices* is reviewed here as extended for ac driven systems by Wagner (1995). We will see how it provides quite straightforwardly the time-independent transmission probabilities by making some reasonable assumptions

about the electronic scattering states in the leads.

2.2.1 Tien-Gordon theory

Motivated by a series of experiments performed by Dayem and Martin (1962) in superconductor/insulator/superconductor (SIS) structures irradiated by microwaves in 1962, Tien and Gordon (1963) formulated a theory for the tunnel transport observed through the insulating barrier between the two superconductors. In spite of its appealing simplicity, this theory gives a correct account of the experimental findings by appropriately linking the time-dependent wave function in the presence of an ac perturbation with the electron distribution that yields the observed dc current.

According to Tien and Gordon, when an ac potential of the form $V(t) = V_0 + V_{\mathrm{ac}} \cos \Omega t$ affects homogeneously one side of a SIS junction, the eigenstates of the Hamiltonian $H = H_0 + V(t)$, with $H_0 = -(\hbar^2/2m^*)\partial^2/\partial x^2$, at one side of the barrier change their form in the static case, $\psi(\mathbf{r}, t) = f(\mathbf{r})\mathrm{e}^{-\mathrm{i}Et/\hbar}$, to

$$\psi(\mathbf{r}, t) = f(\mathbf{r})\mathrm{e}^{-\mathrm{i}(E+eV_0)t/\hbar} \left[\sum_{n=-\infty}^{n=+\infty} B_n \mathrm{e}^{-\mathrm{i}n\Omega t} \right] \tag{2.7}$$

for $H(t) = H_0 + V(t)$. Substituting this into the Schrödinger equation

$$H(t)|\psi(\mathbf{r}, t)\rangle = \mathrm{i}\hbar \frac{\partial}{\partial t} |\psi(\mathbf{r}, t)\rangle \tag{2.8}$$

one obtains $B_n = J_n(eV_{\mathrm{ac}}/\hbar\Omega)$ for the coefficients. The wave function reads

$$\psi(\mathbf{r}, t) = f(\mathbf{r}) \left[\sum_{n=-\infty}^{n=+\infty} J_n \left(\frac{eV_{\mathrm{ac}}}{\hbar\Omega} \right) \mathrm{e}^{-\mathrm{i}(E+n\hbar\Omega)t/\hbar} \right] . \tag{2.9}$$

As seen from the static side, the particles on the driven side behave as if having a probability amplitude $J_n(eV_{\mathrm{ac}}/\hbar\Omega)$ to be displaced in energy by $n\hbar\Omega$ (Tucker and Feldman, 1985). In other words, the action of the ac signal is equivalent to the application of voltages $V_0 + n\hbar\Omega/e$ with a probability $J_n^2(eV_{\mathrm{ac}}/\hbar\Omega)$ across the junction. This results in an effective density of states in the oscillating side of the form

$$\rho_{\mathrm{ac}}^{\mathrm{R}} = \sum_{n=-\infty}^{n=+\infty} J_n^2 \left(\frac{eV_{\mathrm{ac}}}{\hbar\Omega} \right) \rho_{\mathrm{dc}}^{\mathrm{R}}(E + n\hbar\Omega) . \tag{2.10}$$

The tunneling dc current (averaged over a period of the driving)

$$\bar{I} = C \int_{-\infty}^{+\infty} \mathrm{d}E[f(E - V_0) - f(E)]\rho_{\mathrm{dc}}^{\mathrm{L}}(E - V_0)\rho_{\mathrm{dc}}^{\mathrm{R}}(E) \,, \tag{2.11}$$

where C is a constant and $f(E)$ is again the Fermi distribution function, thus becomes

$$\begin{aligned} \bar{I} &= C \sum_{n=-\infty}^{n=+\infty} J_n^2 \left(\frac{eV_{\mathrm{ac}}}{\hbar\Omega} \right) \int_{-\infty}^{+\infty} \mathrm{d}E[f(E - V_0) - f(E + n\hbar\Omega)] \\ &\qquad \times \rho_{\mathrm{dc}}^{\mathrm{L}}(E - V_0)\rho_{\mathrm{dc}}^{\mathrm{R}}(E + n\hbar\Omega) \\ &= \sum_{n=-\infty}^{n=+\infty} J_n^2 \left(\frac{eV_{\mathrm{ac}}}{\hbar\Omega} \right) I_{\mathrm{dc}}(V_0 + n\hbar\Omega) \,. \end{aligned} \tag{2.12}$$

The Tien-Gordon model represents a good attempt to include inelastic channels for the electronic transport in the presence of ac modulation. However, as the implicit assumption for the effective electron distribution is independent of time, it only gives a correct description of the dc current, but does not correctly address any other time-dependent phenomena inherent to ac transport. As an additional drawback, Tien-Gordon can be used only for spatially homogeneous driving, a particular case among various interesting experimental setups.

2.2.2 Floquet theory

This section describes the physical principles of systems whose Hamiltonian depends periodically on time. A convenient starting point is the *Floquet theorem* (Floquet, 1883), which states the following: a time-periodic Hamiltonian such that $H(t + \mathcal{T}) = H(t)$ has a complete set of solutions $|\psi_\alpha(t)\rangle$ in the form

$$|\psi_\alpha(t)\rangle = \mathrm{e}^{-\mathrm{i}\epsilon_\alpha t/\hbar}|u_\alpha(t)\rangle \,, \tag{2.13}$$

where ϵ_α is a real number, termed *quasienergy* (Sambe, 1973), and $|u_\alpha(t)\rangle$ is called a *Floquet state* which conserves the time periodicity of the $H(t)$:

$$|u_\alpha(t + T)\rangle = |u_\alpha(t)\rangle \,. \tag{2.14}$$

A way of demonstrating this theorem (Kohler, 1999) states that the eigenstates of a periodic Hamiltonian can only change by at most a phase factor when acted upon by the symmetry operator

$$\mathcal{S}_{\mathcal{T}} : t \to t + \mathcal{T} \tag{2.15}$$

over one period $\mathcal{T}$ of the driving. This is enough to guarantee that the eigenstates can be decomposed in the way of Eq. (2.13).

Due to their periodic nature, the $|u_\alpha(t)\rangle$ can be decomposed into their Fourier series,

$$|u_\alpha(t)\rangle = \sum_{k=-\infty}^{k=+\infty} \mathrm{e}^{-\mathrm{i}k\Omega t}|u_{\alpha,k}\rangle \ , \tag{2.16}$$

with Fourier coefficients

$$|u_{\alpha,k}\rangle = \frac{1}{T}\int_0^T \mathrm{d}t\, \mathrm{e}^{\mathrm{i}k\Omega t}|u_\alpha(t)\rangle \ . \tag{2.17}$$

The Floquet states satisfy the so-called *Floquet equation*

$$\left(H(t) - \mathrm{i}\hbar\frac{\partial}{\partial t}\right)|u_\alpha(t)\rangle = \epsilon_\alpha|u_\alpha(t)\rangle \ , \tag{2.18}$$

which justifies the name of quasienergies for the ϵ_α, because they appear as the eigenvalues of an equation for the $|u_\alpha(t)\rangle$ in a similar way as do the authentic eigenenergies in the time-*in*dependent Schrödinger equation. This interpretation also follows by analogy with the definition of *quasimomentum* for electrons in a spatially periodic potential in Bloch theory. One can show that these quasienergies are not the eigenvalues by observing that two Floquet states

$$|u_\alpha(t)\rangle \qquad \text{and} \qquad |u'_\alpha(t)\rangle = \mathrm{e}^{\mathrm{i}n\Omega t}|u_\alpha(t)\rangle \tag{2.19}$$

have quasienergies ϵ_α and $\epsilon'_\alpha = \epsilon_\alpha + n\hbar\Omega$ differing in $n\hbar\Omega$, but are otherwise physically equivalent solutions of the Schrödinger equation (2.8). Therefore we only need to know the quasienergies and the corresponding Floquet states in the interval $-\hbar\Omega/2 < \epsilon < \hbar\Omega/2$, known in this context as *first Brillouin zone*. The rest of quasienergies can be constructed by referring to those contained in this part of the spectrum.

Determining the quasienergies is one of the difficult tasks associated with periodically time-dependent problems. However, the appearance of Eq. (2.18) suggests (Sambe, 1973) that the Floquet states are *stationary* eigenstates of the Hamiltonian

$$\mathcal{H}(t) \equiv H(t) - \mathrm{i}\hbar\frac{\partial}{\partial t} \ , \tag{2.20}$$

so one can attempt to compute them exactly by diagonalizing $\mathcal{H}(t)$. With this goal in mind it is convenient to extend the usual Hilbert space where both the

eigenstates of $H(t)$ and the Floquet states are defined, to the Hilbert space formed by the time-periodic functions $f(t+\mathcal{T}) = f(t)$ such that

$$\int_{-\mathcal{T}/2}^{+\mathcal{T}/2} \mathrm{d}t\, |f(t)|^2 < \infty\,, \tag{2.21}$$

with inner product

$$\langle f(t), g(t)\rangle = \frac{1}{\mathcal{T}} \int_{-\mathcal{T}/2}^{+\mathcal{T}/2} \mathrm{d}t\, f^*(t) g(t)\,. \tag{2.22}$$

The plane waves $\{\varphi_n(t) = \mathrm{e}^{-in\Omega t}, n \in \mathbb{Z}\}$ with $\Omega = 2\pi/\mathcal{T}$ form an orthonormal basis in this space. We thus obtain the *composed Hilbert space* of functions defined in $\mathbb{R}^3 \oplus \mathbb{T}$, in which the functions $F(\mathbf{r}, t)$ satisfy

$$\int_{-\mathcal{T}/2}^{+\mathcal{T}/2} \int \mathrm{d}\mathbf{r}\, \mathrm{d}t\, |F(\mathbf{r}, t)|^2 < \infty \tag{2.23}$$

and where the inner product is defined accordingly:

$$\langle F(\mathbf{r}, t), G(\mathbf{r}, t)\rangle = \frac{1}{\mathcal{T}} \int_{-\mathcal{T}/2}^{+\mathcal{T}/2} \int \mathrm{d}\mathbf{r}\, \mathrm{d}t\, F^*(\mathbf{r}, t) G(\mathbf{r}, t)\,. \tag{2.24}$$

A probabilistic interpretation of the Floquet states can only be made if they have a square modulus that is independent of time. This follows from the general properties of unitary evolution of the basis states (Wagner and Sols, 1999). Another way to show it is by means of the Schrödinger equation (2.8):

$$\begin{aligned} \frac{\partial}{\partial t} \int \mathrm{d}\mathbf{r}\, |\psi(\mathbf{r}, t)|^2 &= \int \mathrm{d}\mathbf{r} \left(\frac{\partial \psi(\mathbf{r}, t)^*}{\partial t} \psi(\mathbf{r}, t) + \psi^*(\mathbf{r}, t) \frac{\partial \psi(\mathbf{r}, t)}{\partial t} \right) \\ &= \frac{\mathrm{i}}{\hbar} \int \mathrm{d}\mathbf{r}\, \{[H(t)\psi(\mathbf{r}, t)^*]\psi(\mathbf{r}, t) - \psi(\mathbf{r}, t)^*[H(t)\psi(\mathbf{r}, t)]\} \\ &= 0\,. \end{aligned} \tag{2.25}$$

In an analogous way, the scalar product in $\mathbb{R}^3$ of two Floquet states is independent of time. This is a useful result since it allows to state that two Floquet states with different quasienergies will remain orthogonal at any instant of time. The transport problems investigated later in this thesis will be greatly simplified by it, because for the calculation of currents in the presence of ac driving it is essential to make sure that states which were initially orthogonal (as is the case of plane waves) will still be orthogonal once the ac perturbation has been turned on. This makes calculations easier to handle.

2.2.3 Physical meaning of the Floquet states

The Floquet states and their Fourier series decomposition (see Eqs. 2.14, 2.16-2.17) have been employed up to this point just as a convenient mathematical tool to obtain the energy spectrum of time-dependent systems. Their interpretation depends on the physical system under consideration. A good starting point for this is the calculation of the mean energy $\bar{H}_\alpha$ in one driving period $\mathcal{T}$ that refers to a state $|\psi_\alpha(t)\rangle$. As in a system with a time-dependent Hamiltonian $H(t)$ the energy is no longer a conserved quantity, this is not a trivial result anymore. Thus we have (Grifoni and Hänggi, 1998)

$$\bar{H}_\alpha \equiv \frac{1}{\mathcal{T}} \int_0^{\mathcal{T}} \mathrm{d}t \, \langle \psi_\alpha(t)|H(t)|\psi_\alpha(t)\rangle = \epsilon_\alpha + \mathrm{i}\hbar \langle \langle u_\alpha(t)|\frac{\partial}{\partial t}|u_\alpha(t)\rangle \; ; \tag{2.26}$$

now, using Eq. (2.16), one obtains

$$\bar{H}_\alpha = \sum_{k=-\infty}^{k=+\infty} (\epsilon_\alpha + \hbar k\Omega)\langle u_{\alpha,k}|u_{\alpha,k}\rangle \; . \tag{2.27}$$

According to this equation, the energy stored in a state $|\psi_\alpha(t)\rangle$ is equal to the average over all Fourier components in the wave function at energies $\epsilon_\alpha + k\hbar\Omega$. We can therefore use the expression of the Floquet states *at energies* $E + k\hbar\Omega, k \in \mathbb{Z}$ to understand them as *inelastic scattering channels* by which the electrons exchange energy with the driving field. One often refers to them by the name of *photonic sidebands*.

What is precisely meant by these sidebands depends, as stated above, on the system. When talking of systems with fixed total number of particles, the Fourier coefficients $\langle u_{\alpha,n}|u_{\alpha,n}\rangle$ are taken as the *spectral weights* of the sidebands at energy $E + n\hbar\Omega$. This definition is very common for the calculation of optical absorption spectra of strongly driven systems.

When studying tunneling and other transport-based phenomena, it often proves to be more useful to define the sidebands somewhat differently. Typically one considers an incoming wave with definite wave vector k_0 and energy E, and the reflected and transmitted partial waves after the scattering events with wave vectors k_n and energies $E + n\hbar\Omega$, which can be derive in a wave-packet analysis. These are interpreted as new *transport channels* mediated by the emission or absorption of photon quanta. One is then tempted to say that these partial waves are individual wave functions. But it must be remembered that the Floquet state is still a particular way to describe a single, coherent wave function. Its

components do not have a time dependence given just by $\exp[\mathrm{i}(E + n\hbar\Omega)t/\hbar]$, at difference with the spectral sidebands defined above, but each of them has in general a different one due to their different k_n-vector. When one uses the expression *transport channel at energy* ϵ_n, we mean that this denotes the channel with a wave vector k corresponding to the energy $\epsilon(k) = \epsilon_n$ in the dispersion relation.

There is yet a further type of sidebands of interest both to spectroscopic (isolated) as well as transport problems: as we will see in the case of driven heterostructures, the Floquet states are sometimes decomposed into *free particle solutions* which do not necessarily satisfy the boundary conditions of the problem. A prominent example of this is the expansion into plane waves in a quantum well with infinite barriers (Wagner, 1994), among others. With these free particle states one can nevertheless obtain the right solution to the driven system by combining many of them and therefore *oblige* them to fulfill the boundary conditions of the Schrödinger equation. This is ultimately the foundation of the transfer-matrix method to be described in the next section.

2.3 Scattering formula for transport in ac driven systems

We will examine now how Floquet theory, in slightly different versions, can help us derive an expression for the current in ac driven systems. We argued in the introduction that in a scattering formalism the (time- or energy-dependent) transmission probability is the quantity we need to finally calculate the current, and we review here two useful methods for that purpose. We motivate first, and then show how to go from transmission probabilities to electric current. It should be noted, however, that in the presence of ac perturbations there exist some quantities that cannot be calculated just with the transmission probabilities, but need of the full quantum mechanical probability *amplitudes* with the corresponding phases as, for example the current noise (Kohler *et al.*, 2005).

2.3.1 Heuristic derivation of the dc current

The calculation of the tunnelling current through a semiconductor heterostructure goes back to the formulae of Tsu and Esaki of the 1970s (Esaki and Tsu,

1970; Tsu and Esaki, 1973). Their original derivation can be adapted to ac driven systems by a separate calculation of the fluxes going in left-to-right and right-to-left directions and the subsequent subtraction of both quantities. The current in e.g. L → R direction is defined as the product of the occupation probability of the initial state, given by the Fermi function $f_{\mathrm{L}}(E)$ of Eq. (2.4), the density of states of lead L, the velocity of the electrons $v(E)$, and the inelastic transmission probability $T_{\mathrm{RL}}(E', E) \equiv T_{\mathrm{R}\leftarrow\mathrm{L}}(E \to E')$. In one-dimensional systems the density of states is proportional to $v^{-1}(E)$ and therefore, for a discrete number of channels, one has then

$$I = \frac{2e}{h} \int \mathrm{d}E\, \mathrm{d}E' \{T_{\mathrm{RL}}(E', E) f_{\mathrm{L}}(E) - T_{\mathrm{LR}}(E', E) f_{\mathrm{R}}(E)\} \tag{2.28}$$

This formula holds when the microreversibility of scattering processes is satisfied, meaning that the probability of going from a state at energy E on the left to a state at energy E' on the right is the same of the reversed process:

$$T_{\mathrm{RL}}(E', E) = T_{\mathrm{LR}}(E, E') \,. \tag{2.29}$$

The formula 2.28 should be generalized to take into account of two- and three-dimensional structures. Until now it has been assumed that both leads are just one-dimensional regions connected through point contacts with the driven system. This implicit consideration makes the tight-binding description of section 2.3.3 easy to adapt for molecular wires. But, in semiconductor heterostructures, one is also interested in the cases of planar structures connected through a one-dimensional interface, or of three-dimensional systems. This can be done by including explicitly the density of the leads in the calculations, ignored so far thanks to a lucky cancellation of density of states and the velocity of electrons:

$$\begin{aligned} I = \frac{2e}{h} \int \mathrm{d}E\, \mathrm{d}E' [&T_{\mathrm{R}\leftarrow\mathrm{L}}(E, E') f_{\mathrm{L}}(E) D_{\mathrm{L}\perp}(E_\perp) \\ &- T_{\mathrm{L}\leftarrow\mathrm{R}}(E, E') f_{\mathrm{R}}(E) D_{\mathrm{R}\perp}(E_\perp)] \end{aligned} \tag{2.30}$$

Here, $D_{\ell\perp}(E_\perp)$, with $E_\perp$ representing the density of states of the directions perpendicular to the transport direction in lead $\ell = \mathrm{L}, \mathrm{R}$.

It has been argued that one should include the so-called *Pauli blocking factors* to ensure that the current satisfies Pauli's exclusion principle. This is however not true, since the orthogonality of the dc scattering states from which the corresponding ac counterparts are created is preserved. In any case, if one still insists

in including these factors, they can be shown to cancel for systems with time-reversal, as is our case. The reader is referred to the articles by Sols (1991, 1992).

2.3.2 The method of transfer matrices

Transfer matrices offer a powerful means of treating transport problems of periodically driven by making the *reasonable* hypothesis that (a) the wave functions of the electrons have the Floquet form of Eq. (2.13), and (b) that the Floquet states can be decomposed as a sum of plane waves. This latter assumption makes sense if one accepts that deep inside the external reservoirs, where the dc current is eventually to be calculated (or measured), the initial and final scattering states of the electrons are plane waves. One tries then to express Floquet states in a way such that the final states in the quantum system can be related to the initial scattering states. In doing so the original eigenvalue problem of the time-dependent Schrödinger equation is transformed into a set of coupled *linear* algebraic equations, easier to implement numerically. Another advantage of this procedure is that the plane wave decomposition leads with less effort to the time-independent transmission probabilities of the ac scattering formula for the current. This method has, however, some drawbacks: on the one hand, we disregard in this way all kind of electron–electron interactions, which are of interest in many real problems. We also *lose control* of the precise shape of the Floquet states in the system, and therefore it doesn't allow for a qualitative understanding of the ongoing processes. There have nevertheless been some examples worked out explicitly, as e.g. in the articles by Truscott (1993) and Wagner (1996).

We take advantage of the flat-band conditions that hold for a spatially constant (dc) potential with a time-dependent gate voltage $V_{\mathrm{ac}}(t)$ and, in the spirit of the Floquet theorem, write the solution of the Schrödinger equation as

$$\psi(E,z,t) = \sum_{n=-\infty}^{+\infty} \psi_n(z) \exp\left\{-\frac{\mathrm{i}}{\hbar}(E+n\hbar\Omega)t - \mathrm{i}\phi(t)\right\} \tag{2.31}$$

with the accumulated phase

$$\phi(t) = -\frac{e}{\hbar}\int^{t} \mathrm{d}t' V_{\mathrm{ac}}(t') = \phi(t+\mathcal{T})\,. \tag{2.32}$$

Its time-periodicity follows from the zero time-average of the gate voltage $V_{\mathrm{ac}}(t)$.

Neighbouring layers of a heterostructure may have different ac voltages applied in addition to different band-edges. As a consequence, the wave functions in Eq. (2.31) which satisfy the Schrödinger equation in the asymptotic regions of each layer do not coincide in the general case. However, as the solution for the complete system and its spatial derivative have to be continuous throughout the system, we can construct the total wave function by matching the corresponding partial wave functions at the interfaces between layers. With this goal in mind, we assume that the wave function (2.31) is a solution of the Schrödinger equation for the time-dependent Hamiltonian

$$\begin{aligned} H(z,t) &= H_0(z) + V_{\mathrm{ac}}(t) \\ &= -\frac{\hbar^2}{2}\frac{\partial}{\partial z}\frac{1}{m(z)}\frac{\partial}{\partial z} + V(z) + V_{\mathrm{ac}}\cos\Omega t \end{aligned} \tag{2.33}$$

and that, moreover, $\psi_n(z)$ is an eigenfunction of the time-independent Hamiltonian $H_0\psi_n(z) = E_n\psi_n(z)$ with the spatially piecewise constant effective mass $m(z)$, and has the general form

$$\psi_n(z) = A_n \exp(k_n z) + B_n \exp(-k_n z)\ . \tag{2.34}$$

The wave vector $k_n = \left[2m(V - E - n\hbar\Omega)\right]^{1/2}$ describes travelling as well as decaying waves (bound states) for complex and real values of k_n, respectively. The matching conditions at an interface for $\psi(z,t)$ follow from the fact that both the wave function and the flux have to be continuous, i.e. at $z = z_0$

$$\begin{aligned} \lim_{z\to z_0^+}\psi(z,t) &= \lim_{z\to z_0^-}\psi(z,t) \\ \lim_{z\to z_0^+}\frac{1}{m(z)}\frac{\partial}{\partial z}\psi(z,t) &= \lim_{z\to z_0^-}\frac{1}{m(z)}\frac{\partial}{\partial z}\psi(z,t)\ . \end{aligned} \tag{2.35}$$

This yields an infinite system of algebraic equations for the coefficients A_n and B_n in each layer. Inserting the Fourier expansion of the phase in Eq. (2.32),

$$\exp\left\{-\frac{\mathrm{i}e}{\hbar}V_{\mathrm{ac}}\cos\Omega t\right\} = \sum_{n'=-\infty}^{+\infty} J_{n'}\left(\frac{V_{\mathrm{ac}}}{\hbar\Omega}\right)\exp(-\mathrm{i}n'\Omega t)\ , \tag{2.36}$$

where J_n is the n-th order Bessel function of the first kind, allows one to recast these equations for an interface between layers I and II at $z = z_i$ in matrix form:

$$\mathbf{T}^{\mathrm{I}}_{z_i}\begin{pmatrix} A^{\mathrm{I}}_n \\ B^{\mathrm{I}}_n \end{pmatrix} = \mathbf{T}^{\mathrm{II}}_{z_i}\begin{pmatrix} A^{\mathrm{II}}_n \\ B^{\mathrm{II}}_n \end{pmatrix}\ . \tag{2.37}$$

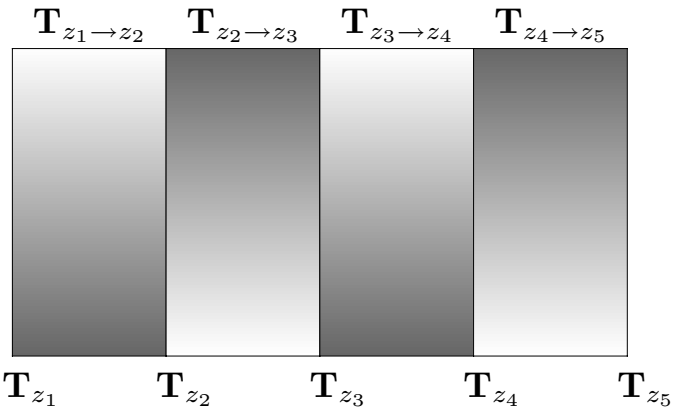

FIGURE 2.1: Layer *vs.* interface usage of transfer matrices (TMs). Defining TMs across layers is physically more sensible, since the matrices depend on the properties of just one layer. They are also numerically easier to implement, as there are fewer qualitatively different matrices to deal with.

The matrices $\mathbf{T}^{\mathrm{I}}_{z_i}$ and $\mathbf{T}^{\mathrm{II}}_{z_i}$ with elements $T^{\mathrm{I}}_{z_i;n,n'}$ and $T^{\mathrm{II}}_{z_i;n,n'}$, respectively, are of infinite dimension, and contain the coefficients of all possible scattering channels, i.e. photon exchanges between the incoming electron and the driving field, at either side of the interface. Their precise form depends of course on whether or not a layer is affected by the time-dependent gate voltage.[4] The transfer matrix $\mathbf{T}_{z_i \to z_j}$ between two sides of a layer of width $z_j - z_i$ is then defined (Wagner and Mizuta, 1993) as

$$\mathbf{T}_{z_i \to z_j} = \mathbf{T}^{\mathrm{I}}_{z_j} \left(\mathbf{T}^{\mathrm{I}}_{z_i} \right)^{-1}. \tag{2.38}$$

A graphical representation of how transfer matrices are defined is presented in Fig. 2.1 above. To calculate the total transfer matrix across the structure, we have to multiply the matrices across all different layers and obtain

$$\mathbf{T}_{\mathrm{L} \to \mathrm{R}} = \mathbf{T}_{z_{\mathrm{R}}} \mathbf{T}_{z_j \to z_{\mathrm{R}}} \cdots \mathbf{T}_{z_{\mathrm{L}} \to z_i} \mathbf{T}_{z_{\mathrm{L}}} \; ; \tag{2.39}$$

where $\mathbf{T}_{z_{\mathrm{L}}}$ and $\mathbf{T}_{z_{\mathrm{R}}}$ represent the initial and final matrices at the ends of the heterostructure. With the elements $T^{n,n'}_{\mathrm{L} \to \mathrm{R}}$ of the total transfer matrix we can find the probability that an electron with energy $E + n\hbar\Omega$ in lead L is scattered into a channel with energy $E' = E + n'\hbar\Omega$ in lead R, with integer n, n'. The diagonal elements $T^{n,n}_{\mathrm{L} \to \mathrm{R}}$ are closely related to the (static) transmission probability T_{RL},

[4] For a detailed description of transfer matrices, see Wagner (1995) or the Appendix.

while the off-diagonal elements $T_{\mathrm{L}\to\mathrm{R}}^{n\neq n'}$ describe the effects of the absorption or emission of $n - n'$ photons on the transmission probability of the electron. With this quantities we can proceed to calculate of the dc current inserting them in a formula like Eq. (2.28) for the time-independent probabilities.

For flat conduction bands on both sides of the heterostructure, the wave functions in the contacts are plane waves, and in this case the proper boundary conditions to describe an electron incident from, say, the left-hand side at energy E are $A_{\mathrm{L}}^n = \delta_{n,0}$ and $B_{\mathrm{R}}^n = 0$. The transmission probability in sideband n is then defined as

$$T_{\mathrm{RL}}^n = \frac{k_{\mathrm{R}}^n}{k_{\mathrm{L}}^0}\frac{m_{\mathrm{L}}}{m_{\mathrm{R}}}\left|\frac{A_{\mathrm{R}}^n}{A_{\mathrm{L}}^0}\right|^2 , \tag{2.40}$$

where k_{R}^n and k_{L}^0 represent the wave vectors on the right- and left-hand side in sidebands n and 0, respectively.

In a numerical implementation of the transfer-matrix technique, it is necessary to truncate the infinite matrices. Thereby for consistency, a proper cut-off has to be so large that unitarity of the scattering process is preserved, i.e.

$$\sum_{n=-N_{\mathrm{low}}}^{+N_{\mathrm{high}}} T_{\mathrm{RL}}^n + \sum_{n=-N_{\mathrm{low}}}^{+N_{\mathrm{high}}} R_{\mathrm{LL}}^n = 1 . \tag{2.41}$$

$N_{\mathrm{low}}, N_{\mathrm{high}} > 0$ denote respectively the lowest and highest sidebands that need to be taken into account to meet a given accuracy (which in our calculations was set to 10^{-10}). This depends essentially on the ratio $eV_{\mathrm{ac}}/\hbar\Omega$, as this is the argument of the Bessel function J_n that determines the weight of each sideband n and sets the values of N_{min} and N_{max}. To proceed, one starts at the initial value of $V_{\mathrm{ac}} = 0$ with a tentative number of sidebands, and increases it for growing driving amplitudes if a check with Eq. (2.41) suggests that unitarity is breaking down. When particle number conservation is restored one can go to a higher V_{ac}. Transfer matrices such as those employed here have the advantage of being easily scalable to arbitrarily complex structures. The combination of flexibility in structural properties and numerical accuracy makes this method well-suited to the study of strongly driven semiconductor heterostructures.

2.3.3 Tight-binding model

As was discussed in the introduction to this thesis, energy levels in heterostructures are not in a one-to-one correspondence with those of the atoms that form the system, but are determined by the interactions of the many atoms in the respective layers of GaAs and AlGaAs forming the tunnel barriers and quantum wells. This discretization by confinement, and the localization inside the wells, along with motivating the name of *artificial atoms* to the resulting structures, suggests a different method to explore the transport properties of these systems. In the tight-binding approximation put forward in this section one treats the quantum dot or quantum well as a structure isolated from the exterior with localized electrons. Electrons go into and out of the structure through tunnel barriers that connect it with the external leads.[5] Using a second quantization description for the occupation of the energy levels, one writes the number operator that counts the electrons in the QD as $N = \sum_i c_i^\dagger c_i$, where the operators $c_i^\dagger$ and c_i create and destroy, respectively, an electron in level i of the QD. The corresponding term in the Hamiltonian is then

$$H_{\mathrm{QDs}}(t) = \sum_{nn'} H_{nn'}(t) c_n^\dagger c_{n'} \,, \tag{2.42}$$

where $H_{nn'}(t)$ represents the matrix element such that $H_{nn}(t) = \epsilon_n(t)$ gives the energy of the electron in site n, and $H_{nn'}(t) = \Delta_{nn'}(t)$ describes the possible interwell interaction between levels in adjacent QDs. The system model we will later use in this thesis will a double QD or double quantum well. Thus our basic Hamiltonian for the QDs, which includes interwell coupling and the effect of an external driving field $V_{\mathrm{ac}}(t)$, reads

$$H_{\mathrm{QDs}}(t) = -\Delta(c_1^\dagger c_2 + c_2^\dagger c_1) + eV_{\mathrm{ac}} \cos(\Omega t) c_1^\dagger c_1 \,. \tag{2.43}$$

We have chosen $\epsilon_1 = \epsilon_2 = 0$ for the time-independent part of the on-site energies $\epsilon(t)$; we have also restricted the action of the ac field to the left QD. If the same description is applied to the leads and to the contacts through which current

[5] The tight-binding method has been used to obtain the energetic levels and transport properties of complex atomic networks from first principles. A detailed account of this procedure can be read in chapters 8-9 in Ashcroft and Mermin (1976), Section 7.3 in Agraït *et al.* (2003), or Ohno *et al.* (1999).

flows in and out of the system, one can write the total Hamiltonian as

$$H(t) = H_{\mathrm{QDs}}(t) + H_{\mathrm{leads}} + H_{\mathrm{contacts}}\,. \tag{2.44}$$

Here, the term

$$H_{\mathrm{leads}} = \sum_{\ell,q} \epsilon_{\ell q} c^{\dagger}_{\ell q} c_{\ell q} \qquad \ell = \mathrm{L}, \mathrm{R} \tag{2.45}$$

describes the electrons in the leads as a non-interacting Fermi gas, while

$$H_{\mathrm{contacts}} = \sum_{q} (V_{\mathrm{L}q} c^{\dagger}_{\mathrm{L}q} c_1 + V_{\mathrm{R}q} c^{\dagger}_{\mathrm{R}q} c_N) + \mathrm{H.\,c.} \tag{2.46}$$

models the interaction between the terminating levels in the QD and the level in the lead $|\ell q\rangle$ through the matrix element $V_{\ell q}$. The lead–dot coupling is effectively described by the *spectral density*

$$\Gamma_\ell(\epsilon) = 2\pi \sum_q |V_{\ell q}|^2 \delta(\epsilon - \epsilon_{\ell q})\,, \tag{2.47}$$

which contains most of the physics of the hopping process between the lead and the dot without being too specific about the details. Furthermore, we will later work in a regime where transport takes place in an energy range much narrower than the conduction band in the leads, so that one can disregard the energy dependence of the coupling and state

$$\Gamma_\ell(\epsilon) \to \Gamma_\ell\,, \tag{2.48}$$

in what is termed as the *wide band limit*.

Calculation of the dc current

To calculate from the Hamiltonian (2.44) the dc component of the current one has to calculate the time average over one period of the driving $\mathcal{T}$

$$\bar{I} = \langle I_\ell(t) \rangle = \frac{1}{\mathcal{T}} \int_0^{\mathcal{T}} \mathrm{d}t I_\ell(t) \tag{2.49}$$

of the current operator in the leads

$$I_\ell(t) = e\dot{N}_\ell(t) = \frac{\mathrm{i}e}{\hbar}[H(t), N_\ell(t)] = \frac{\mathrm{i}e}{\hbar}[H(t), \sum_q c^{\dagger}_{\ell q} c_{\ell q}]\,, \tag{2.50}$$

where we have used the evolution of the operators in the Heisenberg representation. To proceed, one writes the Heisenberg equations of motion for the lead operators and uses Green functions to uncouple the resulting system of equations. By this method (see e.g. Kohler *et al.*, 2005, for details), one arrives at the following expression for the time-averaged current:

$$\bar{I} = \langle I_\ell(t) \rangle = \frac{e}{\hbar} \sum_{k=-\infty}^{\infty} \int \mathrm{d}\epsilon \left\{ T_{\mathrm{LR}}^{(k)}(\epsilon) f_{\mathrm{R}}(\epsilon) - T_{\mathrm{RL}}^{(k)}(\epsilon) f_{\mathrm{L}}(\epsilon) \right\} . \tag{2.51}$$

The transmission probabilities $T_{\ell'\ell}^{(k)}(\epsilon) \equiv T_{\ell' \leftarrow \ell}(\epsilon \to \epsilon + k\hbar\Omega)$ can be expressed in terms of Green functions, and have a straightforward interpretation in terms of electron scattering: they correspond to the processes of absorption ($k > 0$) or emission ($k < 0$) of $|k|$ photons, thus going from an initial energy ϵ to a final one $\epsilon + k\hbar\Omega$. Within this formalism an expression for the dc current can be *derived* that resembles the Landauer formula [Eq. (2.3)] in the ac case right from the definition of the current operator, instead of merely postulating it in some heuristic way. On the other hand, Eq. (2.51) reduces to Eq. (2.3) when $V_{\mathrm{ac}} = 0$, since in that limit $T_{\mathrm{LR}}^{(k)}(\epsilon) = T_{\mathrm{RL}}^{(k)}(\epsilon)$ and the terms with $k \neq 0$ vanish.

The fact that the Hamiltonian of the system is a periodic function of the time t can be used to establish an explicit relation between the Green functions that go into the transmission probabilities of Eq. (2.51) and the Floquet states of Eq. (2.14). With this it is possible to numerically calculate the dc current of Eq. (2.51).

2.3.4 High frequency limit and current suppression

Treating transport problems within a Floquet approach allows the development of a perturbative method in the case when energy scale set by the frequency of the external ac signal, $\hbar\Omega$, is much higher than any other energy scale appearing in the problem. This limit, explored first by Shirley (1965), is a reasonable one to investigate since many of the transport phenomena in the presence of an ac perturbation are greatly amplified when the driving frequency Ω is high. Among them, the coherent destruction of tunnelling and the photo assisted tunnelling addressed in this thesis. Mathematically, this approximation amounts to keeping only the first term in an expansion in the parameter $1/\Omega$. Physically (Kohler *et al.*, 2004), its main advantage is that the original time-dependent problem is mapped into a *static* (or time-independent) one, with the appropriate renormalization of

some quantities, which makes a qualitative understanding easier. In the static case the dc current is calculated with Eq. (2.3), where, again in the wideband limit, transmission probabilities are just $T(\epsilon) = T_{\mathrm{LR}}(\epsilon) = \Gamma_{\mathrm{L}}\Gamma_{\mathrm{R}}|G_{\mathrm{LR}}(\epsilon)|^2$ with the additional condition that $G_{\mathrm{LR}}(\epsilon) = G_{\mathrm{RL}}(\epsilon)$. Setting $V_{\mathrm{ac}} = 0$ in our Hamiltonian (2.44), the transmission can be shown to be

$$T(\epsilon) = \frac{\Gamma^2\Delta^2}{|(\epsilon - \mathrm{i}\Gamma/2)^2 - \Delta^2|^2} \tag{2.52}$$

if the couplings $\Gamma_{\mathrm{L}} = \Gamma_{\mathrm{R}} = \Gamma$ are assumed equal.

The starting point of the high frequency approximation (HFA) is the application of the unitary transformation

$$U_0(t) = \exp\left\{-\frac{\mathrm{i}eV_{\mathrm{ac}}}{\hbar\Omega}\sin(\Omega t)c_{\mathrm{L}}^{\dagger}c_{\mathrm{L}}\right\} \tag{2.53}$$

to the Hamiltonian (2.42):

$$H(t) \to \tilde{H}(t) = U_0^{+}(t)H(t)U_0(t) - \mathrm{i}\hbar U_0^{+}(t)\dot{U}_0(t) \tag{2.54}$$

For very high frequencies $\Omega \gg \Delta/\hbar$, this transformation results in an effective separation of two timescales: that of the ac signal, very short in this limit, and the much longer one of the tunnel dynamics. Thus one can discard the effects of the external driving when averaging over a period $\mathcal{T}$ (Großmann and Hänggi, 1992; Grifoni and Hänggi, 1998). In this way one arrives at an effective Hamiltonian for the QDs

$$\begin{aligned}\bar{H}_{\mathrm{eff}} &= \frac{1}{\mathcal{T}}\int_0^{\mathcal{T}} \mathrm{d}t\, \left(U_0^{\dagger}\, H_{\mathrm{wells}}(t)\, U_0 - \mathrm{i}\hbar\, U_0^{\dagger}\dot{U}_0\right) \\ &= -\Delta_{\mathrm{eff}}(c_{\mathrm{L}}^{\dagger}c_{\mathrm{R}} + c_{\mathrm{R}}^{\dagger}c_{\mathrm{L}}),\end{aligned} \tag{2.55}$$

for the matrix elements $\tilde{H}_{nm}(t) \ll \hbar\Omega$. This effective Hamiltonian has the same form as the static one, but now the tunnel matrix element has been substituted by its effective value

$$\Delta_{\mathrm{eff}} = J_0\left(\frac{eV_{\mathrm{ac}}}{\hbar\Omega}\right)\Delta_0\,, \tag{2.56}$$

where $J_0(x)$ is the Bessel function of the first kind and zeroth order. It logically follows that the static transmission probability has to be replaced in favour of the corresponding effective quantity, $T_{\mathrm{eff}}(\epsilon)$, by substituting $\Delta_0 \to \Delta_{\mathrm{eff}}$ in Eq. (2.52).

The most striking feature of this new transmission is that it appears to be controllable by a proper choice of the driving amplitude and frequency. In particular, the HFA predicts a complete suppression of transport for those values of the argument $V_{\mathrm{ac}}/\hbar\Omega$ for which J_0 goes to zero. This analytical result will be used in the analysis of the results presented in chapter 4.

On the other hand, the transformation (2.53) affects also the contacts between the system and the leads. The principal effect here is the change in the distribution function of the electrons in the leads, which is now replaced by the effective one:

$$f_{\mathrm{L,eff}}(\epsilon) = \sum_{k=-\infty}^{\infty} J_k^2\left(\frac{V_{\mathrm{ac}}}{\hbar\Omega}\right) f_{\mathrm{L}}(\epsilon + k\hbar\Omega)\,. \tag{2.57}$$

The Bessel functions of the first kind and order $k \in \mathbb{Z}$ weigh the contributions of the processes by which an electron goes from an initial energy ϵ to the other side of the structure after emitting or absorbing k photons. This effective Fermi function presents steps at energies $\epsilon = \mu_{\mathrm{L}} + n\hbar\Omega$ and is constant for other values of ϵ.

It is now quite straightforward to show the new form of the current in the HFA: $T_{\mathrm{eff}}(\epsilon)$ is a sharp-peaked function around $\epsilon = 0$, and, for finite voltages, $f_{\mathrm{R}}(0)$ and $f_{\mathrm{L,eff}}(0)$ are constant. The dc current then reads (Kohler *et al.*, 2004)

$$I_{\mathrm{HFA}} = \frac{e\Gamma}{4\hbar}\frac{\Delta_{\mathrm{eff}}^2}{\Delta_{\mathrm{eff}}^2 + (\Gamma/2)^2}\left[1 + \sum_{|k|\leq K(V)} J_k^2\left(\frac{V_{\mathrm{ac}}}{\hbar\Omega}\right)\right] \tag{2.58}$$

using the static Landauer formula with the renormalized parameters. Here, $K(V)$ is an abbreviated form of stating that only the integer part of $e|V|/2\hbar\Omega$ has to be taken into account in the sum over k.

The main achievement of the HFA, namely the mapping of the time dependent problem into a static one, offers yet another way of interpreting its results: transport in static systems, in the absence of other perturbations, can only take place if the charge carriers can be transmitted elastically through the system. The time-dependent gauge transformation $U_0(t)$ takes the part of the Hamiltonian that explicitly depends on time to a static form and, simultaneously, brings the energy levels to an equal energy (in a dynamical way), thus allowing transport *as if it took place elastically*.

3 Coherent suppression of current in heterostructures

As a first application of the time-dependent formalism for transport derived in the previous chapter, we study the effect of an ac gate voltage on the transmission properties of semiconductor heterostructures. The feature of interest here is the possibility of coherently controlling the dc current that traverses the structure by appropriately choosing the parameters of the driving. This effect, predicted at first for isolated systems only (Dunlap and Kenkre, 1986; Grossmann *et al.*, 1991; Holthaus, 1992; Wagner, 1995; Creffield and Platero, 2002), can thus be extended to transport situations by suitably taking into account the coupling to the leads.

We also use this problem as *test bed* for the basic assumptions underlying the analytical and numerical methods used in this thesis. In particular, we check the analytical high-frequency approximation against the exact numerical calculations carried out with the numerical tight-binding and transfer-matrix schemes.

3.1 Dynamic localization and coherent destruction of tunnelling

Motivation for the study of coherent transport suppression comes from different physical systems already mentioned in the introduction: semiconductor quantum wells and their generalization in the form of *superlattices*, envisioned and subsequently built in the early 1970s, and, on the other hand, driven two-level systems, of which various possible realizations exist, which motivated the article of Grossmann *et al.* (1991).

3.1.1 Dynamic localization by irradiation of superlattices

We can consider the pioneering investigations of Tsu and Esaki on negative resistance in superlattices, i.e. a spatially periodic potential created by periodic variation of alloy composition or of impurity densities of semiconductors (Esaki and Tsu, 1970; Esaki, 1974), as the first attempt to control the transport properties by an external field. In the search for "new ultra-high-speed devices" based on semiconductors, and applying the semiclassical theory of transport, a negative differential conductivity appeared when the strength of a dc field reached a certain threshold. The effect was attributed to the negative drift velocity that resulted from an inflection (change of sign in the derivative) in the dispersion relation $\epsilon(k)$ of the electrons.

As an artificial realization of a Kronig-Penney potential (see Ashcroft and Mermin, 1976), superlattices have attracted much attention since their invention. As Tsu and Esaki themselves predicted, they allow the observation of quantum transport properties in a physical scale much bigger than that of the atoms of the host crystal.[1]

The periodic disposition of layers of e.g. GaAs and AlGaAs in a superlattice results in the narrowing of the conduction bands of the starting crystals, justifying the use of the term *miniband*. A tight-binding model for superlattices with separation d and interaction to first neighbours Δ_0 gives a dispersion relation $E(k) = -\hbar\Delta_0 \cos(kd)$ and bandwidth $2\hbar\Delta_0$. The application of an ac field of the form $\hat{e}\cos(\Omega t)/d$ can be shown (Holthaus, 1992) to yield a renormalized dispersion relation $\epsilon'(k) = J_0(\hat{e}/\hbar\Omega)\epsilon(k)$, which translates in a corresponding change in the conduction bandwidth. J_0 is again the zeroth order Bessel function. If $\hat{e}/\hbar\Omega$ equals one of the zeros of J_0, the band will collapse and a particle prepared at a site of the lattice will neither move nor spread. This phenomenon was termed *dynamic localization*.

3.1.2 Coherent destruction of tunnelling in two-level systems

Far from being a mere theoretical tool, two-level systems (TLS) appear often in many problems of chemistry and physics. Double quantum dots and two-site molecular wires, for example, can be described to a good approximation

[1] For a full review of the transport properties of superlattices, see Wacker (2002).

by studying the properties and evolution of just two levels. These are either the lowest-lying in energy above the valence band (for semiconductor dots), or the highest-energy orbitals that are still occupied (for molecular wires). All other levels are then regarded as completely empty or filled, thus not contributing to transport, or too far-lying in energy so as to cause any measurable interaction.[2]

The general properties on TLS of interest to our problem can be summed up as follows. We have in mind a system like those depicted either in Fig. 3.1 or 3.2, that is, a symmetric two-site structure with degenerate levels of energy E_0. Usually, $E_0 = 0$ is chosen for convenience. The degeneracy of the levels is removed by the tunnel interaction Δ. Thus the lowest lying states correspond to the symmetric and antisymmetric combinations of the ground states of the separate wells, which acquire (as shown by elemental first-order perturbation theory) energies $\pm\Delta/2$. A convenient way of writing the Hamiltonian is the *pseudo-spin basis* using the Pauli matrices, because of the identical treatment of this TLS with the standard example of a particle with momentum $J = \hbar/2$ found in text books. The ac perturbation affects the on-site energies only, so one can write

$$H_{\rm TLS}(t) = -\frac{\Delta}{2}\sigma_x + \frac{\epsilon(t)}{2}\sigma_z \ . \tag{3.1}$$

The time-dependent site energy $\epsilon(t)$ will be taken of sinusoidal shape, i.e. $\epsilon(t) = V_{\rm ac}\cos\Omega t$.

The interaction of a TLS with radiation, in the form of an electric or magnetic field, was the subject of a number of relevant papers in the beginnings of quantum mechanics (Rabi, 1937; Bloch and Siegert, 1940). Bloch found in the case of linear polarization that an analytical solution was possible for driving frequencies $\Omega \simeq \Delta/\hbar$, where one could invoke the so-called *rotating wave approximation* and discard terms oscillating very rapidly and keep only the slow oscillations. Then it is possible to analytically solve the coupled system of linear differential equations for the populations $c_1(t)$ and $c_2(t)$ of the energy levels, to find that they oscillate with a frequency $\Omega_{\rm R} = [(\hbar\Omega - \Delta)^2 + V_{\rm ac}^2/4]^{1/2}$. When $\hbar\Omega = \Delta$ the population is transferred periodically between both states.

[2]The basics of TLS can be found in Cohen-Tannoudji *et al.* (1977), and as they apply to driven situations in Sec. 3 of Grifoni and Hänggi (1998). Many experimental results on microwave spectroscopy of TLS in double quantum dots can be found in the review of van der Wiel *et al.* (2003).

But a novel effect appears when one considers this situation in the context of transport. Here one analyzes the problem of a particle, localized initially in site $|\mathrm{L}\rangle$, say, which can tunnel coherently to site $|\mathrm{R}\rangle$. The particle tunnels at a rate $\sim \Delta/\hbar$ in the absence of any other perturbation, and therefore spends typically a time $\sim \hbar/\Delta$ in each well (at least in symmetric systems). The onset of a time-dependent driving that brings the Hamiltonian to the form of Eq. (3.1) changes the picture, and now one must obtain the time-dependent site occupations $c_{\mathrm{L,R}}(t)$ from the Schrödinger equation of the system. This yields for frequencies $\Omega \gg \Delta/\hbar$ the following equation (Grifoni and Hänggi, 1998):

$$\mathrm{i}(\mathrm{d}/\mathrm{d}t)c_{\mathrm{L,R}}(t) = -\frac{1}{2}\Delta J_0(eV_{\mathrm{ac}}/\hbar\Omega)c_{\mathrm{L,R}}(t) \tag{3.2}$$

where $J_0(x)$ is the zeroth-order Bessel function of the first kind. What is interesting of this result is that Eq. (3.2) has the same structure as that of the static system, but with an effective tunnel coupling

$$\Delta \to \Delta_{\mathrm{eff}} \equiv J_0(eV_{\mathrm{ac}}/\hbar\Omega)\Delta \tag{3.3}$$

now multiplied by a function that vanishes at certain values of the argument $eV_{\mathrm{ac}}/\hbar\Omega$. The conclusion that follows is that tunneling in a TLS can be brought to a standstill by the suitable choice of the parameters of the external driving. To explain precisely what is happening here requires a description of the quasienergy levels of the driven TLS: coherent destruction of tunneling takes place when two quasienergies stemming from two quasidegenerate sites (degeneracy removed by tunneling) cross, i.e. are equal at a finite driving. In terms of tunneling process, it is evident that an *effective* tunnel coupling $\Delta_{\mathrm{eff}} \to 0$ takes the tunnel event rate to zero, and correspondingly the dwell time to infinity.

3.1.3 Transport quenching in single quantum dots

Closely related to the transport problem addressed in this chapter, the case of isolated heterostructures under the action of ac driving was considered around a decade ago by Wagner (1994, 1995, 1996). Treating both single- and double semiconductor quantum wells in the presence of either a driving *potential* or a driving *field* (the latter implying a spatially varying potential through the structure), Wagner found that transport channels could be inhibited simultaneously by the action of an external driving. However, as the role of the contacts is not

correctly taken into account, these calculations fail to provide a reliable transport calculation. In any case they are probably the first hint that a transport-related effect, in the way of the coherent destruction of tunneling of Grossmann *et al.*, could be observable.

The approach of Wagner developed in two directions: on the one hand, he used the transfer matrix technique of section 2.3.2 for the numerical computation of transmission probabilities at high amplitude driving, where perturbational approximations are no longer valid. As we know, transfer matrices are a convenient way of expanding the Floquet states in free space — or at least inside layered semiconductor heterostructures, if one can assume flat conduction bands, as has been done there. This is then just a particular case of the more general Floquet theory of periodically driven systems.

But, on the other hand, although numerically exact, the analysis of the results in terms of simple energy (as in the Tien-Gordon case) or transport sidebands is not possible, since the phase of the plain waves retains a certain time- and wave vector dependence. As a way out, (Wagner, 1994, 1995, 1996) developed analytical solutions, either by making some *ansatz* for the transfer matrix coefficients A^n, B^n for driving potentials, or for the wave function itself (in the spirit of Truscott, 1993) for driving electric *fields*. This was done by expanding perutrbatively the general solution for the case $\hbar\Omega \ll E_0$, where E_0 denotes the energy of the level for zero driving. This analytical treatment allowed Wagner to compare with the numerical results, as well as the critical assessment of some experiments of Keay *et al.* (1995) on sequential photon-assisted tunneling in superlattices.

As mentioned above, these findings are still not enough to predict that current will be suppressed in a transport experiment. We need, apart from the rather technical issues of the leads and the relevant integrations in the energy, to find a situation where *all* the relevant transmission probabilities vanish simultaneously, and this is not guaranteed by the theory above. In what follows we explain how a proper comparison with the clearcut physical situation of two level systems brings this closer to experiments.

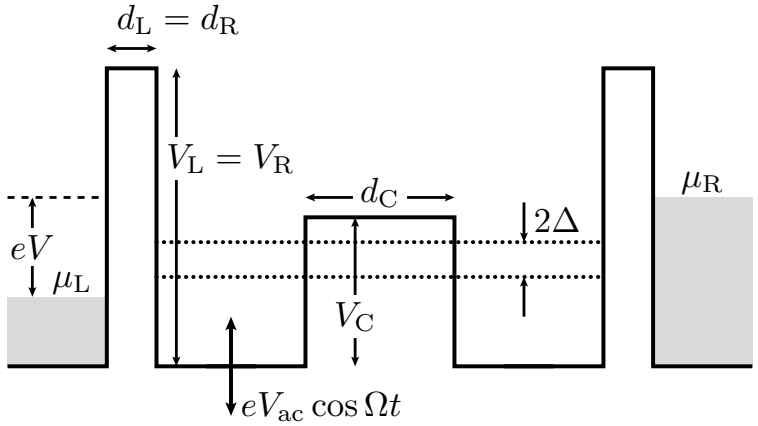

FIGURE 3.1: Double quantum well structure used in the study of coherent current control. Parameters are $d_{\mathrm{L,R}} = 5, d_C = d_{w\mathrm{L,R}} = 15$ nm; $V_{\mathrm{L,R}} = 90, V_C = 40$ meV; $V = 6$ mV.

3.2 Current suppression in semiconductor heterostructures

The investigation of current suppression in a transport context has received attention only recently (Kohler *et al.*, 2004; Camalet *et al.*, 2004). In this section we discuss how a semiconductor heterostructure can be tuned to predict a vanishing of the dc current.[3] The analysis is performed with the tools developed in chapter 2: transfer matrices and tight-binding Floquet theory.

As a system we choose the triple-barrier structure of 3.1. The values of barrier heights and widths correspond roughly to the order of magnitude of typical semiconductor heterostructures (Capasso and Datta, 1990). At zero driving the ground states of the wells are split by $\Delta = 0.23$ meV because of tunneling between them. An equivalent description in terms of the tight-binding model is depicted in Fig. 3.2. In the following we will compare the results of the two approaches, taking advantage of the high precision of numerical transfer-matrix and tight-binding calculations, and the analytical results of the HFA (cf. Section 2.3.4).

In order to be able to compare the transfer-matrix and the tight-binding approaches, we have to ensure that the same physical situation is addressed. As a matching condition we compare the transmission $T(\epsilon)$ in the time-independent case ($eV_\mathrm{ac} = 0$). The level splitting energy 2Δ due to the central tunnel barrier is extracted from the resonance peaks of the doublet states computed with the

[3] This results have already been published in Rey *et al.* (2005).

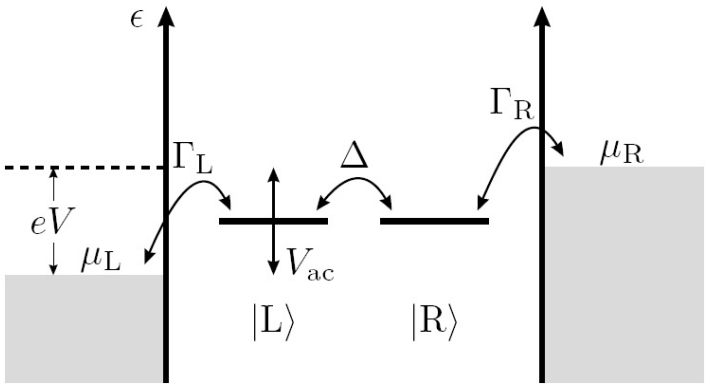

FIGURE 3.2: Tight-binding model for the double quantum well [dot?] of Fig. 3.1. The interwell coupling is given by Δ, while the couplings to the leads are Γ_{L} and Γ_{R}, respectively. The ground state of the left well oscillates by the action of the external ac potential, $V_{\mathrm{ac}}(t)$, and an external bias $V = (\mu_{\mathrm{R}} - \mu_{\mathrm{L}})/e$ is applied.

transfer-matrix method. Solving for Γ in Eq. (2.52), with $\epsilon = 0$ and $T(0)$ and Δ taken from the previous calculation, the corresponding lead–well coupling for the tight-binding system is determined.

Surveying the time-averaged current calculated numerically from the transfer-matrix and the tight-binding method plotted in Fig. 3.3, we observe current minima for distinct values of $eV_{\mathrm{ac}}/\hbar\Omega$ for frequencies in the microwave regime ($\Omega \sim 1\,\mathrm{meV} \sim 200\,\mathrm{GHz}$). By varying the ratio between driving amplitude and frequency, we can thus tune the tunneling between the two wells and thereby control the current (Kohler *et al.*, 2004). To understand this results better we also plot the HFA analytical curve of (2.58), which exhibits minima close to those of the transfer-matrix and tight-binding curves. The analytical expression shows a remarkable agreement with the exact tight-binding result (2.51) for $eV_{\mathrm{ac}} \lesssim eV$. The current (2.58) vanishes whenever the ratio $eV_{\mathrm{ac}}/\hbar\Omega$ assumes a zero of the Bessel function J_0, i.e. for the values 2.405, 5.520, 8.654, ..., since then $\Delta_{\mathrm{eff}} \propto J_0^2 = 0$. That this also happens for the numerical calculations only shows that the parameters ($\hbar\Omega = 5\Delta = 1.15$ meV in our case) have been conveniently chosen so that the HFA, and therfore $\Delta_0 \to \Delta_{\mathrm{eff}} = J_0\Delta_0$, is valid.

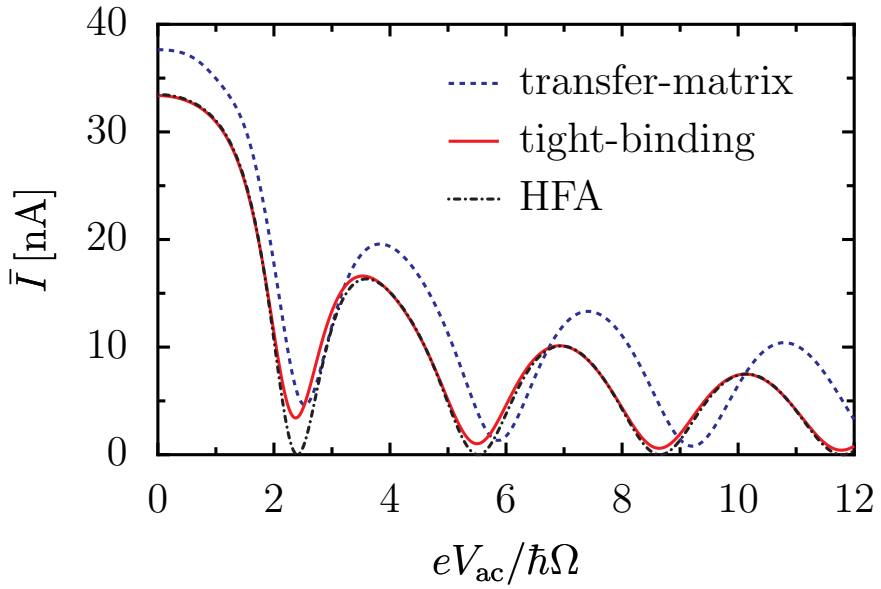

FIGURE 3.3: Average current as function of driving amplitude V_{ac} obtained numerically from transfer-matrix (dashed line) and tight-binding (solid) methods. Also shown is the HFA curve (dash-dotted). The chosen parameters are $\hbar\Omega = 1.15\,\text{meV}$, $V = 6.0\,\text{mV}$, $\Gamma = 0.16\,\text{meV}$ and $\Delta = 0.23\,\text{meV}$. The corresponding parameters for the barriers are the same as those of Fig. 3.1.

3.2.1 Exploration of HFA and tight-binding approximations

As a further check on the correctness of the HFA, Fig. 3.4 shows how the current at the first suppression (around $eV_{ac}/\hbar\Omega = 2.405$ meV) decays as a function of the driving frequency Ω. If the HFA gives a good —though inexact— account of the transport properties in this regime, then $I_{\text{HFA}}(eV_{ac}/\hbar\Omega)$ represents the first order term in the expansion of $\bar{I}(eV_{ac}/\hbar\Omega)$, in the (small) parameter $1/\hbar\Omega$ (Kohler *et al.*, 2004). The current at the minimum does decay as $1/\hbar\Omega$ as predicted by the HFA scheme; higher order contributions are included in the numerically exact calculation of transfer-matrices and tight-binding methods, which results in a non-vanishing current at the minima. These higher order terms can be disregarded for $\hbar\Omega \gtrsim 2$ meV.

While the general shape and magnitude of the current are very similar for both models, there still appears a small difference in the location of the minima for the relatively low barriers chosen in Fig. 3.3. For a continuous potential, the current assumes minima at values of $eV_{ac}/\hbar\Omega$ higher than those predicted by the tight-binding description. We can understand this shift by analysing, for given Ω, the

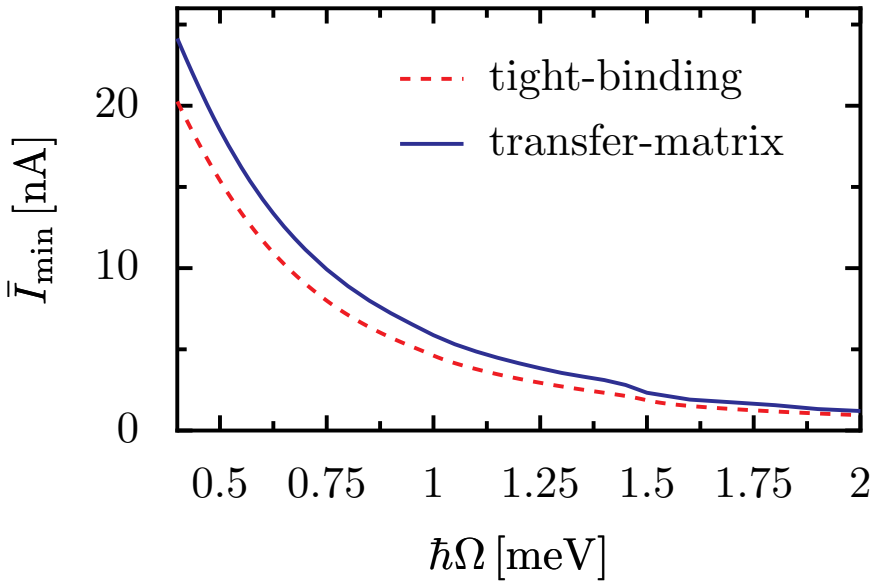

FIGURE 3.4: Value of the first current minimum as a function of the driving frequency. Both transfer-matrix (blue) and tight-binding (red) lines decay approx. as $1/\Omega$, as expected in the HFA approximation.

deviation $\delta V = V_{\min} - V_0$ of the driving amplitude $V_{\min}$ for which the current exhibits its first minimum from $V_0 = 2.405\hbar\Omega$ (the first zero of J_0). In Fig. 3.5 we plot δV as a function of κd, where $d = d_L = d_R$ and

$$\kappa = \frac{1}{\hbar}\sqrt{2m(V - \bar{\mu})}\,; \tag{3.4}$$

i.e. κd is the instanton action in units of $\hbar$, and $\exp(-2\kappa d)$ is the WKB[4] transmission probability of the outer barriers in Fig. 3.1. Here $V = V_L = V_R$ is the corresponding barrier height and $\bar{\mu} = (\mu_L + \mu_R)/2$ is the average chemical potential representing approximately the mean energy of the resonance doublet.

In the derivation of (2.51) for the dc current in the Floquet formalism we considered the lead-well coupling to be completely energy-independent (cf. Eq. 2.47), as assumed in the wide-band limit. But we know this to be an ideal situation, strictly valid only when the external barriers are infinitely high. The wave functions of the well states become then completely localised and Γ is in fact independent of energy. We use κd as a measure of this localization. Figure 3.5 shows that if the width of the outer barriers is kept fixed, δV decreases for growing κd, be-

[4]WKB stands here for the Wentzel, Kramers, and Brillouin semiclassical approximation, cf. Griffiths (1995).

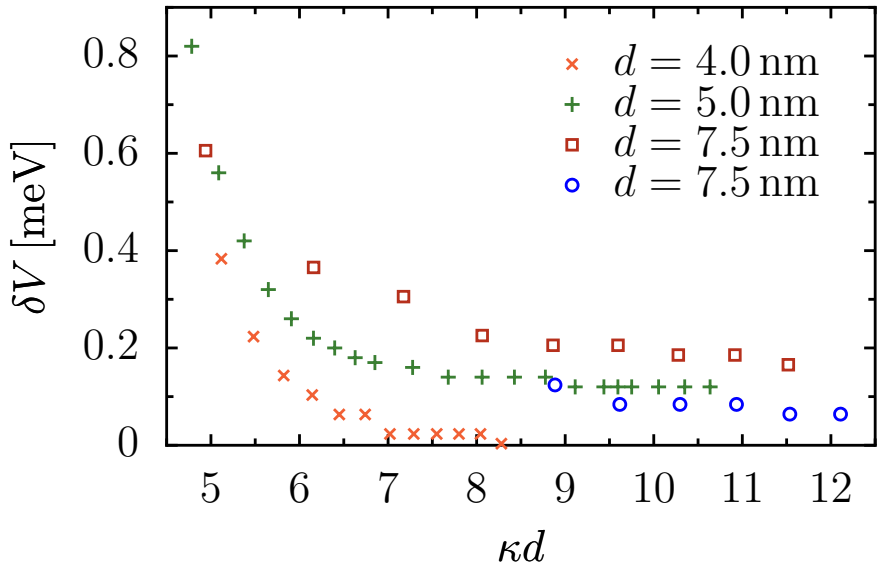

FIGURE 3.5: Deviation of the driving amplitude for the first current minimum from the expected first zero of J_0, $V_0 = 2.405\,\hbar\Omega$, for different barrier widths and heights. The parameters for the first three data sets are $d_C = 15\,\mathrm{nm}$, $\bar{\mu} = 12.0\,\mathrm{meV}$ and $V_C = 40\,\mathrm{meV}$, whereas for the last one (○), we chose $\bar{\mu} = 13.3\,\mathrm{meV}$ and $V_C = 80\,\mathrm{meV}$.

cause then the resonance energies are further away from the barrier edge and the wide-band limit is approached. Furthermore, this argument is used to explain the smaller deviation observed with thinner barriers for the same κd, since V is much larger in that case.

As can be seen by comparing data sets for different central barrier heights in Fig. 3.5, an increase of the height of the central barrier V_C reduces the level splitting 2Δ, that is, the overlap between the localised states in the left and right well in a tight-binding description. Thus the tight-binding and the transfer-matrix results converge as a function of the barrier height. Finally, it is important to note that varying any of the barriers affects the transmission properties of the whole heterostructure, in contrast to the tight-binding model, where the different coupling parameters can be controlled independently.

3.2.2 Other types of driving

A question that arises in view of the results of this section is their stability against possible variations of the driving ac potential, i.e. if the actual experimental conditions are not as ideal as the figure 3.1 suggests. It could well be the case that

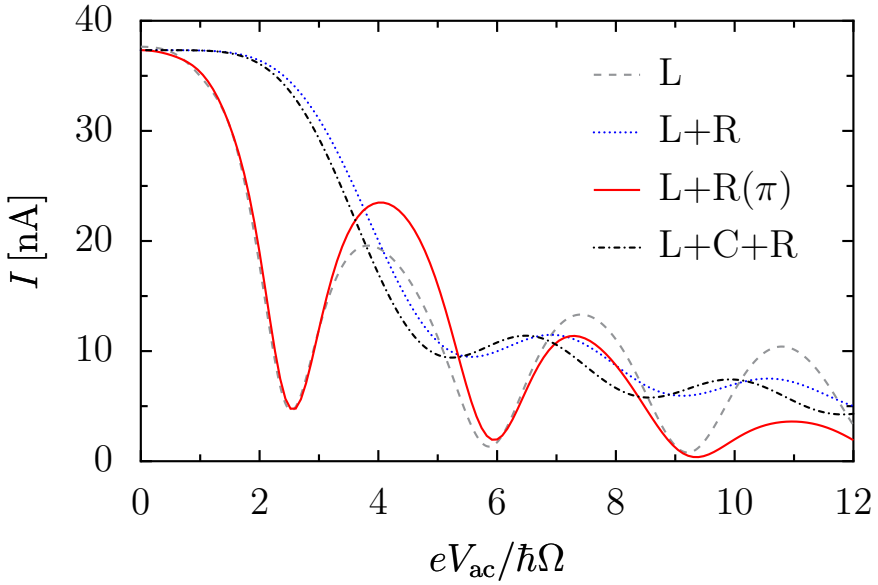

FIGURE 3.6: Current suppression calculated with transfer matrices for different driving setups. Dashed-gray curve corresponds to the situation of Fig. 3.3; for the continuous (red), both wells are driven with a phase difference of π between them. Blue (dotted) and black (dash-dotted) curves represent results for two in-phase driven wells without and with driving the central barrier as well. Parameters are like those of Fig. 3.3.

the localization of the driving to the quantum well is not as perfect as assumed, and that it "invades" adjacent regions as any of the barriers to the left or the right. A numerical test with the transfer matrix approach of these other driving conditions is presented in Fig. 3.6, and the results can be directly compared to the original case of Fig. 3.3. As is evident, all kinds of driving, with minor differences, reproduce the dependence of the dc current with the driving amplitude, with minima at the ratios of the amplitude to the driving frequency that equal zeros of the first order Bessel function. In the case of two in-phase driven wells the results are somewhat different. This difference can be ascribed to the different coupling between the levels when they are raised or lowered simultaneously. Moreover, the HFA scheme presented for the case of a single driven well does not hold, so that we cannot perform the same static-like analysis.

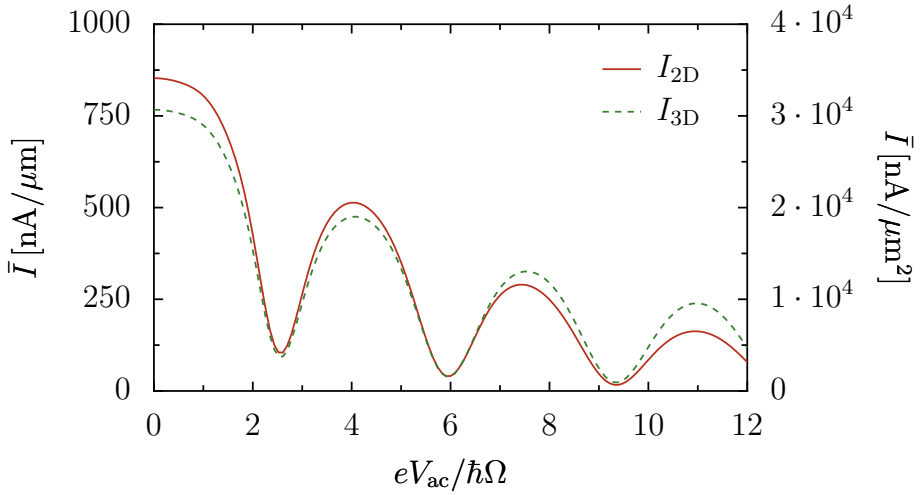

FIGURE 3.7: Time-averaged current through 2- and 3D semiconductor heterostructures. Calculations are carried out with the same ac scattering formalism, but with the corresponding 2D and 3D densities of states in the respective leads. An equivalent suppression effect is also predicted in these cases.

3.2.3 Higher dimensions

The dimensionality of the leads connected to the driven heterostructure has not played any role in the discussion of these results, but in principle it is also interesting to study if this effect is maintained for two- and three-dimensional leads. We assume that the component of the wave vector parallel to the interface across which transport takes place is conserved. Then the main difference with the strictly one-dimensional case treated so far is, as discussed in section 2.3.1, the different densities of state that must be used now. This should however not matter very much for current suppression: as the high-frequency approximation and renormalization of the coupling affect exclusively the driven part of the structure, we expect to observe the same current minima as in one-dimensional systems. The results confirming this is indeed the case are shown in Fig. 3.7.

4 Nonadiabatic pumping in heterostructures

4.1 Introduction

We now turn our attention to the other main topic of the present thesis, namely the nonadiabatic pumping of electrons. This expression is a convenient shorthand for *the transfer of electrons in the absence of, or even against, an externally applied bias, by the action of an ac gate voltage at finite frequency*. Essential ingredients of this rectification effect are nonlinear ac driving and some asymmetry in the spatial structure or in the temporal signal. The general symmetry conditions for pumping in systems described by Floquet Hamiltonians like that of Eq. (2.18) have recently been formulated by Kohler *et al.* (2005). We deal here only with systems without magnetic field, and the structure Hamiltonian possesses time-reversal symmetry. The transmission probabilities $T_{\mathrm{RL}}(\epsilon \to \epsilon + k\hbar\Omega)$ and $T_{\mathrm{LR}}(\epsilon + k\hbar\Omega \to \epsilon)$ are then equal. This implies that to achieve any non-vanishing current a breaking of the generalized parity is required.

The interest in rectified motion of particles by the action of external forces reaches many research areas in physics today. For instance, thermal fluctuations in so-called *thermal ratchets* can result in a net current of particles. When such systems work against a small force opposed to the current they are called *Brownian motors* (Parrondo and de Cisneros, 2002; Astumian, 1997). In solid state devices, the subject of charge pumping was started by the idea of adiabatic charge transfer (Thouless, 1983), and the experiments with single electron turnstiles performed in the early 1990s (see e.g. Geerligs *et al.*, 1990; Devoret *et al.*, 1992). Since then, pumping has been predicted in systems like asymmetric molecules, both undriven (Kornilovitch *et al.*, 2002) and under ac driving (Lehmann *et al.*, 2002), and superconducting-insulator interfaces (Blaauboer, 2002). Experimentally, it

has been found in carbon nanotubes (Leek *et al.*, 2005) and some semiconductor systems such as adiabatically driven quantum dots (Switkes *et al.*, 1999), biased ratchets (Linke *et al.*, 1999), and one dimensional channels driven by the action of surface acoustic waves (Talyanskii *et al.*, 1997).

The reasons for this theoretical and experimental richness are multiple. First, adiabatic pumping holds the promise of providing a precise mechanism for setting a current standard that would complete those already found for voltage in the Josephson effect and for resistance in the Hall effect (Niu, 1990). Second, the miniaturization of electronic devices, almost down to the domain where quantum effects are important, requires the development of new voltage and current sources to be integrated in the circuits (this is the subject of Section 4.3).

In mesoscopic semiconductor systems, pumping has been pursued either via irradiation and subsequent modification of the level structure by an external source, or by the modulation at low frequencies of the gates connecting the system with the environment. The experiments of Kouwenhoven *et al.* (1994) belong to the first group, and partially go back to the proposal of Tien and Gordon (1963) for SIS systems. Switkes *et al.* (1999) achieved pumping through the second mechanism based on Thouless' idea, although this was initially an effect predicted for isolated systems. In this pump the driving frequency produces a dc current while the system does not abandon its ground state, and it is therefore referred to as *adiabatically driven*. These two proposals differ from the single charge pumping method of Devoret *et al.* in the essential feature that the latter, which makes use of the Coulomb blockade effect and the change in the electrostatic energy through a gate voltage, is free from any quantum mechanical fluctuations, and thus is a classical effect.

Adiabatic pumping occurs when the inverse of the driving frequency is much larger than the typical traversal time of the electrons through the system. It requires that at least two parameters be independently varied to produce a nonvanishing dc current (Altshuler and Glazman, 1999). This current has then been shown to be computable from the scattering matrix of the system (Brouwer, 1998) and also to be proportional to the driving frequency. In spite of the theoretical insight it provides on the transport mechanisms of chaotic dots, we are interested here in the opposite regime of moderate-to-high (nonadiabatic) driving frequencies, where a larger current occurs while its accompanying noise can be kept at tolerable values (Strass *et al.*, 2005).

Wagner and Sols (1999) applied this ideas to a semiconductor structure and proposed to introduce a band offset between the leads. This had the consequence of strongly enhancing the pumped current in an otherwise already asymmetric structure. This setup was used to prove that in ac driven systems, in contrast to static situations, the current does not stem exclusively from states with energies close to the Fermi level, but effectively involves electrons at all energies. In the appropriate conditions this results in an interesting resilience of the current to changes in chemical potential or temperature for three dimensional pumps.

We introduce an asymmetry in the structure of chapter 3 by an internal bias in one of the wells. We then follow the formalism of Stafford and Wingreen (1996) to propose a model for a semiconductor heterostructure pump which operates by photon assisted tunnelling (Platero and Aguado, 2004) in the non-adiabatic regime. The last part of the chapter is devoted to the study of the behavior of an electron pump when introduced in an electrical circuit, assuming that it can be treated as a semiclassical device. Most theoretical calculations have dealt so far with the derivation of the pump current, but we argue in section 4.3 that under under some reasonable assumptions the pump, acting as a voltage source, can be characterized by the electromotive force which defines its role in the circuit and the internal resistance. We further show how to calculate these quantities with the scattering matrix of the pump in the limit where coherence effects can be neglected.

4.2 Pump current in asymmetric double quantum wells

Introductory texts to quantum mechanics (see e.g. Cohen-Tannoudji *et al.*, 1977) show how the energy levels of two unequal quantum wells are modified when they are coupled with coupling strength Δ, in the same way as was done to the symmetric structure of Fig. 3.1 (or its tight-binding description in Fig. 3.2). The asymmetry between wells can be characterized by the difference in energy between the ground states of the wells, $\epsilon_0 = E_{02} - E_{01}$, referred to as *internal bias*. The interplay of bias and coupling takes the ground level splitting to $(\Delta^2 + \epsilon_0^2)^{1/2}$. If the coupling is much smaller than the internal bias, the ground states become highly localized in their respective wells. But a current can still be produced if

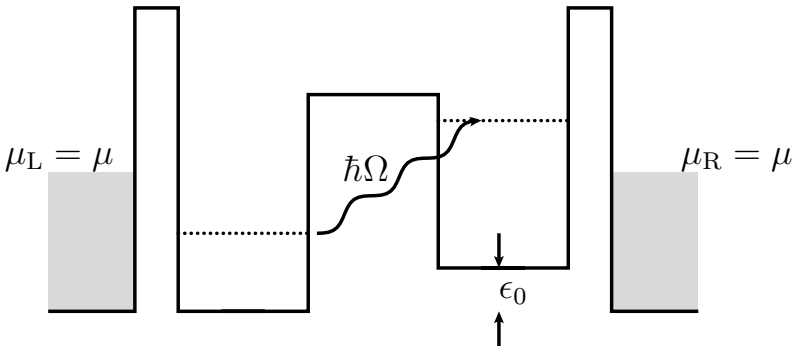

FIGURE 4.1: Double well structure in the asymmetric case. An internal bias ϵ_0 raises the ground level of the right well and thus increases the separation of the ground states. Electrons can however produce a dc current (this time pumped current) if an ac gate voltage is applied.

the structure is driven with a frequency conveniently chosen such that $\hbar\Omega$ equals a multiple of $(\Delta^2 + \epsilon_0^2)^{1/2}$. The physical mechanism of the pumping process considered here should be quite clear from the figure: an electron residing in lead L tunnels through the left barrier to the (modified) ground level E_1 in the left well. It can then absorb one or more quanta of energy $n\hbar\Omega$ and tunnel through the central barrier to the level on the right at E_2; from here, it can finally pass to lead R, therefore producing a current.

To perform the calculation of the pump current with the method of transfer matrices of section 2.3.2, one only needs to modify the band-bottom level of one of the wells, which basically shifts the position of the ground state, and observe the change of the static transmission probability $T(E)$. The Landauer formula Eq. 2.51 for ac transport is of course still valid. Meanwhile, some of the simplifying assumptions of the tight-binding description used in the symmetric case can no longer be applied, and although the derivation of a formula for the current goes along the same lines of Sec. 2.3.4, it needs some appropriate modifications (see Strass *et al.*, 2005).

4.2.1 Tight-binding model

We consider in this section the possibility of changing the static energy levels of the two wells simultaneously, but with an opposite phase. The tight-binding

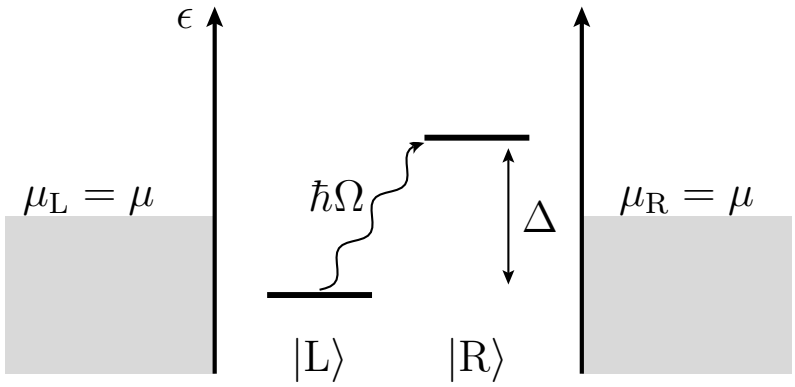

FIGURE 4.2: Tight-binding model of a double quantum well in a pumping setup.

Hamiltonian is then

$$H_{\mathrm{DQD}}(t) = -\frac{\Delta}{2}(c_1^\dagger c_2 + c_2^\dagger c_1) + \frac{\epsilon(t)}{2}(c_1^\dagger c_1 - c_2^\dagger c_2)\ , \tag{4.1}$$

where $\epsilon(t) = \epsilon_0 + V_{\mathrm{ac}}\cos(\Omega t)$ represents the energy *difference* caused by the ac gate voltage and the static bias ϵ_0.

As mentioned above, pumping is expected to show most pronounced features when the frequency meets the resonant condition

$$\hbar\Omega = \frac{(\Delta_0^2 + \epsilon_0^2)^{1/2}}{n} \tag{4.2}$$

for integer n. If, for example, $n = 1$, then electrons at $E = E_1$, absorbing just one photon, acquire the necessary energy to tunnel to the right well and subsequently to lead R. But we can be more precise, since our setup has been designed such that $\epsilon_0 \gg \Delta$, so now we have

$$n\hbar\Omega = (\Delta^2 + \epsilon_0^2)^{1/2} \approx \epsilon_0\ . \tag{4.3}$$

In this regime, the time-dependent part in the Hamiltonian (4.1) dominates over the tunneling term, and this therefore justifies the use of perturbation theory to first order for the calculation of the quasienergies at resonance. Its even possible to obtain a quantitative analytical curve for the current in terms of the Floquet theory of chapter 2, in the HFA. This has been recently done by Strass *et al.* (2005) and, similarly to the analytical results of chapter 3, offers a clear physical interpretation of the numerically exact results.

The main findings of Strass *et al.* are, again, the expressions for the effective tunnel matrix element Δ_{eff} and new electron distribution functions, derived in an

analogous manner as in the case of single-well driving: starting by a new unitary transformation similar to (2.53), an effective Hamiltonian is obtained, to finally arrive at

$$\Delta_{\text{eff}} = (-1)^n J_n \left(\frac{eV_{\text{ac}}}{\hbar\Omega} \right) \Delta \tag{4.4}$$

for the effective coupling, and

$$f_{\text{L/R,eff}}(\epsilon) = \sum_{k=-\infty}^{\infty} J_k^2 \left(\frac{V_{\text{ac}}}{2\hbar\Omega} \right) f_{\text{L/R}} \left(\epsilon + \left[k \mp \frac{n}{2} \right] \hbar\Omega \right) \tag{4.5}$$

for the function that replaces the equilibrium Fermi functions. This functions exhibits steps at $\epsilon = \mu_{\text{L,R}} + (k \mp n/2)\hbar\Omega$ and is constant elsewhere for zero temperature.

4.2.2 Numerical results

To obtain numerical results in the pumping configuration, we start with the double-well structure of Fig. 3.1 to operate in the strongly localized regime of Stafford and Wingreen (1996). With the experience gained in the current suppression comparison of last chapter, we tune the structural parameters so our two independent numerical approaches give better agreement. We choose $\epsilon_0 = 5\Delta$, a value already big enough so that the approximation $\epsilon_0 \gg \Delta$ holds, and accordingly $\hbar\Omega = \epsilon_0 = 5\Delta$ to reach the resonance condition (4.3) for $n = 1$. We note that in the transfer-matrix formalism the whole structure, and in particular the coupling to the leads, is affected by a change in any of its parts, and therefore the new energy splitting differs slightly from the expected $\sqrt{\Delta^2 + \epsilon_0^2}$. The actual level splitting is used then to set the driving frequency. Additionally, and contrary to the two-level tight-binding model, the static transmission is slightly asymmetric around the midpoint energy.

Driving amplitude

In Fig. 4.3 we show the dependence of the pumped current as a function of the driving amplitude V_{ac}. The upper panel (a) shows the results when the two wells are driven with opposite phases, as was considered above. Below the case of a single driven well is presented for comparison. In both cases, the HFA is displayed

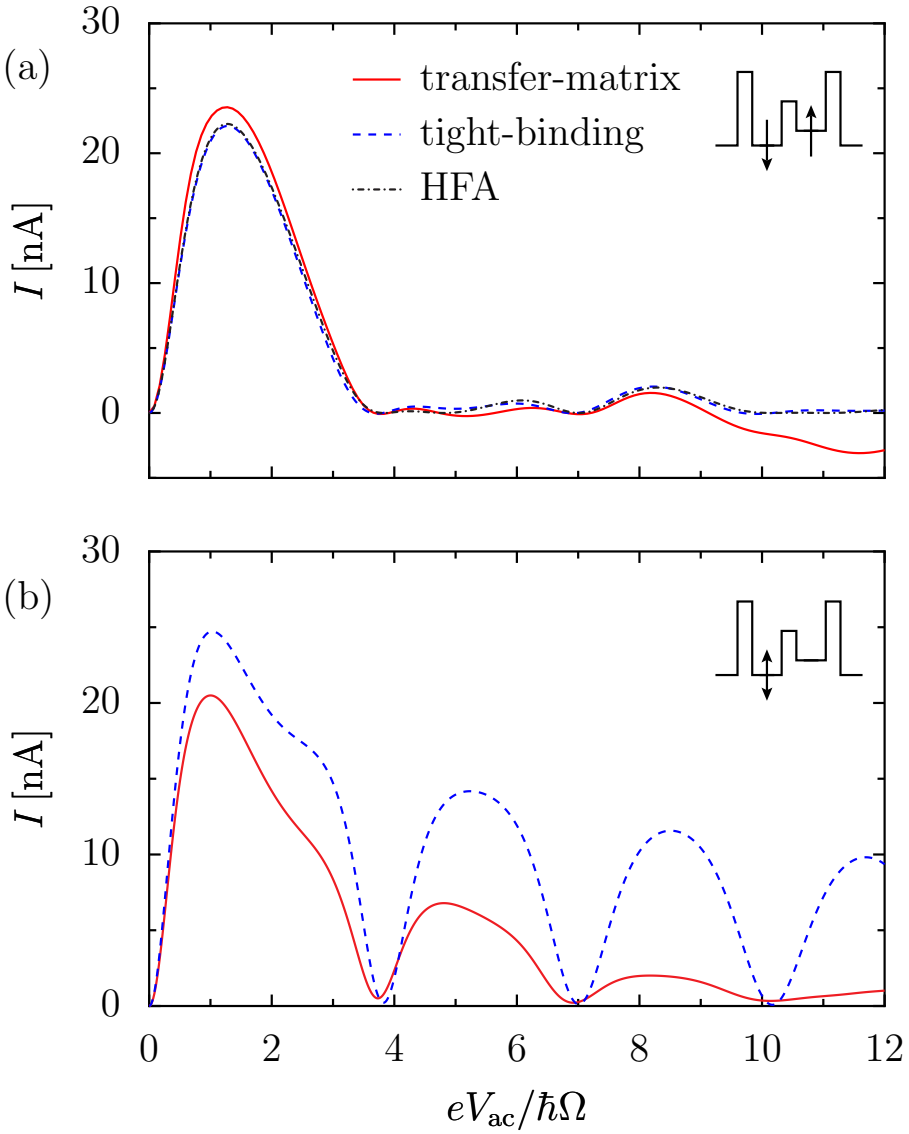

FIGURE 4.3: (a), pump current as a function of the amplitude $eV_{ac}/\hbar\Omega$. (b), pump current for a different driving setup (only one driven well).

as well. When scaled to the driving frequency $\hbar\Omega$, the current is suppressed at the expected values of the quotient $eV_{ac}/\hbar\Omega = 3.812, 7.016, 10.174, \ldots$, i.e. where the Bessel function of first order J_1 vanishes, since we chose $n = 1$ in Eq. (4.3).

We have chosen two different set of parameters in Fig. 4.3: for panel (a) the outer and the center barriers are respectively $d_{L,R} = 3$ and $d_C = 7$ nm wide, while the wells have been *stretched* to 20 nm so that dc levels lie closer in energy; with heights of $V_{L,R} = 140$ and $V_C = 90$ meV, this yields a level splitting (without internal bias) $\Delta = 0.46$ meV, and with the internal bias $\epsilon_0 = 5\Delta$ fixes the driving

frequency as in Eq. (4.3) to $\hbar\Omega = 2.35$ meV.

In panel (b) we have taken the structure of Fig. 3.1 (i.e. $d_{\mathrm{L,R}} = d_C = 5$ nm, well and center barrier 15 nm wide); but now, in order to achieve a better correspondence between our data following the results of Fig. 3.5, with higher outer ($V_{\mathrm{L,R}} = 140$ meV) and central ($V_C = 80$ meV) barriers. Taking again $\epsilon_0 = 5\Delta$ gives $\hbar\Omega = 2.15$ meV.

The agreement of the three different approaches to the calculation of the dc current is in this case highly remarkable; the improvement achieved by the comparison of transfer-matrix and tight-binding calculations of chapter 3 is here clearly demonstrated. There are, however, some deviations from the analytical results for the numerical transfer-matrix: the current remains positive for the numerical tight-binding and HFA calculations, while it takes negative values for higher driving amplitudes in the transfer-matrix results. We ascribe this to the effects of the energy-dependent coupling, not considered in the tight-binding approximation, and the contribution of higher order processes, all of which are "exactly" taken into account in the TM description. The decrease in the pumped current after the first minimum is, according to Stafford and Wingreen, a feature of true photon-assisted tunnelling that distinguishes it from adiabatic electron transfer.

Driving frequency

The HFA predicts (Strass *et al.*, 2005) maxima of the dc pumped current when the driving frequency meets the resonance condition (4.3). Varying the frequency of our transfer-matrix calculations we can observe how the current is enhanced at the values $\hbar\Omega = \epsilon_0/n$, as shown in Fig. 4.4. Displayed here are results for two particular driving amplitudes, together with the tight-binding numerical calculation for the higher driving amplitude $eV_{\mathrm{ac}}/\hbar\Omega = 4$.

We can further check the the non-adiabaticity of the photon-assisted tunneling processes by an exploration of the low-frequency behavior of the pumped current. The results are shown in Fig. 4.5. The double logarithmic plot is a proof of the Ω^2-dependence of the current, clearly different from the $\propto \Omega$ dependence expected if pumping was adiabatic.

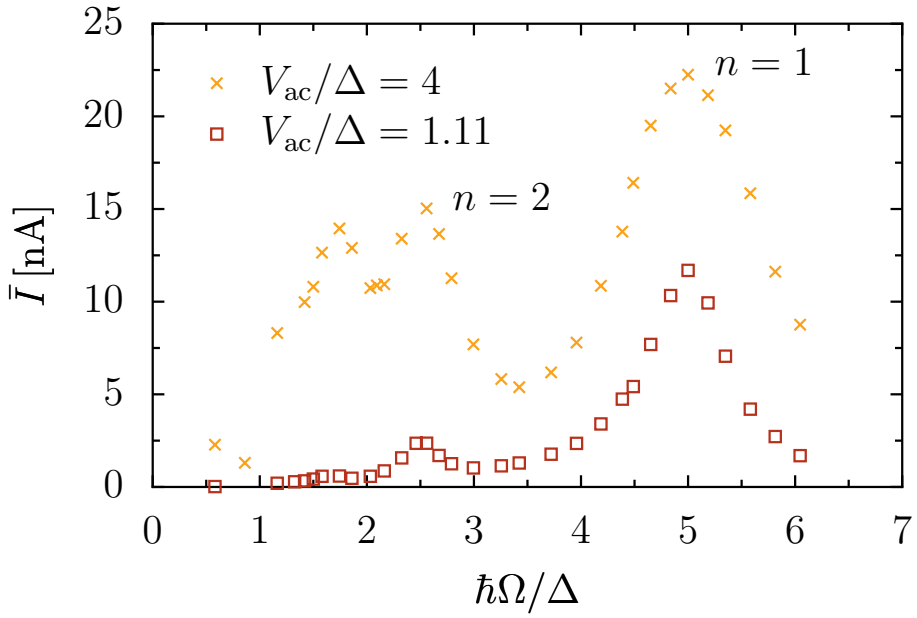

FIGURE 4.4: Pump current as a function of the driving frequency Ω, in units of the splitting Δ. When the resonance condition $\Omega = \epsilon_0/n\hbar$ in the strongly localized regime is fulfilled, the current shows a distinct peak. These peaks are more pronounced for higher driving amplitudes.

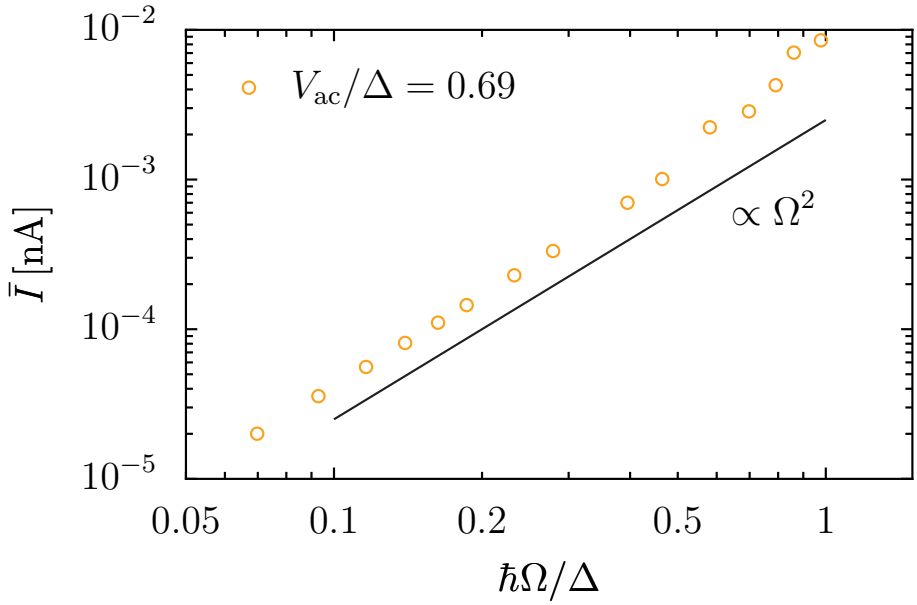

FIGURE 4.5: Going to very low frequencies we can check whether pumping is adiabatic or not; adiabatic pumping implies a $\bar{I} \propto \Omega$ behavior, while in our case it depends quadratically on the driving frequency.

Current-voltage characteristics

Working in the strongly localized regime, again for the first resonance ($\hbar\Omega \approx \epsilon_0 = 5\Delta$ in our case), offers the possibility of studying the current-voltage characteristics of the double-dot pump. The pump current of Fig. 4.6 displays a series of steps of width $2\hbar\Omega = 10\Delta$ as a function of the chemical potential difference $eV = \mu_{\mathrm{L}} - \mu_{\mathrm{R}}$.

To explain these features, the three different situations possible are depicted in Fig. 4.7. When $eV = 0$ we are in the pump configuration studied so far: current is pumped by electrons that travel from the dc ground state on the left well to that of the right one by absorbing one photon.

For positive voltages, the first step appears at $eV = 5\Delta$; that is, when $\mu_{\mathrm{L}} = +\epsilon_0/2$, the energy where —according to Floquet theory— the left well has its first sideband. We must remember that since we chose $\epsilon_0 \gg \Delta$, the level splitting is in effect equal to ϵ_0 (cf. Eq. 4.3), and this places the resonances at $\pm\epsilon_0/2$ symmetrically around the equilibrium situation of $\mu_{\mathrm{L}} = \mu_{\mathrm{R}}$. When this happens electrons can tunnel from lead L to lead R, first through the first sideband of the left dot and, after releasing an energy quantum $\hbar\Omega$, to the sideband at $-\epsilon_0/2$ in the right dot. Therefore, the dc current is enhanced by photon-assisted tunnelling. A similar analysis can be performed for higher steps.

The reverse process takes place for $eV < 0$, which explains the steps at $eV = -5\Delta$. This situation is however not completely symmetric to the one for positive voltage, since in the heterostructure the introduction of the internal bias in the right well has turned the whole structure, and also the static transmission probability, slightly asymmetric: now the resonant peak on the right is higher and wider than that on the left dot, because as it lies somewhat higher in energy due to the internal bias it effectively experiences a lower barrier.

The width of the steps, $2\hbar\Omega$, follows from the fact that the differences of $\mu_{\mathrm{L,R}}$ with respect to their equilibrium value go up and down, respectively, in equal amounts, and they cross the sideband energies at opposite values $\mu_{\mathrm{R}} = -\mu_{\mathrm{L}} = -k\hbar\Omega$.

One could also explain these results by looking at the effective electron distribution of Eq. (4.5) for the HFA. In that case, the interpretation would say that a positive voltage allows static-like processes whenever the two distribution functions differ in energy by the width of one of the steps.

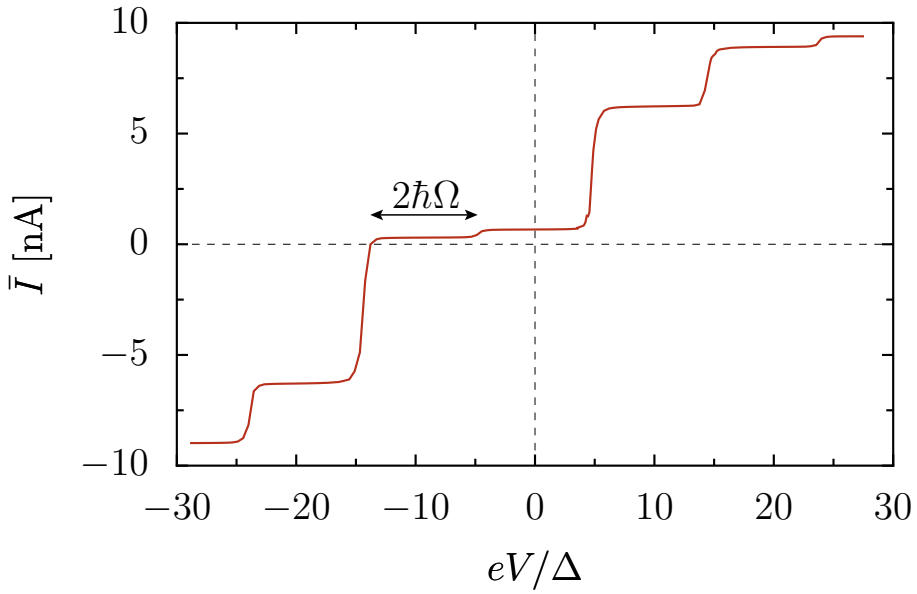

FIGURE 4.6: Photon assisted tunnelling shows steps of width $2\hbar\Omega$ when sweeping in the chemical potential difference $\mu_L - \mu_R$. The driving amplitude is $eV_{ac} = 5\,\text{meV} \simeq 11.1\Delta$.

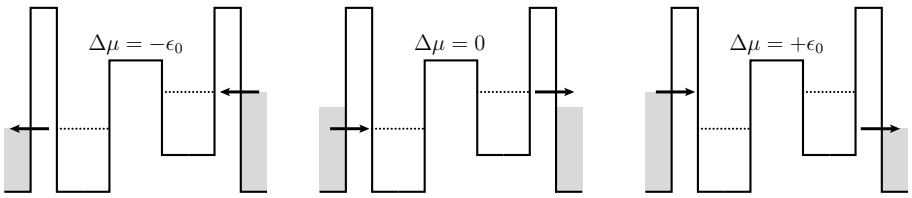

FIGURE 4.7: The three different PAT processes in the electron pump of Fig. 4.1. Current shows steps when $\mu_{L,R} = \mp\epsilon_0/2 \pm n\hbar\Omega$. The dominant process is indicated by the arrows. The rest of the details is given in the text.

4.3 Characterization of an electron pump in the semiclassical regime

In the practical realization of an electron pump, one is likely to be interested in the performance of the pump as a circuit component, something which cannot be predicted from the mere knowledge of the pump current.[1] This creates the need to characterize the electron pump as a battery with a certain *electromotive force* and *internal resistance*. Although the electromotive force can in principle be

[1] The content of this section was published in an slightly different version in Rey and Sols (2004).

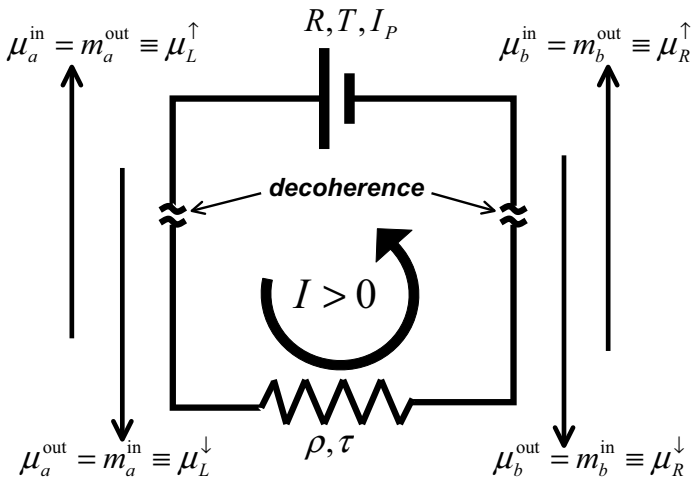

FIGURE 4.8: Schematic representation of an electron pump in series with a generic resistor within a closed circuit where current flows due to the action of the pump.

obtained from the dc bias that exactly cancels the pump current (Switkes *et al.*, 1999; Wagner and Sols, 1999), its derivation within a unified and general scheme seems desirable. On the other hand, there is no obvious ansatz for the calculation of the internal resistance. A potential application of this new class of devices is the generation of current in small closed circuits not attached to broad wires acting as electron reservoirs. Such a setup is schematically depicted in Fig. 4.8. One may also consider a pump in series with a resistor, both within a lead that couples to large reservoirs through ideal contacts, as indicated in Fig. 4.9.

In this section we derive formulae which express the battery parameters in terms of the transmission and reflection probabilities for electrons crossing the pump and the resistor. The scattering theory here presented attempts to play a role for the electromotive force and internal resistance of an electron pump similar to that which the Landauer-Büttiker theory has represented for the conductance of nanostructures. An important difference, however, is that the scenario which we investigate requires a more coarse-grained description if we wish to uniquely characterize the circuit performance of the pump in terms of a small set of parameters. Such an effective self-averaging of the device performance requires the assumption of electron decoherence (i.e. lost of all phase memory) between the pump and the resistor in series. This prevents us from including

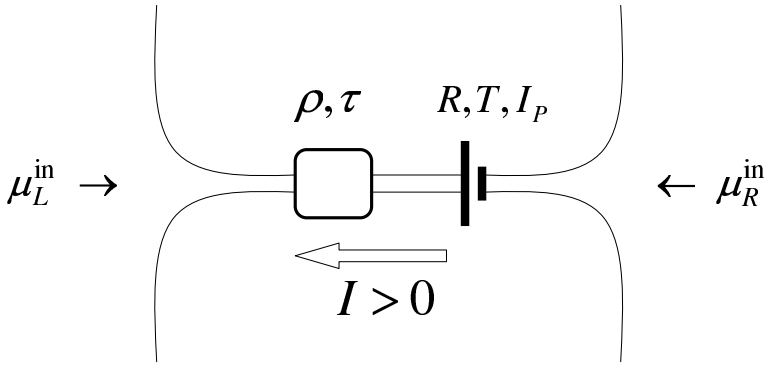

FIGURE 4.9: Electron pump in series with a scattering barrier, both within a multichannel wire that couples through ideal contacts to large electron reservoirs. Both the action of the pump and the difference between the reservoir chemical potentials contribute to drive the current through the wire.

small quantum corrections such as deviations from Ohm's law considered, in adiabatic pumps, in Polianski and Brouwer (2001), and therefore takes our theory into the realm of semiclassical approximations for quantum transport. It might seem a bit odd to obviate quantum effects when pumping as considered here is precisely achieved by another manifestation of the quantum theory. However, unlike Büttiker (1986), we assume that effective phase randomization outside the electron-photon interaction region can be achieved with negligible backscattering. This hypothesis is supported by the fact that a minor distortion of the environment suffices to induce electron dephasing, while a more continued interaction is needed to change the electron energy or direction appreciably (Stern *et al.*, 1990). We find that *reflectionless decoherence* between the circuit elements is still insufficient to permit the characterization in terms of only *two* parameters, and not twice as many as available transverse channels. To achieve a simple and manageable description we must assume that, within the leads, electrons moving in each direction are characterized by a single chemical potential. The adequacy of this assumption, or its replacement by a weaker one within a model of comparable tractability, deserves further study.

For the analysis presented in this Section we will modify slightly the notation used so far. The total current through a two-lead multimode structure in the presence of local ac driving will be written as

$$I = \frac{e}{h} \int \mathrm{d}E_{\mathrm{i}} [f(E_{\mathrm{i}} - \mu_{\mathrm{R}}^{\mathrm{in}}) T_{\mathrm{LR}}(E_{\mathrm{i}}) - f(E_{\mathrm{i}} - \mu_L^{\mathrm{in}}) T_{\mathrm{RL}}(E_{\mathrm{i}})] \tag{4.6}$$

with

$$T_{\mathrm{LR}}(E_{\mathrm{i}}) \equiv \sum_{a\in \mathrm{L}} \sum_{b\in \mathrm{R}} \int \mathrm{d}E_{\mathrm{f}} T^{\mathrm{LR}}_{ab}(E_{\mathrm{f}}, E_{\mathrm{i}}) \; . \tag{4.7}$$

$T^{\mathrm{LR}}_{ab}(E_{\mathrm{f}}, E_{\mathrm{i}})$ represents the probability distribution that an electron incident from the right lead in channel b with energy E_{i} is transmitted into channel a of the left lead with energy E_{f}. For future convenience, we assume $I > 0$ when current flows from right to left. The chemical potentials $\mu^{\mathrm{in}}_L, \mu^{\mathrm{in}}_R$ characterize the population of incoming electrons. These scattering probabilities and chemical potentials include the effective potential which may result from self-consistent dynamic screening (see e.g. Moskalets and Büttiker, 2004), an effect yet to be explored for strictly local pumps.

The pump effect is based on the existence of an asymmetry between the left-to-right and right-to-left transmissions. Thus it is convenient to define:

$$T(E_{\mathrm{i}}) \equiv [T_{\mathrm{LR}}(E_{\mathrm{i}}) + T_{\mathrm{RL}}(E_{\mathrm{i}})]/2 \tag{4.8}$$

$$\delta T(E_{\mathrm{i}}) \equiv T_{\mathrm{LR}}(E_{\mathrm{i}}) - T_{\mathrm{RL}}(E_{\mathrm{i}}) \; . \tag{4.9}$$

If we linearize $f(E - \mu^{\mathrm{in}}_{\mathrm{L,R}})$ around a common reference chemical potential μ_0, we may write the total current of Eq. (4.6) as the sum of a bias and a pump contribution (Pedersen and Büttiker, 1998)

$$I = I_{\mathrm{B}} + I_{\mathrm{P}} \tag{4.10}$$

$$I_{\mathrm{B}} \equiv \frac{e}{h} \Delta\mu^{\mathrm{in}} \int \mathrm{d}E_{\mathrm{i}} [-f'(E_{\mathrm{i}} - \mu_0)] T(E_{\mathrm{i}}) \tag{4.11}$$

$$I_{\mathrm{P}} \equiv \frac{e}{h} \int \mathrm{d}E_{\mathrm{i}} f(E_{\mathrm{i}} - \mu_0) \delta T(E_{\mathrm{i}}) \; , \tag{4.12}$$

with $\Delta\mu^{\mathrm{in}} \equiv \mu^{\mathrm{in}}_{\mathrm{R}} - \mu^{\mathrm{in}}_{\mathrm{L}}$. Hereafter, we take $\mu_0 \equiv 0$, although we note that I_{P}, unlike I_{B}, does in general depend on μ_0.

Let us focus on the current flow in a given channel a on e.g. lead L. For convenience, we define $\tilde{I}_\alpha \equiv (h/e) I_\alpha$ for all future current contributions. To achieve a better perspective, we momentarily abandon the assumption that the chemical potential is channel independent. The total current through channel $a \in \mathrm{L}$ can then be written:

$$\tilde{I}_a = -\mu^{\mathrm{in}}_a + \mu^{\mathrm{out}}_a, \tag{4.13}$$

where μ^{in}_a and μ^{out}_a characterize the population of electrons in L approaching and leaving the pump. We note that even if the *in* population is rigorously thermal, and it can therefore be characterized by a single chemical potential, the *out*

population is generally not. However, one can always find a suitably defined chemical chemical potential μ_a^{out} that reproduces the same current flow (and, in one dimension, the same current density, see Sols and Sánchez-Cañizares, 1999). Like the total current, this *outgoing chemical potential* has a "bias" and a "pump" contribution,

$$\mu_a^{\text{out}} = \mu_a^{\text{out,B}} + \mu_a^{\text{out,P}} \tag{4.14}$$

$$\mu_a^{\text{out,B}} = \sum_b S_{ab}\mu_b^{\text{in}} \tag{4.15}$$

$$\mu_a^{\text{out,P}} = \tilde{I}_{\text{P},a}\ . \tag{4.16}$$

Here, $\tilde{I}_{\text{P},a}$ is the pump current in channel a ($\sum_a \tilde{I}_{P,a} = \tilde{I}_P$). Since the bias contribution depends only on the symmetrized probability (cf. Eq. 4.8), the scattering matrix satisfies the relation $S_{ab} = S_{ba}$. On the other hand, unitarity conditions requires $\sum_b S_{ab} = 1$. The term $\mu_a^{\text{out,P}}$ accounts for the excess (or defect) of electrons generated by the pump. It reflects the fact that an operating battery creates a *population imbalance* which ultimately drives the current through the circuit.

4.3.1 Closed circuit configuration

Assume that, in series with the pump, we introduce a resistor which is also characterized in terms of its scattering probabilities. The resulting circuit is schematically depicted in Fig. 4.8. As the resistor is a passive element, its flow equations do not include a pump term. We write

$$\tilde{I}_a = m_a^{\text{in}} - \sum_b \sigma_{ab} m_b^{\text{in}} \equiv m_a^{\text{in}} - m_a^{\text{out}}, \tag{4.17}$$

where $m^{\text{in}}, m_a^{\text{out}}$ are the chemical potential for the electrons approaching and leaving the resistor, and $\{\sigma_{ab}\}$ are the scattering probabilities by the resistor, which obey $\sigma_{ab} = \sigma_{ba}$ and $\sum_a \sigma_{ab} = 1$. The sign convention in Eq. (4.17) is different from that used in the pump equations because counterclockwise current is taken to be positive (see Fig. 4.8. Now we note that the *out* population of the pump is the *in* population of the resistor, and viceversa. We seal this equivalence by establishing a common notation. For $a \in \text{L}$ we write

$$\mu_a^{\text{in}} = m_a^{\text{out}} \equiv \mu_{\text{L},a}^{\uparrow} \tag{4.18}$$

$$\mu_a^{\text{out}} = m_a^{\text{in}} \equiv \mu_{\text{L},a}^{\downarrow}, \tag{4.19}$$

and similarly for $a \in \mathrm{R}$. The vertical arrows refer to the direction of movement within the convention of Fig. 4.8.

Although a solution of the flow equations that would permit us to predict the total current in terms of $\{I_{\mathrm{P},a}, S_{ab}, \sigma_{ab}\}$ is formally possible, our real goal is the characterization of the pump in terms of two parameters. To achieve this, we have to introduce the simplifying assumption that electrons flowing in a given direction within a lead are all characterized by the same chemical potential. We express it as

$$\mu_{\mathrm{L},a}^{\uparrow\downarrow} = \mu_{\mathrm{L}}^{\uparrow\downarrow} \qquad \mu_{\mathrm{R},a}^{\uparrow\downarrow} = \mu_{\mathrm{R}}^{\uparrow\downarrow} \qquad \forall a \in \mathrm{L}, \mathrm{R}. \tag{4.20}$$

Hereafter we differentiate between reflection and transmission probabilities:

$$S_{ab} \to R_{ab}, T_{ab} \qquad \sigma_{ab} \to \rho_{ab}, \tau_{ab}. \tag{4.21}$$

We further introduce the notation

$$R_a \equiv \sum_b R_{ab} \qquad T_a \equiv \sum_b T_{ab} \qquad (R_a + T_a = 1)\ , \tag{4.22}$$

$$R \equiv \sum_a R_a \qquad T \equiv \sum_a T_a \qquad (R + T = N)\ , \tag{4.23}$$

where N is the number of transverse channels. The resistor parameters $\rho_a, \tau_a, \rho, \tau$ are defined analogously. We introduce an average *pump chemical potential*

$$\mu_{\mathrm{P}} \equiv \sum_a \mu_a^{\mathrm{out,P}} / N = \tilde{I}_{\mathrm{P}} / N \tag{4.24}$$

so that the total current can now be written

$$\tilde{I} = N(\mu_{\mathrm{L}}^{\downarrow} - \mu_{\mathrm{L}}^{\uparrow}) = N(\mu_{\mathrm{R}}^{\uparrow} - \mu_{\mathrm{R}}^{\downarrow})\ . \tag{4.25}$$

These four chemical potential are not independent but are rather related by the flow equations

$$\begin{aligned} N\mu_{\mathrm{L}}^{\downarrow} &= R\mu_{\mathrm{L}}^{\uparrow} + T\mu_{\mathrm{R}}^{\uparrow} + N\mu_{\mathrm{R}}\ , \\ N\mu_{\mathrm{L}}^{\uparrow} &= \rho\mu_{\mathrm{L}}^{\downarrow} + \tau\mu_{\mathrm{R}}^{\downarrow}\ , \\ N\mu_{\mathrm{R}}^{\downarrow} &= T\mu_{\mathrm{L}}^{\uparrow} + R\mu_{\mathrm{R}}^{\uparrow} - N\mu_{\mathrm{P}}\ , \\ N\mu_{\mathrm{R}}^{\uparrow} &= \tau\mu_{\mathrm{L}}^{\downarrow} + \rho\mu_{\mathrm{R}}^{\downarrow}\ . \end{aligned} \tag{4.26}$$

which are physically transparent. The different signs carried by the pump contribution $N\mu_{\mathrm{P}}$ in two of the equations above express the fact that, when $\mu_{\mathrm{P}} > 0$,

there is an excess of outgoing electrons on the left of the pump and a corresponding defect of outgoing electrons on the right. When Eqs. (4.26) are introduced into Eq. (4.25), we obtain for the total current

$$\begin{aligned} \tilde{I} &= -T\Delta\mu^{\uparrow} + N\mu_{\mathrm{P}} \; ; && (4.27) \\ &= \tau\Delta\mu^{\downarrow} \; , && (4.28) \end{aligned}$$

where the chemical potential differences $\Delta\mu^{\uparrow\downarrow} \equiv \mu_L^{\uparrow\downarrow} - \mu_R^{\uparrow\downarrow}$ satisfy

$$\begin{aligned} N\Delta\mu^{\downarrow} &= (R-T)\Delta\mu^{\uparrow} + 2N\mu_{\mathrm{P}} \; ; && (4.29) \\ N\Delta\mu^{\uparrow} &= (\rho-\tau)\Delta\mu^{\downarrow} \; . && (4.30) \end{aligned}$$

We may solve now for $\Delta\mu^{\uparrow\downarrow}$ in Eqs. (4.29) and (4.30) and introduce the solutions in either (4.27) or (4.28) to obtain

$$\tilde{I} = \frac{(N/T)I_{\mathrm{P}}}{\rho/\tau + R/T} \; . \tag{4.31}$$

Calculating the electromotive force $\mathcal{V}_{\mathrm{emf}}$ and the internal resistance $\mathcal{R}_{\mathrm{i}}$ amounts to finding a relation

$$I = \frac{\mathcal{V}_{\mathrm{emf}}}{\mathcal{R} + \mathcal{R}_{\mathrm{i}}} \; , \tag{4.32}$$

where $\mathcal{R}$ is a suitably defined resistance for the resistor. Comparison of Eqs. (4.31) and (4.32) uniquely leads to the result

$$\begin{aligned} \mathcal{V}_{\mathrm{emf}} &= \frac{h}{e^2}\frac{I_{\mathrm{P}}}{T} && (4.33) \\ \mathcal{R}_{\mathrm{i}} &= \frac{h}{Ne^2}\frac{R}{T} \; , && (4.34) \end{aligned}$$

provided that

$$\mathcal{R} = \frac{h}{Ne^2}\frac{\rho}{\tau} \; . \tag{4.35}$$

The prefactors have been chosen to make $\mathcal{V}_{\mathrm{emf}}$ an intensive quantity, while the resistances $\mathcal{R}, \mathcal{R}_{\mathrm{i}}$ vary as $\sim N^{-1}$ for $N \to \infty$.

Application to the pipeline model We may apply these results for to the analytically solvable pipeline model, which assumes that transmission takes place only within a single pair of channels (Wagner and Sols, 1999). This can be expressed as:

$$T_{ab}^{LR}(E_{\mathrm{f}}, E_{\mathrm{i}}) = J\delta_{ab}\delta(E_{\mathrm{f}}^z - E_2)\delta(E_{\mathrm{i}}^z - E_1) \; . \tag{4.36}$$

Here, E_α^z ($\alpha = \mathrm{i}, \mathrm{f}$) is the energy in the direction perpendicular to the planar structure and $(E_2 - E_1)/\hbar = \omega > 0$ is the driving frequency. The other scattering probabilities are determined by time-reversal symmetry in the presence of coherent ac driving ($T_{ab}^{\mathrm{RL}}(E', E) = T_{ba}^{\mathrm{LR}}(E, E')$) and unitarity. For three dimensions, the single pipeline model yields $T = DJ$, where $D = Am/2\pi\hbar^2$ is the two-dimensional transverse density of states, and A is the interface area. Preservation of unitarity requires $DJ < N$. The total pump current is

$$I_{\mathrm{P}} = eDJ\Omega/2\pi \,, \tag{4.37}$$

so we interpret eDJ as the pumped charge per cycle. For the circuit parameters we obtain

$$\mathcal{V}_{\mathrm{emf}} = \hbar\omega/e \,; \tag{4.38}$$

$$\mathcal{R}_{\mathrm{i}} = \frac{h}{Ne^2}\frac{N - DJ}{DJ} \,. \tag{4.39}$$

The result that the electromotive force is just $\hbar\Omega/e$, independently of the transmittivity J, is remarkable if one looks at the structure of the Eqs. (4.12), (4.22), (4.23) and (4.33), but could have been expected from the notion that the pipeline model allows only for an energy gain $\hbar\Omega$ as the electron is pumped from right to left, regardless of the total electron flow. We readily conclude that, in a more general pump structure, $\mathcal{V}_{\mathrm{emf}} \sim \hbar\Omega/e$, in agreement with Switkes *et al.* (1999) and Wagner and Sols (1999). By contrast, the internal resistance is very sensitive to the transmittivity of the pump. In particular, we note that $\mathcal{R}_{\mathrm{i}} \to \infty$ when $J \to 0$.

4.3.2 Open circuit configuration

We now turn our attention to an open setup where the pump and resistor stay in series within a lead coupled through ideal contacts to broad electron reservoirs. As indicated in Fig. 4.9, the chemical potentials in the reservoirs characterize the population of the incoming electrons. Hence, we refer to them also as $\mu_{\mathrm{L,R}}^{\mathrm{in}}$. One may perform an analysis similar to that described for the closed geometry of Fig. 4.8. After some algebra, one obtains

$$I = (e/h)T'(e\mathcal{V}_{\mathrm{emf}} + \Delta\mu^{\mathrm{in}}) \,, \tag{4.40}$$

where $\mathcal{V}_{\mathrm{emf}}$ is given by Eq. (4.33), and

$$T' \equiv \frac{T\tau/N}{1 - R\rho/N^2} \tag{4.41}$$

is the the average transmission through the compound structure formed by the pump plus the resistor.

Interestingly, Eq. (4.40) can also be written as

$$I = \frac{\mathcal{V}_{\rm emf} + \Delta\mu^{\rm in}/e}{(h/Ne^2) + \mathcal{R} + \mathcal{R}_{\rm i}} \,, \tag{4.42}$$

where the resistances $\mathcal{R}$ and $\mathcal{R}_{\rm i}$ are given by Eqs. (4.35) and (4.34), respectively. Thus we see that, in an open geometry, the pump electromotive force adds to the voltage bias generated by the potential difference between the two electron reservoirs. This confirms the intuitive expectation that $\mathcal{V}_{\rm emf}$ can be obtained from the the voltage difference $\Delta\mu^{\rm in}$ needed to cancel the pump current (Switkes *et al.*, 1999; Wagner and Sols, 1999).

A striking difference between Eqs. (4.32) and (4.42) is the role of the contact resistance h/Ne^2, which is absent in the case of a closed structure. Comparison of the underlying models suggests that the contact resistance disappears under the assumption that the flow of outgoing electrons on the left of the resistor-pump structure of the open circuit setup is identified with the flow of incoming electrons from the right, and equivalently for electrons moving in the opposite direction. We conclude that, within a closed circuit of uniform width, there is no natural lower limit to the resistance that the electron current must face as it is generated by the electron pump. This result appears reasonable if one notes that contact resistances along the circuit are generated by narrow-wide contacts where the width of the wire (and thus the number of available electron channels) changes (Imry, 1997), a feature which doesn't apply to the open configuration.[2]

The denominators of Eqs. (4.32) and (4.42) suggest that the resistances which we have introduced should be additive. Unfortunately, the ratios R/T and ρ/τ cannot be guaranteed to be additive in general. That is possible only in one dimension, where the ration R/T is known to be additive for barriers compounded incoherently (Datta, 1995) or, for multichannel wires, in the particular case where the scattering probabilities are independent of the channel index ($R_{ab} = R/N^2$,

[2]This question is directly related to the famous *two- vs. four-terminal conductance* dispute of section 2.1. It has been experimentally —and definitely— answered by de Picciotto *et al.* (2001) in recent times: it is the contacts who give a ballistic wire its resistance, and this vanishes when the current enters and leaves the sample through two terminals different from the ones through which the voltage drop is measured.

$T_{ab} = T/N^2$, and similarly for ρ_{ab}, τ_{ab}). In such a case, the assumption of a common chemical potential for all incoming electrons ($\mu_a^{\text{in}} = \mu_{\text{L,R}}^{\text{in}}$ for all $a \in \text{L,R}$) automatically guarantees an outgoing population with a common chemical for all outgoing electrons ($\mu_b^{\text{out}} = \mu_{\text{L,R}}^{\text{out}}$ for any $b \in \text{L,R}$). Within that scheme, the assumption of a common chemical potential for all electrons moving in a given direction [see Eq. 4.20] is internally consistent in the sense that a scenario may be conceived where the outgoing population from a barrier or pump is guaranteed to be a suitable incoming population for the following obstacle. Interestingly, it is also in the channel-independent scattering limit where the resistance defined by Büttiker *et al.* (1985),

$$\mathcal{R} \equiv G^{-1} = \frac{\pi\hbar}{e^2}\left(\sum_i T_i\right)^{-1} \frac{\sum_i (1 + R_i - T_i) v_i^{-1}}{2\sum_i v_i^{-1}} \tag{4.43}$$

becomes additive and equivalent to the resistance defined in Eq. (4.35).

On closer inspection, one realizes that the assumption of channel independent scattering is hard to justify within an independent electron picture, where no naturally additive resistance can be defined for multichannel wires without invoking impurity averaging. In particular, such a hypothesis is not satisfied by the pipeline model invoked above, since its transmission depends on the perpendicular energy. We conclude that the question of the definition of an electron pump internal resistance is directly connected to the discussion on the additivity of resistances in multichannel wires. As long as this fundamental issue is not satisfactorily resolved, the transport equations (4.32) and (4.42), together with Eqs. (4.26), which we have derived, will have to be viewed as approximations obtained from a reasonable and appealing scheme.

5 ac-cooling of nanoscale conductors

5.1 Introduction

It is a well-known fact that the flow of charge carriers is accompanied by the transfer of energy. The development of a temperature difference when a current is driven through a metal, named the *Seebeck effect* after its discoverer, and its inverse, the appearance of a voltage difference when a temperature gradient is maintained between its extremes, or *Peltier effect*, are based on this fact. Since their discovery in the 19th century it has led to many technological applications, from thermocouples to thermal diodes and thermoelectric generators. They have also contributed to the understanding of the properties of the solid state. The ongoing miniaturization of electronic devices has opened a new field for the study of the interplay of thermal and electric effects, since in small systems the currents which heat up the structure can damage the performance of the device and must therefore be taken into account.

In this chapter we describe how the dc current between two unbiased leads could be used to pump heat from one reservoir to the other by means of a driven asymmetric semiconductor heterostructure. We first discuss the definition of heat production for ac driven systems and, subsequently, show how to derive the correct formula by extending the Floquet-Green scattering formalism of section 2.3.3. This gives a sound basis to the *counting arguments* of energy balance between the reservoirs. In this derivation the role of phonons is not taken into account. We assume that the thermal conductivity of the lattice is much smaller than electronic thermal conductivity, a result that usually holds for moderately doped semiconductors at sufficiently low temperatures (Mahan *et al.*, 1997).

It is also discussed how an appropriate choice of parameters can yield a *negative* heat production, i.e. a cooling of one of the reservoirs. This is in itself not such a novel idea in view of traditional thermoelectric effect. The novelty of our calcu-

lations is that the ac driving can be used to select the sign of the heat production and, most importantly, that cooling can be achieved in conditions of no net flow of electrons between the leads. The idea is to replace *hot* electrons, i.e. electrons with an energy above the chemical potential of the lead, with *cold* electrons from the other lead of the structure. We implement the resulting expressions with the transfer-matrix method to perform numerical calculations.

5.2 General remarks on heat transfer

Classical thermodynamics describes the production of heat due to a change in internal energy and particle number (volume is assumed to be fixed) as

$$\mathrm{d}Q = T\mathrm{d}S = \mathrm{d}U - \mu\mathrm{d}N \,. \tag{5.1}$$

In a semiconductor structure, heat is produced by the exchange of carriers. Thus, entropy is increased when electrons arrive at states above the chemical potential μ, or leave states below μ. Conversely, entropy is reduced when hot electrons (i.e. with energy above μ) leave, or cold electrons arrive.

In solids, the first estimates of thermal currents were calculated with the Drude theory for conduction in metals. It successfully accounted for the ratio of thermal to electrical conductivity, κ/σ (the empirical Wiedemann-Franz law), but estimated in about two orders of magnitudde the *thermopower* or coefficient of the thermoelectric (Seebeck) effect.

Semiclassical band-theories of conduction removed many of the inconsistencies of the Drude model (see e.g. Ashcroft and Mermin, 1976). Electrical and energy currents are expressed by averages over the distribution of the electrons, weighted respectively by the charge ($-e$) or the energy transported per electron ($\epsilon - \mu$). Assuming a linear relation between the currents $\mathbf{J}$ and the *forces* $\mathbf{X}$ that create them (electric fields, and temperature or chemical potential gradients) of the form $\mathbf{J}_i = \sum_j \mathsf{Z}^{(ij)}\mathbf{X}_j$, all electrical and thermal conductivities and thermoelectric coefficients can be found with the coefficients $\mathsf{Z}^{(ij)}$.

5.3 Some thermodynamic identities

Considering cooling from a purely thermodynamical point of view offers some insight on the physical process involved. We consider a noninteracting gas of Fermi particles with well defined chemical potential. Our goal is to calculate the variations of entropy and temperature of the system when it exchanges particles with another reservoir. We note here some useful thermodynamical relations. First, we note

$$\left(\frac{\partial U}{\partial N}\right)_T = \mu + T\left(\frac{\partial S}{\partial N}\right)_T = \mu - T\left(\frac{\partial \mu}{\partial T}\right)_n , \tag{5.2}$$

where $n \equiv N/V$ is the particle density and Maxwell relations have been used. Now, noting the cyclic property

$$\left(\frac{\partial T}{\partial N}\right)_U = -\left(\frac{\partial T}{\partial U}\right)_N \left(\frac{\partial U}{\partial N}\right)_T , \tag{5.3}$$

we may write

$$\left(\frac{\partial T}{\partial N}\right)_U = \frac{1}{C_v}\left[\mu - T\left(\frac{\partial \mu}{\partial T}\right)_n\right] . \tag{5.4}$$

where $(\partial T/\partial U)_N = 1/C_v$ is the inverse of the volume heat capacity. Thus we can write the temperature variation in the form

$$\begin{aligned} \mathrm{d}T &= \left(\frac{\partial T}{\partial U}\right)_N \mathrm{d}U + \left(\frac{\partial T}{\partial N}\right)_U \mathrm{d}N \\ &= \frac{1}{C_v}\left\{\mathrm{d}U - \left[\mu - T\left(\frac{\partial \mu}{\partial T}\right)_n\right]\mathrm{d}N\right\} . \end{aligned} \tag{5.5}$$

For a noninteracting gas we can assume $\mathrm{d}U = \epsilon \mathrm{d}N$, where ϵ is the energy of the electron state involved in a given elementary process. Thus, Eq. (5.5) becomes

$$\mathrm{d}T = \frac{1}{C_v}\left[\epsilon - \mu + T\left(\frac{\partial \mu}{\partial T}\right)_n\right]\mathrm{d}N , \tag{5.6}$$

or

$$\mathrm{d}T = \frac{1}{C_v}[\epsilon - \sigma(T)]\mathrm{d}N \qquad \text{with} \qquad \sigma(T) \equiv \mu(T) - T\left(\frac{\partial \mu}{\partial T}\right)_n . \tag{5.7}$$

The meaning of this new quantity $\sigma(T)$ can be elucidated by the direct comparison of the entropy and temperature variations, namely

$$\mathrm{d}S = \frac{\epsilon - \mu(T)}{T}\mathrm{d}N \qquad vs. \qquad \mathrm{d}T = \frac{\epsilon - \sigma(T)}{C_v}\mathrm{d}N . \tag{5.8}$$

This shows that *entropy and temperature variations are not necessarily proportional to each other*. From the low-temperature Sommerfeld expansion of $\mu(T)$,

$$\mu(T) = \epsilon_{\mathrm{F}} - \frac{\pi^2}{12}\frac{(k_{\mathrm{B}}T)^2}{\epsilon_{\mathrm{F}}} \tag{5.9}$$

so that

$$\sigma(T) = \epsilon_{\mathrm{F}} + \frac{\pi^2}{12}\frac{(k_{\mathrm{B}}T)^2}{\epsilon_{\mathrm{F}}}\,, \tag{5.10}$$

The fact that $\mu(T) < \sigma(T)$ suggests that an arriving electron increases entropy more easily than temperature.

For convenience we refer to a given scattering process by the generic name λ. Summing over all scattering process, we can write Eq. (5.8) as

$$\begin{aligned}\frac{\partial S}{\partial t} &= \sum_{\lambda}\frac{\epsilon_\lambda - \mu(T)}{C_v}\Delta N_\lambda \Gamma_\lambda \\ \frac{\partial T}{\partial t} &= \sum_{\lambda}\frac{\epsilon_\lambda - \sigma(T)}{T}\Delta N_\lambda \Gamma_\lambda\,.\end{aligned} \tag{5.11}$$

where Γ_λ is the probability per unit time that a certain scattering process takes place, and $\Delta N_\lambda = \pm 1$ is the number variation in the electrode under consideration. For systems of charged carriers, particle accumulation in a given electrode is undesirable because of the high energy of Coulomb repulsion. For such systems, the most interesting situation is that of $\dot{N} = \sum_\lambda \Delta N_\lambda \Gamma_\lambda = 0$. In this case we can identify entropy increase with temperature increase provided a proper summation over all scattering processes is performed. Thus, if electrons leave the system at energies above the chemical potential and are replaced by electrons below it, one can effectively cool the system at zero net electrical current. We base our cooling proposal on this idea.

5.4 Cooling in mesoscopic systems

The cooling of systems by means of electrical currents has been used in a number of recent experimental proposals (Manninen *et al.*, 1999; Clark *et al.*, 2005). We emphasize that in general all these approaches have treated the case of cooling by transfer of heat from the hot to the cold part of the system. This is in high contrast to the idea of *heat pumping*, or transfer of heat against a temperature difference, which we will find in ac driven nanostructures.

5.4.1 Experiments

Many details about the present state of cooling through phonon transport can be found in the recent review of Cahill *et al.* (2003). Phonons are the main subject of interest because in insulators it represents the most important contribution to the heat conductivity. Usually this research is motivated by the increasing interest in the dissipation of heat in field-effect transistors, required by the miniaturization of the devices.

Solid-state microscopic refrigerators built on junctions of a normal metal and a superconductor with an insulator spacer, have been investigated recently (Manninen *et al.*, 1999; Clark *et al.*, 2005). A bulk system is cooled by the emission of hot electrons to a superconductor. The absence of free states below the superconductor gap prevents cold electrons (i.e. below the chemical potential) to leave the metal, resulting in an overall cooling. These systems offer interesting prospects for cooling at very low temperatures (in the sub-Kelvin range), and at moderate cooling powers ($\sim 1 - 100$ pW), two requirements that have to be fulfilled for possible applications: analytical instruments for radiation detectors, sensitive low-temperature detectors, and refrigerators (see Pekola, 2005; Giazotto *et al.*, 2006, for details).

5.4.2 Theory

Heat transfer theories in mesoscopic systems have been centered in the calculation of the coefficient of performance in molecular heat pumps (Segal and Nitzan, 2006) and classical ratchets (Parrondo and de Cisneros, 2002), while the interest in semiconductor quantum dots has been generally put on obtaining the transport coefficients, either using a scattering formalism (Sivan and Imry, 1986; Guttman *et al.*, 1995, 1996) or a rate equation approach for a dot in the Coulomb blockade (Beenakker and Staring, 1992). The formulation of Sivan and Imry shows that the formula for heat transfer is a natural generalization of the Landauer idea, and can be derived from general thermodynamical and scattering arguments. They find that the energy U transferred by electrons is

$$U = \theta J_S = \frac{1}{h} \int_0^\infty \mathrm{d}\epsilon \sum_{i=1}^{N} T_i(\epsilon - \epsilon_i^T)(\epsilon - \mu) \times [f_\mathrm{L}(\epsilon) - f_\mathrm{R}(\epsilon)] \,, \tag{5.12}$$

where θ is the temperature and J_S the entropy current. This formula resembles Landauer's Eq. (2.3), but the charge $-e$ has been substituted by the energy carried by each electron, i.e. $(\epsilon - \mu)$.

The link between classical heat transfer expressions and a scattering formalism for phonons has been provided by Blencowe (2004).[1]

5.5 Heat production in the presence of ac driving

The introduction of an ac signal changes the static picture that has been common to all theoretical and experimental research on heat transfer so far. When, in addition to chemical potential or temperature imbalances, an external source of energy is present in the system, the production of heat is affected as happened with the electrical current in the previous chapters of this work. Prior to us, work has been done on the adiabatic transfer of electrons against a negative temperature in an adiabatically driven quantum well (Humphrey *et al.*, 2002). The motivation behind is the search of quantum engines with efficiencies as close as possible to those predicted by Carnot. A possible implementation of this scheme is an adiabatically driven quantum well coupled to two leads at different temperatures, which can be analyzed with the scattering formulas of Sivan and Imry (1986) of above. We describe our proposal for achieving a similar effect with a driving that operates in the opposite limit of high frequencies. These formulas will be the basis of the numerical calculations presented in section 5.6.

5.5.1 Finite frequencies

Adiabatic heat transfer mechanism is by its construction restricted to very slow heat pumping. It neither can make any statement about the general case of finite driving frequencies. In the following we show how to define the heat production[2]

[1] The naturally arising issue of whether heat transport is quantized; i.e. whether a quantum of thermal conductance exists, analogously to the quantum of electrical conductance, was elucidated in recent experiment by Schwab *et al.* (2000), who found the thermal current in a quantum electromechanical system (suspended insulating nanowires) at very low temperatures T to be quantized in units of $\pi^2 k_B^2 T/3h$. Since these data were taken on insulating Si, this value refers to the quantum of *phonon* thermal conduction.

[2] We avoid such terms as entropy or heat current as a given microscopic electron transfer process induces different entropy changes in the exit and arrival leads.

in the leads when a (dc) electron current flows in the presence of an ac potential far from the adiabatic limit. The notation we will adopt here is as follows: the heat produced in lead $\ell = \mathrm{L}, \mathrm{R}$ is

$$\dot{Q}_\ell = \sum_q (\epsilon_q - \mu_\ell)\dot{n}_{\ell q} = \sum_q \epsilon_q \dot{n}_{\ell q} - \frac{\mu_\ell}{e} I \tag{5.13}$$

$$= \dot{E}_\ell - \mu_\ell \dot{N}_\ell \, . \tag{5.14}$$

Here, $\dot{E}_\ell$ represents the energy current and $\dot{N}_\ell$ the particle current. In this formula, the energy transfer processes are referred to the corresponding local chemical potential.

In the first place we present here a derivation of the heat production formulas in a scattering, Landauer-like formalism. Our *counting arguments* of considering the various processes that take place here and writing the respective contributions to the total energy balance are then derived within a Green function approach, as it is done for the electrical current (see section 2.3.3).

There are three different processes contributing to the energy transfer which have to be included in the total $\dot{E}_\ell$ formula: the electrons leaving and arriving to the lead, and the electrons reflected which do not actually traverse the structure, but which do exchange one or more energy quanta with the ac driving and therefore must be explicitly considered. For convenience we consider in the following the right lead only:

- Electrons transmitted R $\to$ L: they leave lead R with energy ϵ *before* they interact with the driving. Their contribution to the total energy balance, $-\sum_k \epsilon T^{(k)}_{\mathrm{LR}}(\epsilon) f_{\mathrm{R}}(\epsilon)$, is independent of sideband index k.

- Electrons transmitted L $\to$ R: these leave lead L with an initial energy ϵ, but reach lead R with $\epsilon + k\hbar\Omega$. This time the term does depend on index k: $(\epsilon + k\hbar\Omega) T^{(k)}_{\mathrm{RL}}(\epsilon) f_{\mathrm{L}}(\epsilon)$.

- Reflected electrons R $\to$ R: they start with energy ϵ but, scattered by the driven structure, go back to lead R with $\epsilon + k\hbar\Omega$, so that their total contribution is just proportional to the energy *difference* $k\hbar\Omega$; the corresponding energy term is therefore $k\hbar\Omega R^{(k)}_{\mathrm{RR}}(\epsilon) f_{\mathrm{R}}(\epsilon)$.

The total energy balance is then written as

$$\dot{E}_{\mathrm{R}} = \frac{1}{h}\sum_k \int \mathrm{d}\epsilon[\,-\epsilon T^{(k)}_{\mathrm{LR}}(\epsilon) f_{\mathrm{R}}(\epsilon) + (\epsilon + k\hbar\Omega) T^{(k)}_{\mathrm{RL}}(\epsilon) f_{\mathrm{L}}(\epsilon) + k\hbar\Omega R^{(k)}_{\mathrm{RR}}(\epsilon) f_{\mathrm{R}}(\epsilon)]\,.$$

On the other hand, only transmission processes contribute to a change in the particle number in the leads; therefore,

$$\dot{N}_{\mathrm{R}} = \frac{1}{h}\sum_k \int \mathrm{d}\epsilon[T^{(k)}_{\mathrm{RL}}(\epsilon) f_{\mathrm{L}}(\epsilon) - T^{(k)}_{\mathrm{LR}}(\epsilon) f_{\mathrm{R}}(\epsilon)]\,. \tag{5.15}$$

Thus, the total heat production in lead R is

$$\dot{Q}_{\mathrm{R}} = \frac{1}{h}\sum_k \int \mathrm{d}\epsilon[(\mu_{\mathrm{R}} - \epsilon) T^{(k)}_{\mathrm{LR}}(\epsilon) f_{\mathrm{R}}(\epsilon) + k\hbar\Omega R^{(k)}_{\mathrm{RR}}(\epsilon) f_{\mathrm{R}}(\epsilon) + (\epsilon + k\hbar\Omega - \mu_{\mathrm{R}}) T^{(k)}_{\mathrm{RL}}(\epsilon) f_{\mathrm{L}}(\epsilon)]\,. \tag{5.16}$$

A similar expression (exchanging L and R) can be derived analogously for $\dot{Q}_{\mathrm{L}}$.

Starting from the definition of the energy current as $\dot{E} = \langle \epsilon \dot{N}(\epsilon) \rangle$, the tight-binding method described in section 2.3.3 for the calculation of the electrical current offers a way to properly derive the terms of the equation above. In doing so, one obtains first an expression for the time-dependent electrical current:

$$\dot{E} = \langle \epsilon \dot{N}(\epsilon) \rangle = \dot{E}_{\mathrm{R}\leftarrow\mathrm{L}} + \dot{E}_{\mathrm{R}\leftarrow\mathrm{R}} \tag{5.17}$$

(the R $\rightarrow$ L seems to be included by hand) and writes the different terms with the creation and destruction operators of the leads and the system. It is convenient here to introduce the system's Green function

$$G(t, t') = -\frac{\mathrm{i}}{\hbar} U(t, t') \Theta(t - t') \tag{5.18}$$

as an alternative way of describing the time evolution of the system. $U(t, t')$ is the evolution operator and $\Theta(t - t')$ represents the step function.[3] Their importance, as mentioned in section 2.3.3, lies in that with them one can formally solve the Heisenberg equations of motion for the creation and destruction operators in the

[3] The application of Green function theory to transport problems can be found in Jauho *et al.* (1994). Details for ac driven systems are described in Kohler *et al.* (2005). A tight-binding approach to pumps has been recently published (see Arrachea, 2005).

quantum wells and, subsequently, obtain the time-average of the current operator. This results for the electrical current in the equivalent of the Landauer formula for ac driven systems. To do this, the following correspondence between Green functions and transmission probabilities is used:

$$T_{\mathrm{LR}}^{(k)}(\epsilon) = \Gamma_{\mathrm{L}}\Gamma_{\mathrm{R}}|G_{1N}^{(k)}(\epsilon)|^2 \,. \tag{5.19}$$

Here, $\Gamma_{\mathrm{L,R}}$ are the wide-band limit coupling with the leads and $G_{1N}^{(k)}(\epsilon)$ is the k-component of the Fourier-transformed Green function. We use here this formalism for heat production. One proceeds by writing e.g. the term corresponding to $\dot{E}_{\mathrm{R}\leftarrow\mathrm{L}}$ in Eq. 5.17 with the Green functions,

$$\begin{aligned}\dot{E}_{\mathrm{R}\leftarrow\mathrm{L}} =& \frac{1}{2\pi\hbar^2}\int \mathrm{d}\epsilon\Gamma_{\mathrm{L}}(\epsilon)\epsilon\int_0^\infty \mathrm{d}\tau \mathrm{e}^{-\mathrm{i}\epsilon\tau/\hbar} \\ & \frac{1}{(2\pi)^2}\times\sum_\ell\int \mathrm{d}\epsilon' \mathrm{e}^{\mathrm{i}\epsilon' t/\hbar}\mathrm{e}^{-\mathrm{i}\epsilon'(t-\tau)/\hbar}G_{1\ell}^*(t,\epsilon')G_{1\ell}(t-\tau,\epsilon') \\ & \times 2\pi\Gamma_\ell(\epsilon')f_\ell(\epsilon') + [\text{H. c.}]\end{aligned} \tag{5.20}$$

and, using the Fourier transform of $G_{1\ell}(t,\epsilon')$, eliminates one of the energy integrals in favour of a sum over Fourier coefficients k. Then, after performing a time-average, this equation takes the simplified form

$$\dot{E}_{\mathrm{R}\leftarrow\mathrm{L}} = \frac{1}{h}\sum_{\ell k}\int \mathrm{d}\epsilon(\epsilon+k\hbar\Omega)\Gamma_{\mathrm{L}}(\epsilon+k\hbar\Omega)|G_{1\ell}^{(k)}(\epsilon)|^2\Gamma_\ell(\epsilon)f_\ell(\epsilon) \tag{5.21}$$

Now, with $G_{1\ell}^{(k)}(\epsilon)$ interpreted in terms of transmission probability as above, we finally obtain

$$\dot{E}_{\mathrm{R}\leftarrow\mathrm{L}} = \frac{1}{h}\sum_{\ell k}\int \mathrm{d}\epsilon(\epsilon+k\hbar\Omega)T_{\mathrm{L}\ell}^{(k)}(\epsilon)f_\ell(\epsilon)\,. \tag{5.22}$$

A similar analysis can be performed with the rest of the contributions to the total energy balance to justify Eq. (5.15).

5.5.2 Fundamental limits to cooling: per degree of freedom (acting on volume)

In a thermodynamic system, the quantity C_v/k_{B} is a good measure of the "active" degrees of freedom, i.e. of those dynamic variables whose characteristic lowest

energy scale is lower than $k_B T$. Here we estimate the maximum rate at which we can extract heat from a given degree of freedom. Such an extraction will result from many elementary processes. The maximum energy we can expect to extract in each of those elementary processes is of order $k_B T$. On the other hand, the rate must be lower than $k_B T/\hbar$, since otherwise we may heat up the system because of Heisenberg's uncertainty principle. This yields

$$\frac{k_B^2 T^2}{\hbar} \tag{5.23}$$

as the order of magnitude of the maximum rate at which we can cool a given degree of freedom. Summing over all active degrees of freedom, we find for the rate of internal energy variation

$$\frac{\mathrm{d}U}{\mathrm{d}t} \simeq -\frac{C_v}{k_B}\frac{k_B^2 T^2}{\hbar} \,. \tag{5.24}$$

On the other hand, the temperature variation is

$$\frac{\mathrm{d}T}{\mathrm{d}t} = \frac{1}{C_v}\frac{\mathrm{d}U}{\mathrm{d}t} \,. \tag{5.25}$$

From these equations we conclude

$$\left|\frac{\mathrm{d}T}{\mathrm{d}t}\right|_{\max} \simeq \frac{k_B^2 T^2}{\hbar} \tag{5.26}$$

and, therefore,

$$T(t) \geq \frac{T(0)}{1 + (k_B^2/h)T(0)t} \tag{5.27}$$

for any cooling process starting from $T = T(0)$.

5.5.3 Fundamental limits to cooling: per outgoing channel (acting on surface)

We can give here an estimate of the maximum cooling rate that can be attained in a mesoscopic structure. This occurs for a perfectly transmitting interface between the R electrode and the zero-temperature L electrode. Roughly, the heat produced in e.g. lead R is

$$\begin{aligned} \dot{Q}_R &= \frac{1}{\pi\hbar}\int_{-\infty}^{+\infty} \mathrm{d}\epsilon\, \epsilon[f_L(\epsilon)(\epsilon-\mu_R) + f_R(\epsilon)(\mu_R-\epsilon)] \\ &= \frac{1}{\pi\hbar}\int_{-\infty}^{+\infty} \mathrm{d}\epsilon\, (\epsilon-\mu_R)[f_L(\epsilon) - f_R(\epsilon)] = -2\frac{1}{\pi\hbar}\int_0^{\infty} \mathrm{d}\epsilon\, \epsilon f_R(\epsilon) \,. \end{aligned} \tag{5.28}$$

In the last equation, we have taken $\mu_{L,R} = 0$, and used the fact that $f_L(\epsilon)$ is a step function. The change of variables $\epsilon/k_B T = x$ yields

$$\dot{Q}_R = -\frac{2}{\pi\hbar} k_B^2 T^2 \int_0^\infty dx \frac{x}{e^x + 1} = \frac{\pi^2}{3} \frac{k_B^2 T^2}{h} \tag{5.29}$$

where we have used the definite integral $\int_0^\infty dx\, x/(e^x + 1) = \pi^2/12$. This suggests

$$|\dot{Q}_R|_{max} = -\frac{\pi^2}{3} \frac{k_B^2 T^2}{h} \tag{5.30}$$

as an upper limit to the cooling rate per outgoing channel. We wish to note that Eq. (5.30) has different prefactors from those which would be obtained from replacing ΔT by T in the quantum of thermal conductance.

5.6 Heat production in a double-well heterostructure

The theory developed in the preceding sections of this chapter will now be applied for the calculation of heat production in semiconductor heterostructures. Here we propose a double-well structure which, if properly tuned, shows the remarkable feature of pumping heat from the right lead by emitting *hot* electrons (i.e. above the chemical potential) while absorbing *cold* electrons from lead L, in the absence of a chemical potential or even temperature bias between the leads. It is of particular importance the possibility of extracting heat *against* a temperature bias, i.e. pumping heat from the cold to the hot electron reservoir.

5.6.1 Structure of the double-well

To achieve this *cooling* effect we need at least the four-level structure depicted in Fig. 5.1. These resonant levels (ordered by increasing energy) E_{1L}, E_{1R}, E_{2R} and E_{2L}, originate from two different quantum wells placed between tunnel barriers, neglecting for transport calculations all higher-lying states in each well. The structure is designed as follows: the two levels of the wider well on the right can be placed symmetrically in the energy axis between the other two levels, which are correspondingly more separated if the left well is narrower, by introducing an internal bias ϵ_0 that shifts the levels to higher energies. Left and right chemical potentials of the leads are then placed halfway between the four levels, and an ac

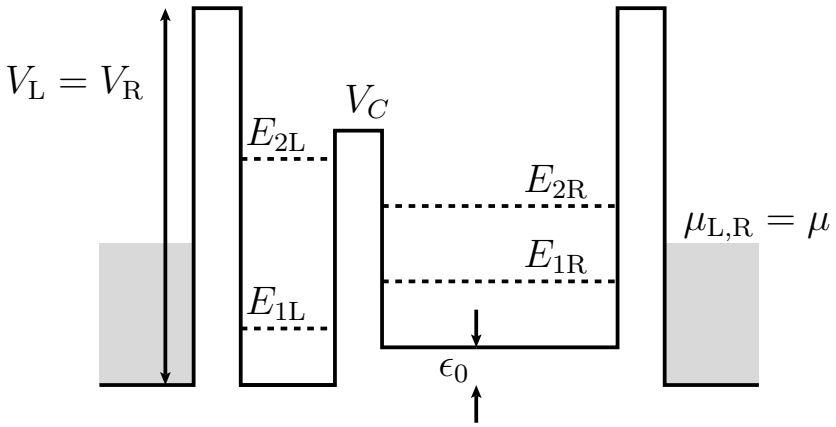

FIGURE 5.1: Asymmetric double-well heterostructure used for heat production calculations. Energy levels are symmetrically placed around the equal Fermi levels of the leads. See text for further details.

gate voltage is applied to the structure in the same way as in the electron pump of chapter 4. Now, we choose the driving frequency to be as close as possible to the energy difference between the two highest levels, that is, $\hbar\Omega \approx E_{2\mathrm{L}} - E_{2\mathrm{R}}$, which ideally corresponds to $E_{1\mathrm{R}} - E_{1\mathrm{L}}$.

Thus we try to favor the following processes (see Fig. 5.2): first, electrons in lead R can tunnel through the right barrier to $E_{2\mathrm{R}}$ and then absorb one photon to hop to $E_{2\mathrm{L}}$. These electrons leave the structure through the left barrier and reach lead L, thus producing a current. At the same time, electrons in lead L can follow a similar process and travel from left to right through the levels $E_{1\mathrm{L}}$ and $E_{1\mathrm{R}}$. These two contributions have the effect of taking away electrons above the chemical potential μ_{R} in the direction R→L, while replacing them by electrons below μ_{R} stemming from the left lead. We are effectively replacing hot electrons (above μ_{R}) by cold electrons (below μ_{R}), i.e. we are cooling the R electrode. Importantly, this transmission-induced cooling must overcome the reflection term in Eq. (5.16).

On the other hand, we expect cooling to be more efficient at low driving amplitudes. We explore this regime since this allows for a a fine control of the relevant inelastic processes. For low amplitudes, the term $k = 1$ will dominate over higher order processes, which might transfer electrons to higher energies contributing to spoil the cooling effect.

As a further requirement, temperature must be carefully chosen. Too low temperatures would leave the states at energies around $E_{2\mathrm{R}}$ completely empty, so

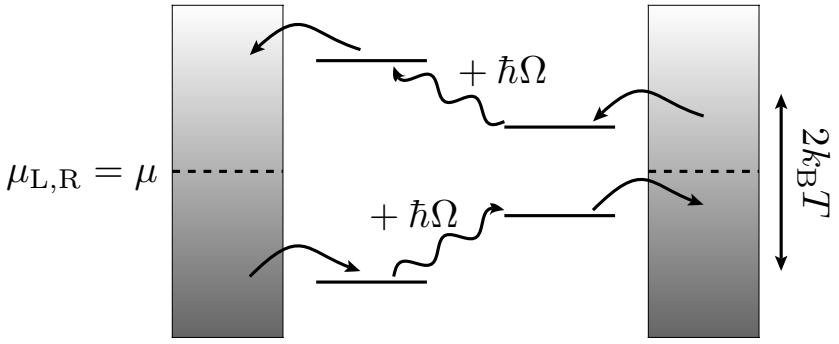

FIGURE 5.2: Dominant transmission processes to cool lead R: *hot* electrons in the low-populated states up to $\sim k_{\mathrm{B}}T$ above μ leave lead R, and are replaced by *cold* electrons from lead L, stemming from highly occupied states at energies as much as $\sim k_{\mathrm{B}}T$ below μ. It is assumed that $T_{\mathrm{L}} = T_{\mathrm{R}} = T$.

there would be very few electrons to be transferred to lead L. By contrast, too high temperatures (assuming $\mu_{\mathrm{L,R}} = (E_{2\mathrm{R}} + E_{1\mathrm{R}})/2$) would have the opposite effect of too high occupation of $E_{2\mathrm{L}}$. The electron current from L to R would prevent any efficient cooling. The optimal temperature for cooling of lead R is therefore expected for temperatures such that $E_{2\mathrm{L}} - E_{2\mathrm{R}} \approx 2k_{\mathrm{B}}T$. This intuition is confirmed by both the numerical results and an analytical model.

The structure was developed by surveying the dc transmission probabilities, calculated via transfer-matrices, of the separate wells without internal bias. This is shown in panel (a) of Fig. 5.3. In this situation we can ascribe each of the resonances to either of the wells. The two wells are then coupled through a central barrier. The full $T(E)$ curve (gray dashed in panel (b) of the same figure) was then finely tuned to arrive at the solid blue curve, which displays a four level structure symmetrically placed around $E \sim 6.03$ meV. There is a further level at $E \sim 2$ meV, about ~ 0.2 meV below the one we actually consider, but if the frequency is properly tuned with $E_{2\mathrm{L}} - E_{2\mathrm{R}}$ so that it differs from it by less than the level width, then we expect its contribution to transport to be negligible. We emphasize here that this modelling is realistic in that it does not neglect other resonances present in the structure. This makes our transfer matrix approach more reliable for numerical results than a tight-binding calculation where the number and position of the levels can be adjusted at will.

Our assumptions on the relevance of the $k = 1$ process is checked in Fig. 5.4. Here we show the transmission probability at a finite value of the driving ampli-

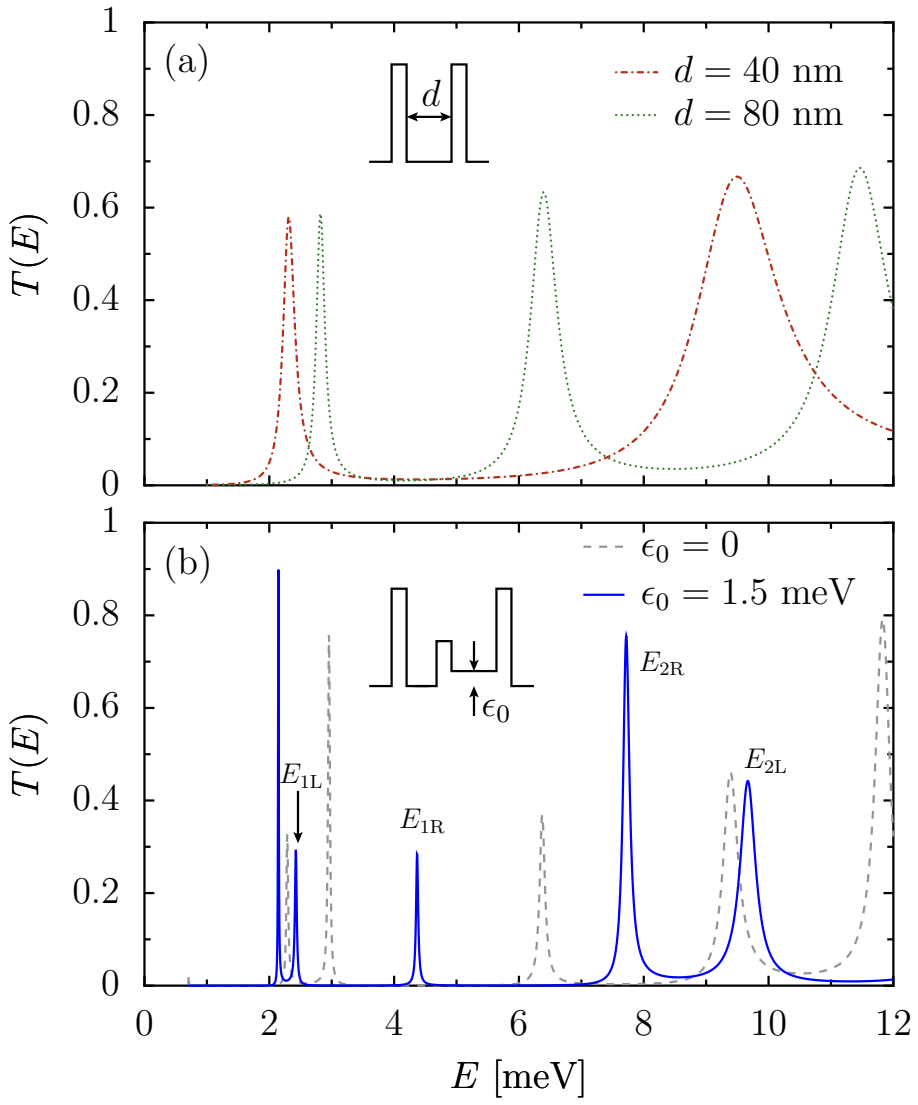

FIGURE 5.3: dc transmission probability as a function of energy. Upper panel (a) shows $T(E)$ of the separate wells (depicted in the inset), while lower panel (b), with the corresponding inset, displays the transmission of the full double-well structure. See text for some comments.

tude. Left-right and right-left transmissions are no longer equal because of the ac driving. A peak appears in e.g. R→L transmission for $E \sim E_{2R}$, indicating that there is a strong resonance for the $E \to E + \hbar\Omega$ process. The same analysis can be performed with the rest of the peaks.

For our calculations we have chosen two wells 40 and 80 nm wide, respectively, coupled through 4 nm barriers of 60 meV to the leads and with a central barrier 5

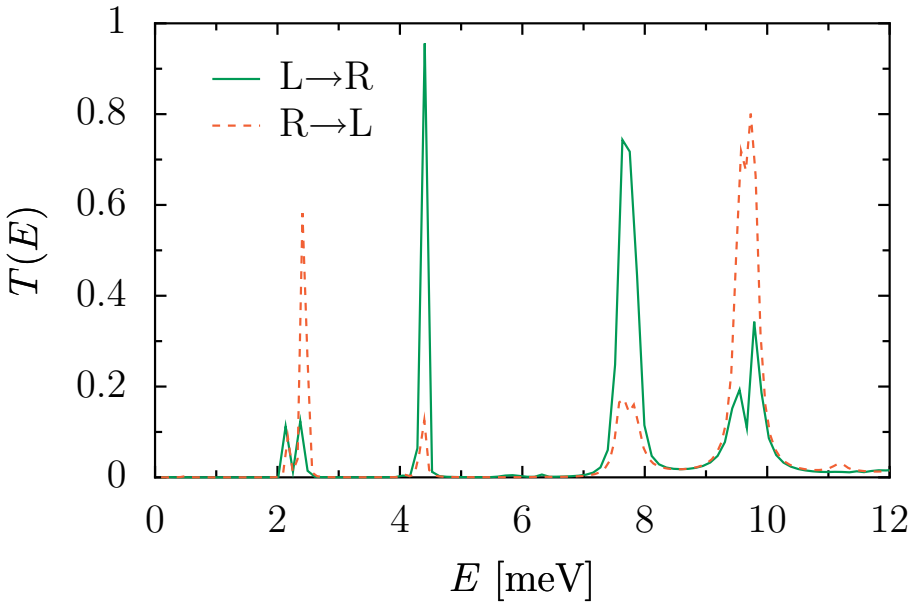

FIGURE 5.4: ac transmission probability of the structure of Fig. 5.1 for $eV_{ac} = 0.4$ meV. Peaks correspond to the L→R and R→L processes relevant for heat transport calculations.

nm wide and 30 meV high. The levels of the right well fall symmetrically between those of the left one for $\epsilon_0 = 1.5$ meV, as shown in Fig. 5.3. The dc transmission probability thus obtained is still highly asymmetric, in the sense that peaks are of different heights and widths; but this, hard to avoid in practice, does not spoil the numerical results, although it does make them a little less transparent when it comes to their interpretation. The four levels have in this case the energies $E_{1L} = 2.43$, $E_{1R} = 4.36$, $E_{2R} = 7.70$, and $E_{2L} = 9.65$ meV, respectively. This determines the driving frequency of the ac potential as $\hbar\Omega \approx E_{2L} - E_{2R} \approx E_{1R} - E_{1L} \simeq 1.94$ meV (i.e. $\sim$ 400 GHz), and an optimal temperature for cooling is expected at $k_B T \sim (E_{2R} - E_{1R})/2 \approx 1.7$ meV or equivalently $T \approx 20$ K.

5.6.2 Numerical results

We consider now the numerical implementation of the formulas of section 5.5. In addition to the basic plot of $\dot{Q}_R$ as a function of the driving amplitude, we perform various numerical tests to check the assumptions made on transport model and its robustness against departures from ideal behavior. The exploration of the parameter space can help optimize the structure to achieve higher cooling

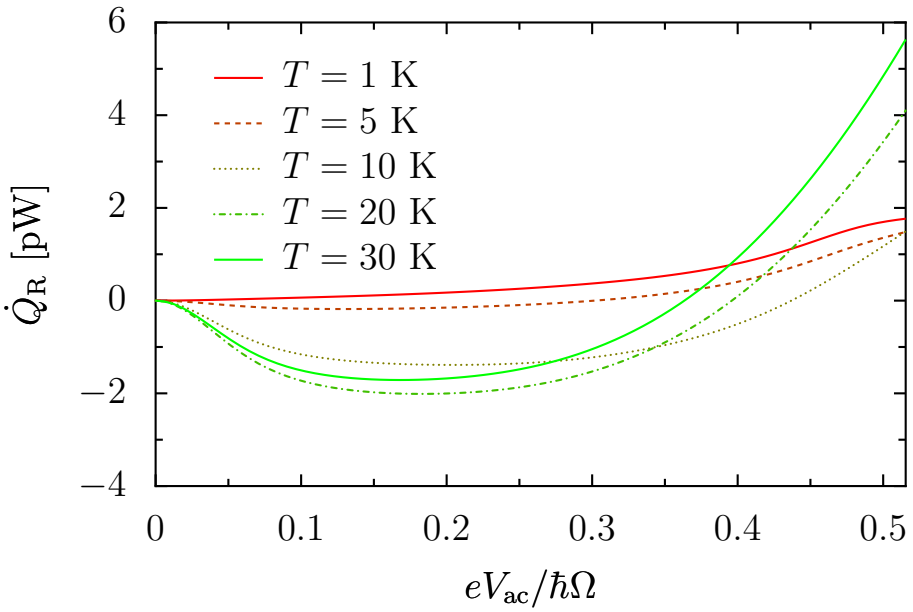

FIGURE 5.5: Heat production in lead R for the structure of Fig. 5.1 as a function of the driving amplitude eV_{ac} for various temperatures of the leads. Panel (b) shows the case of $T = 20$ K together with the electrical current and the contribution of reflected electrons, which remains always positive. The driving frequency is $\hbar\Omega = 1.94$ meV.

rate. In particular, we check the dependence of $\dot{Q}_R$ on the driving frequency, the temperature of the leads and the chemical potential. We also show negative heat production in the experimentally interesting case of vanishing electric current is also possible.

Driving amplitude

Typical data for $\dot{Q}_R$ for the structure defined above are shown in Fig. 5.5. We plot here the dependence of $\dot{Q}_R$ on the driving amplitude eV_{ac} for different temperatures $T_L = T_R = T$ of the reservoirs. We restrict the calculations to low amplitudes. Heat production remains positive at very low temperatures, but decreases with growing T until it begins to take negative values at $T \gtrsim 5$ K. The highest cooling power is observed, as expected from the reasons given in the introduction to this section, for temperatures around 20 K.

In Fig. 5.6 we plot the specific case of $T = 20$ K. Here, the contribution of reflected electrons to the total heat production and the electrical current as a reference. The accompanying electrical current is also shown as a reference. As

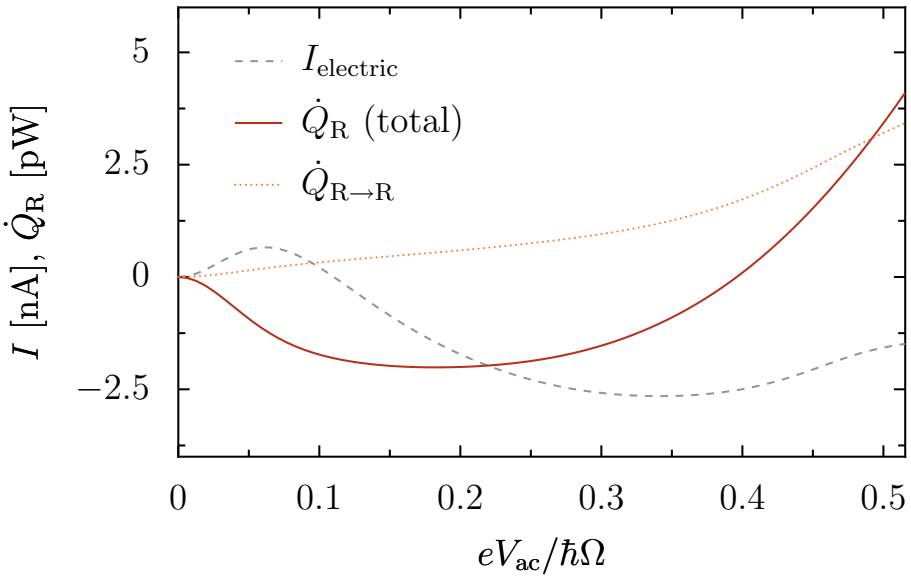

FIGURE 5.6: $\dot{Q}_{\text{R}}$ for $T = 20$ K, plotted together with the electrical current and the contribution of reflected electrons, which remains always positive.

expected from very general principles, reflection always tends to heat the system, eventually dominating at high driving amplitudes. There exists however a regime at low amplitudes where transmission terms dominate, resulting in a negative heat.

The magnitude obtained for the cooling power of these devices remains low, $\sim 10^{-12}$ W, but comparable to the experimental results reported (see Pekola, 2005, and references therein).

Dependence of heat production with driving frequency

We show in the following some numerical results to explore the qualitative behavior expected from Fig. 5.2 against the variation of some parameters. In the first place, we check that the resonance condition for the driving frequency $E_{2\text{L}} - E_{2\text{R}} \approx \hbar\Omega$ is in fact a maximum condition for the negative heat production. Similar results but with lower output are expected for frequencies which differ from the resonant case. This is indeed the case, as can be seen in Fig. 5.7: heat production at specific temperature and driving amplitude conditions is plotted against the frequency of the driving. If the energy absorbed by the electrons does not match any of the inelastic transmission channels, electrical current and therefore heat production are effectively blocked. The graph shows that whenever $\hbar\Omega$

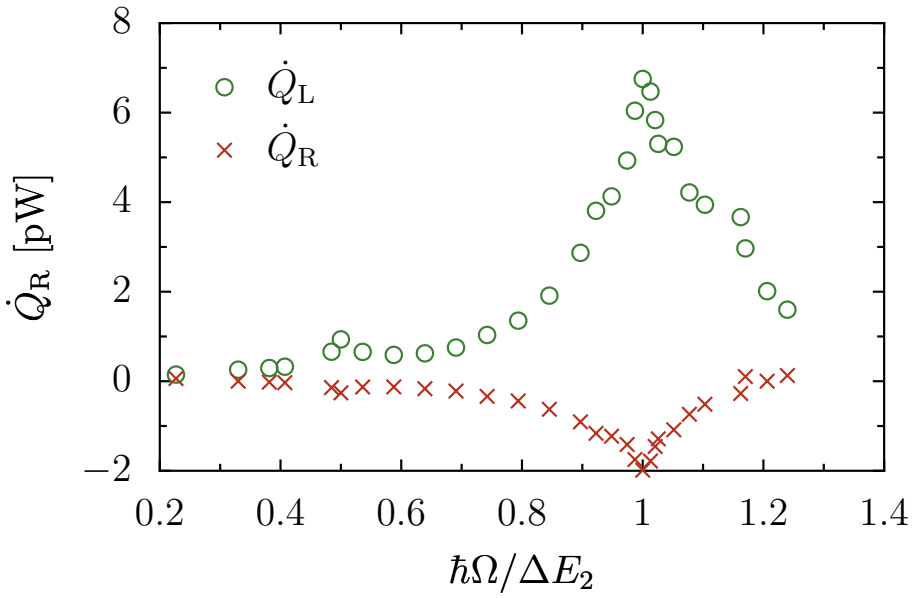

FIGURE 5.7: Maximum pumped heat, plotted against the deviation of the driving frequency $\hbar\Omega$ from the resonant frequency $\Delta E_2 = E_{2\rm L} - E_{2\rm R} \simeq \Delta E_1$. The temperature is 20 K and the driving amplitude $eV_{\rm ac} = 0.3$ meV.

differs from $E_{2\rm L} - E_{2\rm R}$ in more than about ~ 0.5 meV, which is approximately the width of the resonances in Fig. 5.3(b), then heat production goes to zero. This illustrates the need to carefully choose the driving parameters so that they meet all necessary requirements.

Note further that $\dot{Q}_{\rm L}$ remains always bigger than $|\dot{Q}_{\rm R}|$. This indicates that, as expected, in global terms heat is produced in the system. A general proof of this is given in the Appendices.

Dependence on chemical potential

The direction of the electrical current as well as the sign of heat production in the leads can be controlled through the variation of the common chemical potential of the leads. We show this in Fig. 5.8. We have chosen the optimal temperature ($T_{\rm L,R} = 20$ K) and driving amplitude ($eV_{\rm ac} \sim 0.2\hbar\Omega$ meV) conditions of maximum negative heat production of Fig. 5.6.

The curves of $\dot{Q}_{\rm L}$ and $\dot{Q}_{\rm R}$ as a function of μ can be understood qualitatively in terms of our model of Fig. 5.2. The transition $E_{1\rm L} \to E_{1\rm R}$ dominates for low chemical potential, and this results in a small negative $\dot{Q}_{\rm L}$ and positive $\dot{Q}_{\rm R}$. With

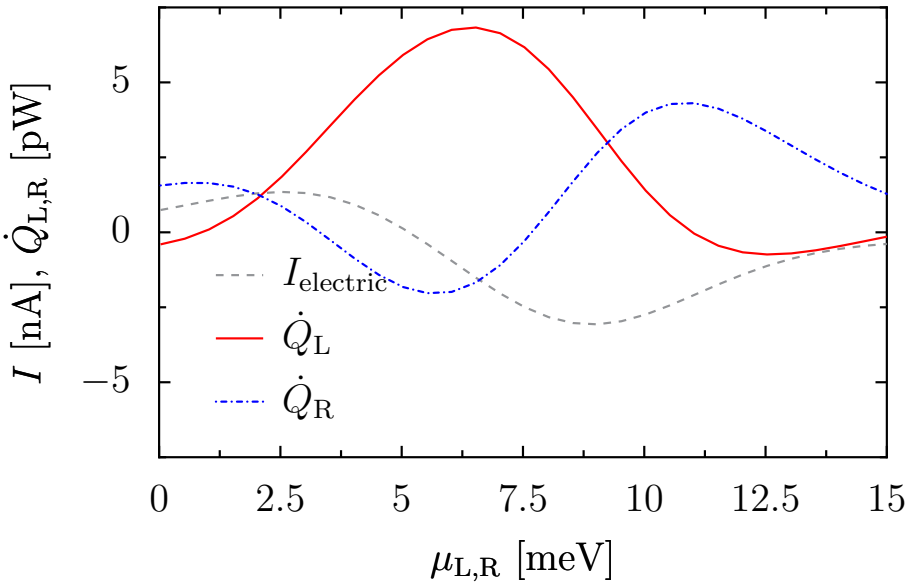

FIGURE 5.8: Dependence of $\dot{Q}_{\mathrm{L,R}}$ with the chemical potential $\mu_{\mathrm{L}} = \mu_{\mathrm{R}} = \mu$. Other parameters are $T_{\mathrm{L,R}} = 20$ K, $eV_{\mathrm{ac}} = 0.3$ meV. Maximum cooling power is attained when μ reaches the mid-point between levels of the right dot, i.e. $(E_{2\mathrm{R}} + E_{1\mathrm{R}})/2 \approx 6$ meV.

increasing μ we begin to populate states around $E_{1\mathrm{R}}$, and since the process $E_{1\mathrm{R}} \to E_{1\mathrm{L}}$ is slightly more probable than its reverse, we soon obtain a certain cooling of lead R. This tendency is maintained for higher chemical potentials, reaching maximal negative heat production for lead R when μ lies around the mid-point between resonances on the right and, simultaneously, the temperature is such that $k_{\mathrm{B}}T \approx (E_{2\mathrm{R}} - E_{1\mathrm{R}})/2$. Then, a few states are populated at $E \sim E_{2\mathrm{R}}$, so that the transition $E_{2\mathrm{R}} \to E_{2\mathrm{L}}$ effectively removes *hot* electrons from lead R, while electrons coming from lead L with energies around $k_{\mathrm{B}}T$ below μ_{R} still have some free states when arriving to R through the *lower* transmission channel $E_{1\mathrm{L}} \to E_{1\mathrm{R}}$. A further increase of μ fills these levels, so that lead R can only *cool* by the leaving electrons, which reduces the overall efficiency. Eventually, for high chemical potentials $\gtrsim 10$ meV it is the $E_{2\mathrm{L}} \to E_{2\mathrm{R}}$ which dominates, which causes a small negative $\dot{Q}_{\mathrm{L}}$.

Figure 5.8 also shows that there even exist some conditions when heat can be pumped from lead R at vanishing electrical current (e.g. for $\mu \approx 6$ meV). This is explored in detail next.

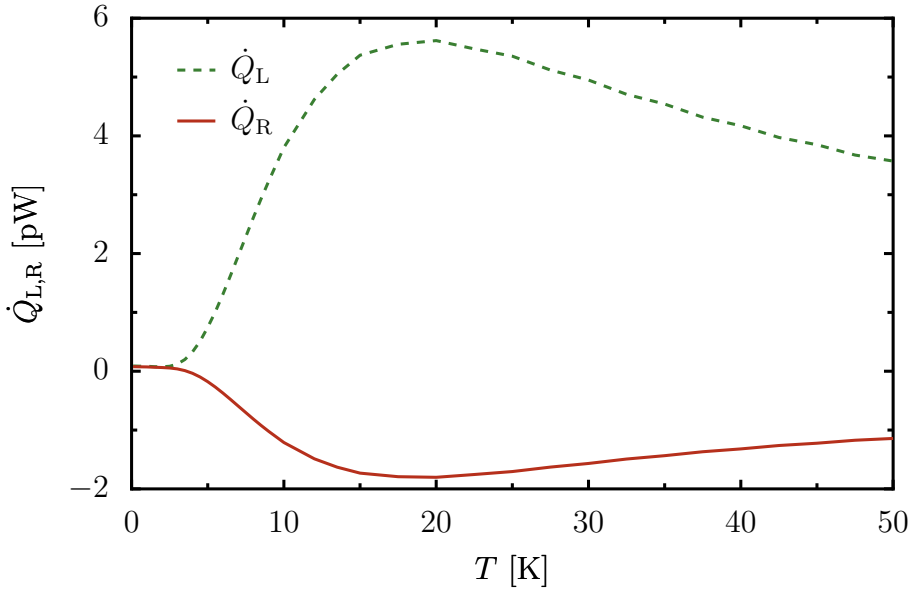

FIGURE 5.9: Dependence of $\dot{Q}_{\mathrm{L,R}}$ with temperature $T_{\mathrm{L}} = T_{\mathrm{R}} = T$ at $I_{\mathrm{electric}} = 0$. Driving amplitude is $eV_{\mathrm{ac}} \sim 0.21$ meV. Heat production goes again through a maximum for $k_{\mathrm{B}}T \sim (E_{2\mathrm{R}} - E_{1\mathrm{R}})/2 \approx 20$ K.

Heat production at zero electric current

While a negative heat production is an interesting result in itself for driven heterostructures, a desirable situation would be to obtain it in the absence of electric current across the system. The various thermoelectric effects confirm that the passage of electrical current involves in general the transfer of heat, too, so the most interesting situation arises when *no* current flows through the double well structure. To achieve this, one could search for a current suppression effect as discussed in chapter 3. This is however not useful, since by blocking the flow of electrons prevents also the flow of heat. We are rather interested in vanishing electrical current by *cancellation* of left- and right-moving currents of electrons. That this is possible can be noted by assuming particle-hole symmetry around the chemical potential, and it is confirmed by the $I(eV_{\mathrm{ac}})$ curve of Fig. 5.6. The current appears to vanish at $eV_{\mathrm{ac}} \approx 0.1\hbar\Omega$. Since the electrical current depends essentially on the ratio $eV_{\mathrm{ac}}/\hbar\Omega$ —although here in a far more complicated manner than in the cases studied so far—, it should be no surprise that for different temperatures and under the same driving conditions there still exists a zero-current point at the same value of the driving amplitude. We plot in Fig. 5.9 how $\dot{Q}_{\mathrm{L}}$

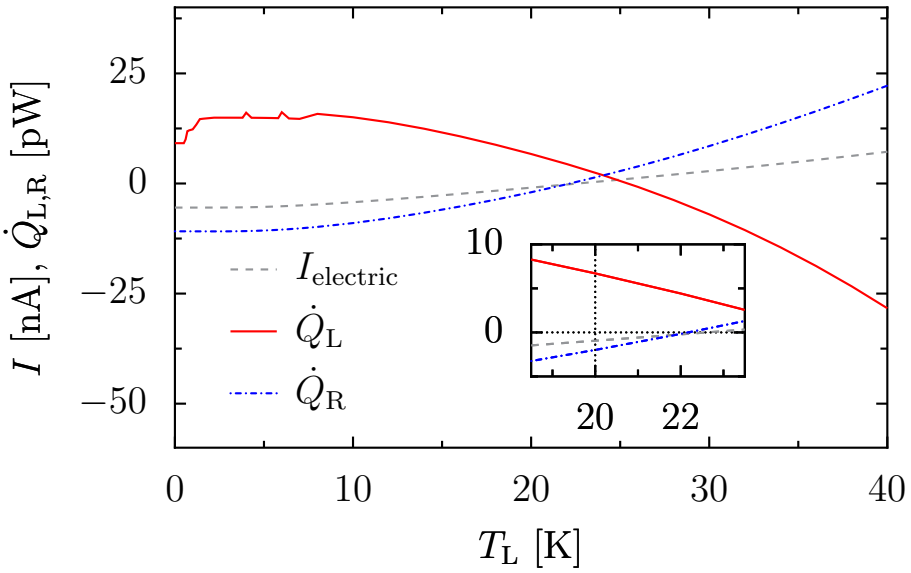

FIGURE 5.10: Dependence of $\dot{Q}$ with temperature at fixed $T_{\mathrm{R}} = 20$ K, and fixed driving amplitude $eV_{\mathrm{ac}} = 0.3$ meV. Chemical potential is $\mu_{\mathrm{L,R}} = 6.03$ meV. The inset shows the region around $\Delta T = 0$, where pump occurs despite equal temperatures and chemical potentials.

and $\dot{Q}_{\mathrm{R}}$ change with temperature in this situation. Although there is some heat pumping for low temperatures, the effect is more pronounced again at the optimal temperature $T_{\mathrm{L,R}} \sim 20$ K, and it is still appreciable for higher temperatures.

Dependence on temperature difference

We explore here the dependence of the heat production with the temperature *difference* between the leads. Figure 5.10 shows the results for fixed $T_{\mathrm{R}} = 20$ K and varying temperature of the left lead, T_{L}. The chemical potentials $\mu_{\mathrm{L,R}} = 6.03$ meV are set half-way between resonances. Two interesting features can be observed: first, as displayed in the inset, heat production and electrical current are negative for *zero* temperature difference. In the small region with $T_{\mathrm{L}} > T_{\mathrm{R}}$ the double well structure acts as a true heat pump, i.e. heat flows against the temperature gradient. Such a device may be viewed as a *nanorefrigerator*.

The second regime of interest is that of very low temperatures. When $T_{\mathrm{L}} \to 0$, $\dot{Q}_{\mathrm{R}}$ reaches its maximum value. From a simple thermodynamical analysis it is expected that the highest cooling rate attains its maximum efficiency when the temperature of the coldest reservoir goes towards absolute zero. The non-zero

electrical current flowing from lead R to L (thus its negative sign) still puts some heat into lead L.

Dependence of heating with coupling: two-pipeline model

In our previous analysis we have implicitly considered that the width of the resonances is very small. Our qualitative discussion assumed that electrons entered and left the structure at the energies of the resonances. But a rapid check with Fig. 5.3 or 5.4 shows that this is not strictly true. We show here that a simple, but more realistic, model for the shape of the resonance of the right well helps to demonstrate that the cooling rate cannot attain any desired value, but is limited by the interplay between the coupling to the leads, fixed by the width of the resonances and of the Fermi distribution, and the distance of the resonances to the middle energy between them.

This model is based on the idea of inelastic transmissive channels or *pipelines* (Wagner and Sols, 1999; Sols and Wagner, 2000). Pipelines are conceived as the dominant channels of the inelastic transmission induced by the ac driving. The rest of possible transfer process, resulting from the absorption or emission of more than one photon, or from different energies, is neglected.

For the double-well structure of Fig. 5.1 our model goes as follows. Choosing $E = 0$ at the middle energy between $E_{1\mathrm{R}}$ and $E_{2\mathrm{R}}$, the transmission in the presence of ac driving is modelled by two pipelines, named $T_u(E)$ and $T_d(E)$, which peak at energies $E_{2\mathrm{R}} \equiv +E_0$ and $E_{1\mathrm{R}} \equiv -E_0$, respectively. Any electron entering the heterostructure at $\pm E_0$ will be transmitted in either case to $E_0 + \hbar\Omega$ and $-E_0 - \hbar\Omega$. We take $\mu_{\mathrm{L,R}} = 0$ for convenience. If temperature is chosen such that $\hbar\Omega \gg k_{\mathrm{B}}T$, then

$$f_{\mathrm{L}}(E_0 + \hbar\Omega) \approx 0\,, \qquad f_{\mathrm{L}}(-E_0 - \hbar\Omega) \approx 1\,, \tag{5.31}$$

i.e. the corresponding energy levels are completely empty or filled. Note that this is compatible with $T_{\mathrm{L}} > T_{\mathrm{R}}$, i.e. with lead L being hotter than lead R. In this case the electrical current reads

$$\begin{aligned}\frac{h}{e}I = \int \mathrm{d}E\{&[f_{\mathrm{L}}(E+\Omega) - f_{\mathrm{R}}(E)]T_u(E) \\ &+ [f_{\mathrm{L}}(E-\Omega) - f_{\mathrm{R}}(E)]T_d(E)\}\,,\end{aligned} \tag{5.32}$$

while for heat production in lead R we have

$$h\dot{Q}_{\mathrm{R}} = \int \mathrm{d}E\{[f_{\mathrm{L}}(E+\Omega) - f_{\mathrm{R}}(E)](E-\mu_{\mathrm{R}})T_u(E) + [f_{\mathrm{L}}(E-\Omega) - f_{\mathrm{R}}(E)](E-\mu_{\mathrm{R}})T_d(E)\} \,. \tag{5.33}$$

If we take the pipelines to be symmetric, $T_u(E) = T_d(-E) \equiv T_0(E)$ and use Eq. (5.31), it is easy to show that the electrical current vanishes and, furthermore,

$$h\dot{Q}_{\mathrm{R}} = -\int_{-\infty}^{\infty} \mathrm{d}E f_{\mathrm{R}}(E) E T_0(E) \,. \tag{5.34}$$

A possible model for the transmission peaks is to assume they are Gaussians of width Γ_0 centered around the energies $\pm E_0$.[4] It follows that the cooling rate is given by

$$\dot{Q}_{\mathrm{R}} = -\frac{\pi^2}{3}\frac{(k_{\mathrm{B}}T)^2}{h} T_0 H(\beta E_0, \beta\Gamma_0) \,, \tag{5.35}$$

with $\beta \equiv 1/k_{\mathrm{B}}T$ (T stands here for temperature), $T_0 = \max_E\{T_0(E)\}$ is the maximum value of $T_0(E)$, and

$$H(x,y) \equiv y\frac{3}{\pi^2}\int_{-\infty}^{+\infty} \mathrm{d}t \frac{t}{\mathrm{e}^t+1}\frac{1}{2y}\,\mathrm{e}^{-(t-x)^2/y^2} \,. \tag{5.36}$$

This function is basically a measure of the overlap between the Fermi function and the resonance. Note that in the limit of small widths,

$$\lim_{y\to 0}\frac{1}{2y}\exp[-(t-x)^2/y^2] = \delta(t-x) \,, \tag{5.37}$$

i.e. the transmission becomes a Dirac delta.

This expression for $\dot{Q}_{\mathrm{R}}$ should be compared with the upper limit for cooling, estimated in Eq. (5.30) to be of order $\sim (k_{\mathrm{B}}T)^2/h$. Thus the maximum cooling rate for this model will be given by the highest value of $H(x,y)$ times T_0, which is a function independent of the scale. Numerical exploration suggests that the maximum of $H(x,y)$ is of order 0.1. This allows us to conclude that for any lead R there is always a $T_0(E)$ which produces optimal cooling.

On the other hand, the cooling rates obtained are still of the order of ~ 10 pW even in the most favorable of the cases studied. This is about an order of magnitude below the highest possible cooling rate of Eq. (5.30), which for temperatures

[4] We take Gaussian shapes for the resonances to avoid the divergences that would appear for Lorentzian curves.

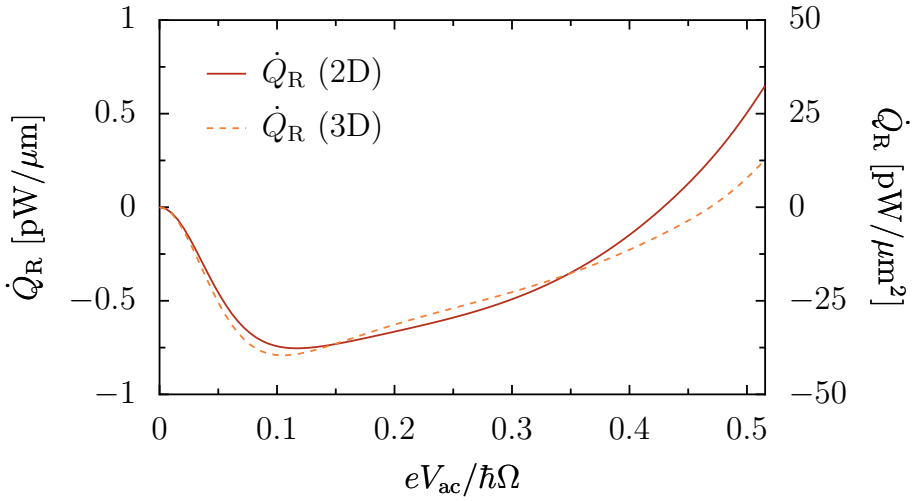

FIGURE 5.11: Heat production for two and three dimensional structures. The parameters are the same as in Figs. 5.5 and 5.6.

in the range of 10 K predicts $\sim$ 100 pW for this quantity. Given the crudeness of the two-pipeline model and the absolutely fundamental nature of the upper limit (5.30), it is probably not such a bad result. Moreover, the model captures the main features of an optimal heat transfer process.

Heat production in systems of higher dimensions

Finally, we study the situation when the heterostructure is part of a two- or three-dimensional system. As happened in chapter 3 with this issue, the way in which the calculation is done amounts to making certain assumptions about the conditions of transmission through the interface. Here we stick to our previous choice of considering that the wave vector $\vec{k}_{\parallel}$ of the electrons parallel to the interface is conserved. The results, shown in Fig. 5.11, indicate that a negative cooling rate is also observed. As a general remark we note that while not all $\vec{k}_{\parallel}$ may operate optimally, none of them will oppose cooling, i.e. all of them will contribute to cool the lead R albeit with varying efficiency.

6 Conclusions and outlook

Was sich überhaupt sagen lässt,
lässt sich klar sagen; und
wovon man nicht reden kann,
darüber muß man schweigen.[1]

(Ludwig Wittgenstein)

We summarized here the main conclusions. In this thesis, we have studied the behaviour of semiconductor quantum heterostructures under the action of external ac driving. We have found that these systems offer a physical mechanism to achieve coherent current control of the electrical current, for sufficiently localized states an moderately wide external barriers. This effect is also observed in situations that depart from the ideal one, i.e. when the driving is not localized to one of the wells, and for two- and three dimensional systems, in which it was assumed that the component of the wave vector parallel to the transmission interface, $\vec{k}_{\|}$, is conserved.

The high-frequency approximation (HFA) for the tight-binding formalism predicts the driving amplitudes of current suppression in accordance with numerically exact results obtained within a transfer-matrix formalism and a numerical implementation of the tight-binding approach. The discrepancies can be explained by an analysis of the assumptions made for the HFA and tight-binding approaches: HFA represents the first order term in a $(\hbar\Omega)^{-1}$ expansion, so it is the dominant contribution at high frequencies, and predicts $I = 0$ for zeros of the Bessel functions; on the other hand, the tight-binding description uses an

[1] What can be said at all can be said clearly; and whereof one cannot speak thereof one must be silent.

energy-independent coupling, which disregards higher order contributions that spoil the exact $eV_{\mathrm{ac}}/\hbar\Omega$ dependence.

We also studied asymmetrically driven double quantum wells. The asymmetry is introduced by an internal bias ϵ_0. When properly tuned, this systems can yield a nonzero dc current at vanishing external bias. We have shown that in this situation transport presents the features of photon-assisted tunneling predicted by Stafford and Wingreen (1996). In particular, the current presents peaks at resonance frequencies $\Omega \approx n\epsilon_0/\hbar$ in the strongly localized regime $\epsilon_0 \gg \Delta$, and a Ω^2 dependence for low frequencies. Our numerical results are confirmed again by the analytical curves of a Floquet calculation in the high frequency approximation.

The dependence on an external ac bias demonstrates the enhancement of the current by the absorption of one or more photons. The current steps indicate the adequacy of the Floquet analysis, in terms of sidebands, for ac transport.

Assuming electron decoherence between a pump and a resistor connected in series, and equal chemical potentials for all channels in the leads, it is possible to derive in a semiclassical scheme the two parameters (electromotive force and internal resistance) which characterize the pump when considered as an element in a circuit. In our analysis we have disregarded nonlinear effects and a possible dependence of the scattering events on the incident channel. These issues deserve further study and we hope to address them in forthcoming investigations.

Perhaps our most interesting results are the matter of chapter 5, where we have described heat production in electron reservoirs caused by electrical current. This current is produced by the action of ac driving in semiconductor heterostructures. We have extended Landauer's scattering formulation to heat transfer in an ac context, and have proved that this agrees with a derivation along the lines of the Floquet-Green formalism explained in Kohler *et al.* (2005).

We have shown that by properly choosing the structure and the driving parameters heat production in one of the leads can be negative, i.e. we predict a negative cooling rate for ac driven double quantum wells. The cooling rate predicted falls somewhat below the order of magnitude of other experimentally accomplished setups (Pekola, 2005), but presents some advantages over them: first, it the driving provides a means to control the amount of heat produced and even the direction of heat flow. Second, cooling should be attainable in the experimentally relevant conditions of zero electrical current, i.e. without charging

of the leads, and even against a thermal gradient, so the proposed device would act as a heat pump or nanorefrigerator.

To gain a better understanding of the physical model, we have explored part of the vast parameter space that defines the double well heterostructure. Our calculations show that the achievement of a negative heat production depends on the relation of the temperature of the leads and the level structure of the wells. Although in our particular model the highest cooling rates were expected at temperatures of the order of $\sim$ 20 K, the scaling arguments of sections 5.5.2 and 5.5.3 make it clear that the scheme can operate at any temperature.

Heat production depends strongly on the driving frequency. Optimal cooling rates appear when the energy of the driving, $\hbar\Omega$, matches the difference between energy levels in the wells. The chemical potential of the leads is a further parameter that can be used to adjust the amount of heat produced. Finally, by modelling the resonances as pipelines, we have shown that the cooling rate can always come close to the fundamental limits for completely transparent systems with an electrode at zero temperature, provided that the frequency is correctly tuned and both resonance level widths and difference are comparable to the temperature of the electrode we wish to cool.

Taking the resonances as pipelines of Gaussian shape, we have modelled the heat produced and found it to agree roughly with the fundamental limits expected in the most favourable conditions of completely transparent systems.

Besides the nonlinear effects on pumps mentioned above, there are other issues which we have not taken into account in this work. The most important might be that of screening effects in the reservoirs, which is overestimated systematically in our calculations. More effort is needed to understand realistic conditions of driven heterostructures. Besides, all electron–electron interactions have also been completely disregarded, and while this might be a valuable approximation in vertical quantum dots populated with few atoms, this does not address many situations in other types of dots. Regarding the ac-cooling of nanostructures, we think we have captured the essential ingredients of the physics, but we are also aware that the formalism is still not as sound as existing transport theories for electrical current in mesoscopic systems. We hope to fill this gap in forthcoming research projects.

Conclusiones

En esta tesis hemos estudiado el comportamiento de heteroestructuras semiconductoras bajo la acción de potenciales externos dependientes del tiempo. Hemos utilizado las propiedades de transporte coherente a través de dobles pozos cuánticos, y hemos demostrado que es posible controlar la corriente eléctrica que atraviesa una de estas estructuras escogiendo de forma adecuada la amplitud del voltaje aplicado y su frecuencia. Estos resultados se mantienen también para señales alternas con diferente dependencia espacial y en estructuras de dos y tres dimensiones.

La supresión coherente de la corriente eléctrica nos ha permitido comparar cálculos numéricos exactos, realizados mediante los formalismos de *matrices de transferencia* y *enlaces fuertes* (*tight-binding*). Mientras que el primero describe de forma más realista las heteroestructuras, la aproximación de altas frecuencias del segundo permite dar una explicación cualitativa de problemas de transporte en sistemas con Hamiltoniano periódico en el tiempo. Mediante cálculos adicionales hemos evaluado algunos de los supuestos sobre los que se sustenta esta aproximación.

El estudio del *bombeo de electrones* en dobles pozos cuánticos asimétricos ha centrado la segunda parte de nuestra investigación. Hemos calculado la corriente de bombeo en ausencia de un voltaje continuo (de polarización) externo y hemos comprobado que se corresponde con los supuestos de que el transporte tiene lugar mediante la absorción de fotones del campo (alterno) aplicado. También en este caso las curvas de la aproximación de altas frecuencias reproducen los resultados numéricos y permiten una clara interpretación cualitativa.

Por otro lado, hemos comprobado que bajo las hipótesis de decoherencia electrónica completa de los electrones en su desplazamiento entre la bomba y el resistor, y de igualdad de potencial químico de todos los canales de transporte, el comportamiento del dispositivo de bombeo de electrones al formar parte de un circuito puede caracterizarse por dos parámetros: la fuerza electromotriz y

la resistencia interna. Ambas cantidades pueden calcularse en términos de las propiedades de dispersión de los elementos que forman el circuito.

En último lugar hemos considerado la producción de calor debida al paso de la corriente eléctrica en los electrodos. Hemos propuesto un modelo para una heteroestructura en la que la acción de voltajes alternos y una elección precisa de los parámetros de la heteroestructura permiten controlar la dirección del flujo de calor. La corriente predicha por nuestros cálculos queda por debajo de los resultados experimentales en otros sistemas, pero sobre ellos presenta las ventajas de ser controlable, y de poder operar en condiciones en las que la corriente eléctrica neta en los electrodos se anula. Esta situación es de gran interés para sistemas mesoscópicos, puesto que los procesos de carga conllevan un gran coste energético por la repulsión de Coulomb entre los electrones.

Para comprender mejor el modelo descrito, hemos explorado el espacio de parámetros que define la heteroestructura. Según nuestros cálculos, la posibilidad de enfriar un electrodo está fijada por la relación entre la estructura de niveles energéticos y la temperatura de funcionamiento. Aunque en el caso particular estudiado el enfriamiento alcanza su valor óptimo en $T \sim 20$ K, los argumentos teóricos indican que este esquema de funcionamiento puede operar a cualquier temperatura. Los cálculos numéricos realizados permiten afirmar que nuestro modelo contiene la física esencial de la producción de calor en heteroestructursa.

Appendix A: Transfer matrices and Bessel functions

Little has been said in chapter 2 about the actual content of the transfer matrices. For the interested reader we offer here some insight into their structure as defined in chapter 2. In many occasions, their manipulation involves using Bessel functions in some way; therefore,a couple of useful relations of these mathematical objects are stated here for completeness.

A.1 What is inside a transfer matrix?

Transfer matrices (TMs) are obtained matching wave functions across an interface. This means that one takes the plane-wave expansion of the scattering states on one side of a layer, which we take to be non-driven (static), and has to match all the coefficients, and those of its spatial derivative, to the plane-wave expansion at the other side of the interface, which is driven by e.g. $V_{\rm ac}(t) = V_{\rm ac}\cos\Omega t$. An important point in this derivation is that the matching equates time-dependent wave functions that have to be equal *at all times*. With the definition

$$a_n^{\rm I}(z) = \begin{pmatrix} {\rm e}^{k_l^{\rm I} z} & {\rm e}^{-k_l^{\rm I} z} \\ k_l^{\rm I}{\rm e}^{k_l^{\rm I} z} & -k_l^{\rm I}{\rm e}^{-k_l^{\rm I} z} \end{pmatrix} \tag{A-1}$$

for the spatial part of the wave functions and its derivatives for layer I (an equal expression, of course, appears for layer II), and using Bessel functions, this means

$$\sum_n a_n^{\rm I}(z){\rm e}^{-{\rm i}n\Omega t} = \sum_n a_n^{\rm II}(z)\sum_l J_l {\rm e}^{-{\rm i}(n+l)\Omega t}\ . \tag{A-2}$$

We need to re-arrange the terms on the rhs of this equation in order to get rid of the time-dependent factors by matching *term by term* the corresponding coefficients. This can be done with the addition theorems for Bessel functions (see

below):

$$\sum_n a_n^{\mathrm{II}}(z) \sum_l J_l \mathrm{e}^{-\mathrm{i}(n+l)\Omega t} = \sum_n \sum_l a_l^{\mathrm{II}}(z) J_{n-l} \mathrm{e}^{-\mathrm{i}n\Omega t} \,, \tag{A-3}$$

and then the infinite set of algebraic equations of Eq. (A-2) becomes

$$a_n^{\mathrm{I}}(z) = \sum_l a_l^{\mathrm{II}}(z) J_{n-l} \tag{A-4}$$

or, in a more explicit manner,

$$\sum_l \underbrace{\delta_{z;n,l} \begin{pmatrix} \mathrm{e}^{k_l^{\mathrm{I}} z} & \mathrm{e}^{-k_l^{\mathrm{I}} z} \\ k_l^{\mathrm{I}} \mathrm{e}^{k_l^{\mathrm{I}} z} & -k_l^{\mathrm{I}} \mathrm{e}^{-k_l^{\mathrm{I}} z} \end{pmatrix}}_{\mathbf{T}^{\mathrm{I}}_{z;n,l}} \begin{pmatrix} A_l^{\mathrm{I}} \\ B_l^{\mathrm{I}} \end{pmatrix} = \sum_l \underbrace{J_{n-l} \begin{pmatrix} \frac{V_{\mathrm{ac}}}{\hbar\Omega} \end{pmatrix} \begin{pmatrix} \mathrm{e}^{k_l^{\mathrm{II}} z} & \mathrm{e}^{-k_l^{\mathrm{II}} z} \\ k_l^{\mathrm{II}} \mathrm{e}^{k_l^{\mathrm{II}} z} & -k_l^{\mathrm{II}} \mathrm{e}^{-k_l^{\mathrm{II}} z} \end{pmatrix}}_{\mathbf{T}^{\mathrm{II}}_{z;n,l}} \begin{pmatrix} A_l^{\mathrm{II}} \\ B_l^{\mathrm{II}} \end{pmatrix} \tag{A-5}$$

which defines the transfer matrices corresponding to the layers I and II at the common interface at coordinate z. So the matching takes place between the matrix on the left, made up of 2×2-blocks along the diagonal (note that we have introduced a Kronecker delta $\delta_{z;n,l}$ for this TM), and the TM on the right, which has 2×2-blocks also for non-diagonal elements:

$$\begin{pmatrix} \ddots & & \vdots & & \\ \cdots & \mathbf{t}_{n-1,-1} & \mathbf{t}_{n-1,0} & \mathbf{t}_{n-1,+1} & \cdots \\ \cdots & \mathbf{t}_{n,-1} & \mathbf{t}_{n,0} & \mathbf{t}_{n,+1} & \cdots \\ & & \vdots & & \ddots \end{pmatrix} \tag{A-6}$$

where each sub-matrix $\mathbf{t}_{n,l}$ is of the form

$$\mathbf{t}_{n,l} = \begin{pmatrix} J_{n-l} \mathrm{e}^{k_l^{\mathrm{II}} z} & J_{n-l} \mathrm{e}^{-k_l^{\mathrm{II}} z} \\ J_{n-l} k_l^{\mathrm{II}} \mathrm{e}^{k_l^{\mathrm{II}} z} & J_{n-l} (-k_l^{\mathrm{II}}) \mathrm{e}^{-k_l^{\mathrm{II}} z} \end{pmatrix} \,. \tag{A-7}$$

The index n increases from top to bottom, and we have omitted further blocks to the left and right of $k = \pm 1$. The compact form of (2.37) does in fact mean that one must equate each block of the diagonal matrix on the left to the corresponding sum on the right, as shown above. This represents the mixing of the sidebands on either side of the interface: one of the undriven layer and a sum over sideband index l on the right. This is the way to interpret correctly Eq. (A8) of the Appendix A in Wagner (1995). It is these matrices that one needs to invert in order to build up the total TM across a driven system.

To do this, we have the option of operating with TMs across an *interface* or a *layer*. As was discussed in chapter 2, we prefer to use the latter. Across a layer of width $(d = z_j - z_i)$ driven by a monochrome ac potential, one applies two times the same wave matching procedure as explained above; the total TM is then obtained as

$$\begin{aligned}\left(\mathbf{T}^{\mathrm{II}}_{z_i\to z_j}\right)_{n,n'} &= \mathbf{T}^{\mathrm{II}}_{z_j;n,l} \times \left(\mathbf{T}^{\mathrm{II}}_{z_i}\right)^{-1}_{l,n'} = \\ \sum_{l=-\infty}^{\infty} J_{n-l} \begin{pmatrix} \mathrm{e}^{k_l^{\mathrm{II}} z_j} & \mathrm{e}^{-k_l^{\mathrm{II}} z_j} \\ k_l^{\mathrm{II}} \mathrm{e}^{k_l^{\mathrm{II}} z_j} & -k_l^{\mathrm{II}} \mathrm{e}^{-k_l^{\mathrm{II}} z_j} \end{pmatrix} &\times \frac{1}{2} J_{n'-l} \begin{pmatrix} \mathrm{e}^{-k_l^{\mathrm{II}} z_i} & \frac{m_{\mathrm{II}}}{k_l^{\mathrm{II}}} \mathrm{e}^{-k_l^{\mathrm{II}} z_i} \\ \mathrm{e}^{k_l^{\mathrm{II}} z_i} & -\frac{m_{\mathrm{II}}}{k_l^{\mathrm{II}}} \mathrm{e}^{k_l^{\mathrm{II}} z_i} \end{pmatrix} \\ = \sum_{l=-\infty}^{\infty} J_{n-l} J_{n'-l} &\times \begin{pmatrix} \cosh(k_l^{\mathrm{II}} d) & \frac{m_{\mathrm{II}}}{k_l^{\mathrm{II}}} \sinh(k_l^{\mathrm{II}} d) \\ \frac{k_l^{\mathrm{II}}}{m_{\mathrm{II}}} \sinh(k_l^{\mathrm{II}} d) & \cosh(k_l^{\mathrm{II}} d) \end{pmatrix} \end{aligned} \tag{A-8}$$

(across a layer that is not driven this is easier to accomplish, since one simply needs to invert $\mathbf{T}^{\mathrm{I}}_{z;n,l}$ —which is a block-diagonal matrix— and calculate $\mathbf{T}_{z_i\to z_j} = \mathbf{T}^{\mathrm{I}}_{z_j;n,l} \left(\mathbf{T}^{\mathrm{I}}_{z_i}\right)^{-1}_{l,n'}$). For readability only we have omitted the (common) argument of the Bessel functions, e.g. $J_{n-l} = J_{n-l}(V_{\mathrm{ac}}/\hbar\Omega)$.

This TM is too made up of 2×2-blocks relating coefficients $A^{\mathrm{II}}_{n'}$ and $B^{\mathrm{II}}_{n'}$ on one side of a layer with those on the other side; taking $z_i = z_{\mathrm{L}}$ and $z_j = z_{\mathrm{R}}$, we have

$$\begin{aligned}\begin{pmatrix} A^{\mathrm{II}}_n \\ B^{\mathrm{II}}_n \end{pmatrix}_{\mathrm{R}} &= \sum_{n'} \left(\mathbf{T}^{\mathrm{II}}_{\mathrm{R}\leftarrow\mathrm{L}}\right)_{n,n'} \begin{pmatrix} A^{\mathrm{II}}_{n'} \\ B^{\mathrm{II}}_{n'} \end{pmatrix}_{\mathrm{L}} \\ = \sum_{n'} \sum_{l=-\infty}^{\infty} J_{n-l} J_{n'-l} &\times \begin{pmatrix} \cosh(k_l^{\mathrm{II}} d) & \frac{m_{\mathrm{II}}}{k_l^{\mathrm{II}}} \sinh(k_l^{\mathrm{II}} d) \\ \frac{k_l^{\mathrm{II}}}{m_{\mathrm{II}}} \sinh(k_l^{\mathrm{II}} d) & \cosh(k_l^{\mathrm{II}} d) \end{pmatrix} \begin{pmatrix} A^{\mathrm{II}}_{n'} \\ B^{\mathrm{II}}_{n'} \end{pmatrix}_{\mathrm{L}} \end{aligned} \tag{A-9}$$

so that we can now write

$$\begin{pmatrix} \vdots \\ A^{\mathrm{II}}_n \\ B^{\mathrm{II}}_n \\ \vdots \end{pmatrix}_{\mathrm{R}} = \begin{pmatrix} & \vdots & \vdots & \\ \cdots & \sum_l J_{n-l} J_{n'-l} \cosh k_l^{\mathrm{II}} d & \sum_l J_{n-l} J_{n'-l} \frac{m^{\mathrm{II}}}{k_l^{\mathrm{II}}} \sinh k_l^{\mathrm{II}} d & \cdots \\ \cdots & \sum_l J_{n-l} J_{n'-l} \frac{k_l^{\mathrm{II}}}{m^{\mathrm{II}}} \sinh k_l^{\mathrm{II}} d & \sum_l J_{n-l} J_{n'-l} \cosh k_l^{\mathrm{II}} d & \cdots \\ & \vdots & \vdots & \end{pmatrix} \begin{pmatrix} \vdots \\ A^{\mathrm{II}}_{n'} \\ B^{\mathrm{II}}_{n'} \\ \vdots \end{pmatrix}_{\mathrm{L}} \tag{A-10}$$

From the matrix above, using the usual conditions $A^{\mathrm{II}}_{n,\mathrm{L}} = \delta_{n,0}$, $B^{\mathrm{II}}_{n',\mathrm{R}} = 0$, etc., one

finally gets the transmission probabilities

$$T^n_{\mathrm{R}\leftarrow\mathrm{L}} = \frac{k^n_{\mathrm{R}}}{k^0_{\mathrm{L}}}\frac{m_{\mathrm{L}}}{m_{\mathrm{R}}}\left|\frac{A^n_{\mathrm{R}}}{A^0_{\mathrm{L}}}\right|^2$$
$$= \frac{k^n_{\mathrm{R}}}{k^0_{\mathrm{L}}}\frac{m_{\mathrm{L}}}{m_{\mathrm{R}}}\left|\frac{\sum_{n'}\left[\sum_l J_{n-l}J_{n'-l}\left(\cosh(k^{\mathrm{II}}_l d)A^{\mathrm{II}}_{n'} + \frac{m^{\mathrm{II}}}{k^{\mathrm{II}}_l}\sinh(k^{\mathrm{II}}_l d)B^{\mathrm{II}}_{n'}\right)\right]}{A^0_{\mathrm{L}}}\right|^2 \tag{A-11}$$

This transmission probability is energy dependent because of the k vectors ($\hbar k^{\mathrm{II}}_l = [2m^{\mathrm{II}}(V - E - l\hbar\Omega)]^{1/2}$, for example). It is evident that these are not easy formulas to operate with, or even to be simplified. One therefore restricts to the numerical results or, with some intuition and practice, substitutes a *reasonable* ansatz for the coefficients to obtain whenever possible some analytical results. This was achieved for some cases by Wagner (1994, 1995). We can note further that the hyperbolic functions turn into normal trigonometric ones for complex values of the wave vector, and this is precisely what happens for travelling states ($E + l\hbar\Omega > V, l \in \mathbb{Z}$).

A.1.1 TM with phase shifts

Now let's see what happens if the driving comes with a phase shift of π, i.e. $V_{\mathrm{ac}}(t) = V_{\mathrm{ac}}\cos(\Omega t + \pi)$. This driving has been used in the calculation of the dc current in the pump (asymmetric double quantum dot) of chapter 4, and most of the results in chapter 5 on heat production. On the static side nothing changes. On the driven side we now, the algebraic equations become

$$\sum_l \underbrace{\delta_{z;n,l}\begin{pmatrix} \mathrm{e}^{k^{\mathrm{I}}_l z} & \mathrm{e}^{-k^{\mathrm{I}}_l z} \\ k^{\mathrm{I}}_l \mathrm{e}^{k^{\mathrm{I}}_l z} & -k^{\mathrm{I}}_l \mathrm{e}^{-k^{\mathrm{I}}_l z}\end{pmatrix}}_{\mathbf{T}^{\mathrm{I}}_{z;n,l}}\begin{pmatrix} A^{\mathrm{I}}_l \\ B^{\mathrm{I}}_l\end{pmatrix} = \sum_l \underbrace{J_{l-n}\begin{pmatrix} \mathrm{e}^{k^{\mathrm{II}}_l z} & \mathrm{e}^{-k^{\mathrm{II}}_l z} \\ k^{\mathrm{II}}_l \mathrm{e}^{k^{\mathrm{II}}_l z} & -k^{\mathrm{II}}_l \mathrm{e}^{-k^{\mathrm{II}}_l z}\end{pmatrix}}_{\mathbf{T}^{\mathrm{II}}_{z;n,l}}\begin{pmatrix} A^{\mathrm{II}}_l \\ B^{\mathrm{II}}_l\end{pmatrix} \tag{A-12}$$

An expansion like that of Eq. (A-6) shows that this system has the same structure,

$$\begin{pmatrix} \ddots & & \vdots & & \\ \cdots & \mathbf{t}'_{n-1,-1} & \mathbf{t}'_{n-1,0} & \mathbf{t}'_{n-1,+1} & \cdots \\ \cdots & \mathbf{t}'_{n,-1} & \mathbf{t}'_{n,0} & \mathbf{t}'_{n,+1} & \cdots \\ & & \vdots & & \ddots \end{pmatrix}, \tag{A-13}$$

but now the sub-matrices $\mathbf{t}'_{n,l}$ are

$$\mathbf{t}'_{n,l} = \begin{pmatrix} J_{l-n}\mathrm{e}^{k_l^{\mathrm{II}}z} & J_{l-n}\mathrm{e}^{-k_l^{\mathrm{II}}z} \\ J_{l-n}k_l^{\mathrm{II}}\mathrm{e}^{k_l^{\mathrm{II}}z} & J_{l-n}(-k_l^{\mathrm{II}})\mathrm{e}^{-k_l^{\mathrm{II}}z} \end{pmatrix} . \tag{A-14}$$

This shows distinctly that, although similar, the matrices in Eqs. (A-6) and (A-13) are slightly different. There is yet no simple way of relating elements of this latter matrix to elements of the former one except for $l = 0$.

In the end one arrives at a new TM:

$$\begin{aligned} \left(\mathbf{T}^{\mathrm{II},\pi}_{z_i\to z_j}\right)_{n,n'} &= \mathbf{T}^{\mathrm{II},\pi}_{z_j;n,l} \times \left(\mathbf{T}^{\mathrm{II},\pi}_{z_i}\right)^{-1}_{l,n'} = \\ &= \sum_{l=-\infty}^{\infty} J_{l-n}J_{l-n'} \times \begin{pmatrix} \cosh(k_l^{\mathrm{II}}d) & \frac{m_{\mathrm{II}}}{k_l^{\mathrm{II}}}\sinh(k_l^{\mathrm{II}}d) \\ \frac{k_l^{\mathrm{II}}}{m_{\mathrm{II}}}\sinh(k_l^{\mathrm{II}}d) & \cosh(k_l^{\mathrm{II}}d) \end{pmatrix} . \end{aligned} \tag{A-15}$$

A.2 Some relations for Bessel functions

The importance of Bessel functions for driven systems stems from the expansion in plane waves of the time-dependent phase of Eq. 2.32, as was done in Eq. 2.36 for the case of sinusoidal driving. Their usage for TMs is even more relevant, since here they appear in matrices that have to be inverted, which can be an expensive numerical task in terms of computer operations for large matrices. The addition theorem stated below simplifies many of these calculations.

A.2.1 Addition theorem

The addition theorem for Bessel functions of the first kind (see Arfken and Weber, 2001, ex. 11.1.3),

$$J_n(y+z) = \sum_m J_m(y)J_{n-m}(z) \tag{A-16}$$

can be proven with help of the generating function

$$\mathrm{e}^{(x/2)(t-1/t)} = \sum_{n=-\infty}^{\infty} J_n(x)t^n , \tag{A-17}$$

used to define Bessel functions, in the following way: set $x = y + z$ so that

$$\begin{aligned} \mathrm{e}^{(y+z/2)(t-1/t)} &= \mathrm{e}^{(y/2)(t-1/t)}\mathrm{e}^{(z/2)(t-1/t)} = \\ &= \left(\sum_{n=-\infty}^{\infty} J_n(y)t^n\right)\left(\sum_{m=-\infty}^{\infty} J_m(z)t^m\right) \\ &= \sum_{n=-\infty}^{\infty} J_n(y+z)t^n \ ; \end{aligned} \tag{A-18}$$

now we re-arrange terms on the two infinite sums on the left side of the equal sign:

$$\sum_{n=-\infty}^{\infty} J_n(y)t^n \sum_{m=-\infty}^{\infty} J_m(z)t^m = \sum_{n,m} J_n(y)J_m(z)t^{n+m} = \sum_{n,m} J_{n-m}(y)J_m(z)t^m \ . \tag{A-19}$$

Equating now term by term Eqs. (A-18) and (A-19) we arrive at the expression of Eq. (A-16), which completes the proof.

A.2.2 Other results

Obtaining the TM across a layer amounts, in some sense, to solving the algebraic system of equations for the coefficients of the wave function; this operation, in turn, is done by matrix inversion and multiplication. To show that summing over one common index one can get rid of Bessel functions, we use the addition theorem above in a special case: set $z = -y$ so that

$$J_n(0) = \sum_m J_m(y)J_{n-m}(-y) \ . \tag{A-20}$$

We now remember that Bessel functions have even or odd parity, according to the following rule:

$$J_n(x) = (-1)^n J_n(-x) \ \Rightarrow \ J_n(-x) = (-1)^{-n} J_n(x) \tag{A-21}$$

so that $J_{n-m}(-y) = (-1)^{m-n} J_{n-m}(y)$; then

$$\begin{aligned} J_n(0) = \sum_m J_m(y)(-1)^{m-n} J_{n-m}(y) = (-1)^{-n} \sum_m J_{-m}(y)J_{n-m}(y); \\ J_{-n}(0) = \sum_m J_{-m}(y)J_{n-m}(y) \ . \end{aligned} \tag{A-22}$$

For the last line we have used the property $J_{-n}(x) = (-1)^n J_n(x)$.

Now $J_n(0) = J_{-n}(0) = \delta_{n,0}$ (all J_n are 0 at $x = 0$ except for $n = 0$, where $J_0(0) = 1$). Suppose in addition that we perform the change $-m \to n' - m$, so that, *mutatis mutandis*,

$$J_{-n}(0) = \sum_m J_{n'-m}(y) J_{n+(n'-m)}(y) \;\Rightarrow\; J_{n''-n'}(0) = \sum_m J_{n'-m}(y) J_{n''-m}(y) \quad \text{(A-23)}$$

and finally (changing index names)

$$\delta_{n,n'} = \sum_m J_{n-m}(y) J_{n'-m}(y)\ . \quad \text{(A-24)}$$

Because m ranges from $-\infty$ to $+\infty$, we can change its name to $-m$ without changing the value of this expression. It then follows this version of the above:

$$\delta_{n,n'} = \sum_m J_{m-n}(y) J_{m-n'}(y). \quad \text{(A-25)}$$

Appendix B: Entropy production

We provide here a proof that the reflection part in the heat production formula contributes always to the heating of the corresponding lead. We begin by writing the total entropy production in the system in the following way:

$$\begin{aligned}\frac{h}{k_{\mathrm{B}}}(\dot{S}_{\mathrm{L}}+\dot{S}_{\mathrm{R}}) = \int \mathrm{d}E\,\mathrm{d}E'[&T_{\mathrm{LR}}(E,E')f_{\mathrm{R}}(E')(\beta_{\mathrm{L}}E-\eta_{\mathrm{L}}-\beta_{\mathrm{R}}E'+\eta_{\mathrm{R}})\\ &+T_{\mathrm{RL}}(E,E')f_{\mathrm{L}}(E')(\beta_{\mathrm{R}}E-\eta_{\mathrm{R}}-\beta_{\mathrm{L}}E'+\eta_{\mathrm{L}})\\ &+R_{\mathrm{LL}}(E,E')f_{\mathrm{L}}(E')(\beta_{\mathrm{L}}E-\beta_{\mathrm{L}}E')\\ &+R_{\mathrm{RR}}(E,E')f_{\mathrm{R}}(E')(\beta_{\mathrm{R}}E-\beta_{\mathrm{R}}E')]\ .\end{aligned} \tag{B-1}$$

We have defined for convenience $\eta_\ell \equiv \mu_\ell/k_{\mathrm{B}}T_\ell$, and we have used $\beta_\ell = 1/k_{\mathrm{B}}T_\ell$. Consider first the reflection part of e.g. lead L. We can rewrite it, invoking the time-reversal symmetry $R_{\mathrm{LL}}(E,E') = R_{\mathrm{LL}}(E',E)$, as

$$\frac{h}{k_{\mathrm{B}}}(\dot{S}_{\mathrm{L}})_{\mathrm{refl.}} = \frac{1}{2}\int \mathrm{d}E\,\mathrm{d}E'\beta_{\mathrm{L}}R_{\mathrm{LL}}(E,E')[f_{\mathrm{L}}(E')-f_{\mathrm{L}}(E)](E-E')\ . \tag{B-2}$$

It is easy to prove that this is a *definite positive* quantity: $R_{\mathrm{LL}}(E,E') > 0$ by definition. With $f_{\mathrm{L}}(E)$ being a monotonically decreasing function of E, the product of $[f_{\mathrm{L}}(E')-f_{\mathrm{L}}(E)]$ and $(E-E')$ must remain always positive.

On the other hand, it can be shown that the *total* entropy production is also a positive quantity. If one takes the terms proportional to the transmission probabilities in Eq. (B-1) and uses time-reversal properties, i.e. $T_{\mathrm{RL}}(E,E') = T_{\mathrm{LR}}(E',E)$, this can be written in the form

$$\begin{aligned}\frac{h}{k_{\mathrm{B}}}(\dot{S}_{\mathrm{L}}+\dot{S}_{\mathrm{R}})_{\mathrm{trans.}} = \int \mathrm{d}E\,\mathrm{d}E'&T_{\mathrm{LR}}(E,E')\\ &\times[f_{\mathrm{R}}(E')-f_{\mathrm{L}}(E)](\beta_{\mathrm{L}}E-\eta_{\mathrm{L}}-\beta_{\mathrm{R}}E'+\eta_{\mathrm{R}})\ .\end{aligned} \tag{B-3}$$

The positive sign of this expression follows from similar considerations to those used for Eq. (B-2), this time comparing the monotonically decreasing function

with the full argument $\beta_L E - \eta_L$. Therefore we can conclude that

$$\frac{h}{k_B}(\dot{S}_L + \dot{S}_R)_{\text{total}} > 0 \,. \tag{B-4}$$

Bibliography

Agraït, N., A. L. Yeyati, and J. M. van Ruitenbeek, 2003, Phys. Rep. **377**, 81. (cited on pages 9 and 26)

Alhassid, Y., 2000, Rev. Mod. Phys. **72**, 895. (cited on p. 7)

Altshuler, B. L., and L. I. Glazman, 1999, Science **283**, 1864. (cited on p. 44)

Anderson, P. W., D. J. Thouless, E. Abrahams, and D. S. Fisher, 1980, Phys. Rev. B **24**, 3519. (cited on p. 12)

Arfken, G. B., and H. J. Weber, 2001, *Mathematical methods for physicists* (Harcourt/Academic Press, London), 5th edition. (cited on p. 97)

Arrachea, L., 2005, Phys. Rev. B **72**, 125349. (cited on p. 70)

Ashcroft, N. W., and N. D. Mermin, 1976, *Solid State Physics* (Saunders College, Philadelphia). (cited on pages 26, 32, and 64)

Ashoori, R. C., 1996, Nature **379**, 413. (cited on pages 5 and 7)

Astumian, R. D., 1997, Science **276**, 917. (cited on p. 43)

Aviram, A., and M. Ratner, 1974, Chem. Phys. Lett **29**, 277. (cited on p. 8)

Baibich, M. N., J. M. Broto, A. Fert, F. N. Van Dau, F. Petroff, P. Eitenne, G. Creuzet, A. Friederich, and J. Chazelas, 1988, Phys. Rev. Lett. **61**, 2472. (cited on p. 1)

Beenakker, C., and H. van Houten, 1991, Sol. Stat. Phys. **44**, 1. (cited on pages 4, 5, and 7)

Beenakker, C. W. J., and A. A. M. Staring, 1992, Phys. Rev. B **46**, 9667. (cited on p. 67)

Blaauboer, M., 2002, Phys. Rev. B **65**, 235318. (cited on p. 43)

Blencowe, M., 2004, Phys. Rep. **395**, 159. (cited on p. 68)

Blick, R. H., R. J. Haug, J. Weis, D. Pfannkuche, K. von Klitzing, and K. Eberl, 1996, Phys. Rev. B **53**, 7899. (cited on p. 8)

Bloch, F., and A. Siegert, 1940, Phys. Rev. **57**, 522. (cited on p. 33)

Brouwer, P. W., 1998, Phys. Rev. B **58**, R10135. (cited on p. 44)

Büttiker, M., 1986, Phys. Rev. Lett. **57**, 1761. (cited on pages 14 and 55)

Büttiker, M., Y. Imry, R. Landauer, and S. Pinhas, 1985, Phys. Rev. B **31**, 6207. (cited on pages 13 and 62)

Cahill, D. G., W. K. Ford, K. E. Goodson, G. D. Mahan, A. Majumdar, H. J. Maris, R. Merlin, and S. R. Phillpot, 2003, J. Appl. Phys **93**, 793. (cited on p. 67)

Camalet, S., S. Kohler, and P. Hänggi, 2004, Phys. Rev. B **70**, 155326. (cited on p. 36)

Camalet, S., J. Lehmann, S. Kohler, and P. Hänggi, 2003, Phys. Rev. Lett. **90**, 210602. (cited on p. 9)

Capasso, F., and S. Datta, 1990, Phys. Today **43**, 74. (cited on p. 36)

Clark, A. M., N. A. Miller, A. Williams, S. T. Ruggiero, G. C. Hilton, L. R. Vale, J. A. Beall, K. D. Irwin, and J. N. Ullom, 2005, Appl. Phys. Lett. **86**, 173508. (cited on pages 66 and 67)

Cohen-Tannoudji, C., B. Diu, and F. Laloë, 1977, *Quantum Mechanics* (Hermann & John Wiley & Sons, Cambridge), 2nd edition. (cited on pages 33 and 45)

Creffield, C. E., and G. Platero, 2002, Phys. Rev. B **65**, 113304. (cited on p. 31)

Das, M. P., and F. Green, 2003a, in *Proceedings of XXVI International Workshop on Condensed-Matter Theories* (Nova Science, New York). (cited on p. 13)

Das, M. P., and F. Green, 2003b, J. of Phys – Condensed Matter **15**, L687. (cited on p. 13)

Datta, S., 1995, *Electronic Transport in Mesoscopic Systems* (Cambridge University Press, Cambridge). (cited on p. 61)

Dayem, A. H., and R. J. Martin, 1962, Phys. Rev. Lett. **8**, 246. (cited on p. 15)

Devoret, M. H., D. Esteve, and C. Urbina, 1992, Nature **360**, 547. (cited on p. 43)

Dunlap, D. H., and V. M. Kenkre, 1986, Phys. Rev. B **34**, 3625. (cited on p. 31)

Esaki, L., 1974, Rev. Mod. Phys. **46**, 237. (cited on p. 32)

Esaki, L., and R. Tsu, 1970, IBM J. Res. Dev. **14**, 61. (cited on pages 20 and 32)

Feynman, R. P., 1960, Eng. Sci. **23**, 22, talk delivered at the 1959 APS meeting. For a transcription, see `http://www.its.caltech.edu/~feynman/plenty.html`. (cited on p. 1)

Field, S. B., M. A. Kastner, U. Meirav, J. H. F. Scott-Thomas, D. A. Antoniadis, H. I. Smith, and S. J. Wind, 1990, Phys. Rev. B **42**, 3523. (cited on p. 4)

Floquet, G., 1883, Ann. de l'Ecole Norm. Sup. **12**, 47. (cited on p. 16)

Geerligs, L. J., V. F. Anderegg, P. A. M. Holweg, J. E. Mooij, H. Pothier, D. Esteve, C. Urbina, and M. H. Devoret, 1990, Phys. Rev. Lett. **64**, 2691. (cited on p. 43)

Giazotto, F., T. T. Heikkilä, A. Luukanen, A. M. Savin, and J. Pekola, 2006, Rev. Mod. Phys. **78**, 217. (cited on p. 67)

Griffiths, D. J., 1995, *An Introduction to Quantum Mechanics* (Prentice Hall), 1st edition. (cited on p. 39)

Grifoni, M., and P. Hänggi, 1998, Phys. Rep. **304**, 229. (cited on pages 19, 29, 33, and 34)

Grossmann, F., T. Dittrich, P. Jung, and P. Hänggi, 1991, Phys. Rev. Lett. **67**, 516. (cited on p. 31)

Grossmann, F., and P. Hänggi, 1992, Europhys. Lett. **18**, 571. (cited on p. 29)

Guttman, G. D., E. Ben-Jacob, and D. J. Bergman, 1995, Phys. Rev. B **52**, 5256. (cited on p. 67)

Guttman, G. D., E. Ben-Jacob, and D. J. Bergman, 1996, Phys. Rev. B **53**, 15856. (cited on p. 67)

Holthaus, M., 1992, Z. Phys. B **89**, 251. (cited on pages 31 and 32)

Humphrey, T. E., R. Newbury, R. P. Taylor, and H. Linke, 2002, Phys. Rev. Lett. **89**, 116801. (cited on p. 68)

Imry, Y., 1997, *Introduction to Mesoscopic Physics*, volume 1 of *Mesoscopic Physics and Nanotechnology* (Oxford University Press, New York).
(cited on pages 4 and 61)

Imry, Y., and R. Landauer, 1999, Rev. Mod. Phys. **71**, S306. (cited on p. 13)

Jauho, A.-P., N. S. Wingreen, and Y. Meir, 1994, Phys. Rev. B **50**, 5528. (cited on p. 70)

Kastner, M. A., 1993, Physics Today **46**, 24. (cited on p. 6)

Keay, B. J., S. Zeuner, S. J. A. Jr., K. D. Maranowski, A. C. Gossard, U. Bhattacharya, and M. J. W. Rodwell, 1995, Phys. Rev. Lett. **75**, 4102. (cited on p. 35)

Kohler, S., 1999, *The interplay of chaos and dissipation in driven quantum systems*, Ph.D. thesis, Universität Augsburg, Augsburg. (cited on p. 16)

Kohler, S., S. Camalet, M. Strass, J. Lehmann, G.-L. Ingold, and P. Hänggi, 2004, Chem. Phys. **296**, 243. (cited on pages 28, 30, 36, 37, and 38)

Kohler, S., J. Lehmann, and P. Hänggi, 2005, Phys. Rep. **406**, 379. (cited on pages xvi, 14, 20, 28, 43, 70, and 88)

Kornilovitch, P., A. Bratkovsky, and R. Stanley Williams, 2002, Phys. Rev. B **66**, 165436. (cited on p. 43)

Kouwenhoven, L. P., D. G. Austing, and S. Tarucha, 2001, Rep. Prog. Phys. **64**, 701. (cited on pages 5 and 6)

Kouwenhoven, L. P., S. Jauhar, J. Orenstein, P. L. McEuen, Y. Nagamune, J. Motohisa, and H. Sasaki, 1994, Phys. Rev. Lett. **73**, 3443. (cited on p. 44)

Landauer, R., 1957, IBM J. Res. Dev. **1**, 223. (cited on pages xvi, 2, 11, and 12)

Landauer, R., 1987, Z. Phys. B – Condensed Matter **68**, 217. (cited on pages 11 and 12)

Leek, P. J., M. R. Buitelaar, V. I. Talyanskii, C. G. Smith, D. Anderson, G. A. C. Jones, J. Wei, and D. H. Cobden, 2005, Phys. Rev. Lett. **95**, 256802. (cited on p. 44)

Lehmann, J., S. Kohler, P. Hänggi, and A. Nitzan, 2002, Phys. Rev. Lett. **88**, 228305. (cited on p. 43)

Likharev, K. K., and A. B. Zorin, 1985, J. Low Temp. Phys **59**, 347. (cited on p. 4)

Linke, H., T. E. Humphrey, A. Löfgren, A. O. Shuskov, R. Newbury, R. P. Taylor, and P. Omling, 1999, Science **286**, 2314. (cited on p. 44)

Loss, D., and D. P. DiVincenzo, 1998, Phys. Rev. A **57**, 120. (cited on p. 5)

Mahan, G., B. Sales, and J. Sharp, 1997, Phys. Today **50**, 42. (cited on p. 63)

Manninen, A. J., J. K. Suoknuuti, M. M. Leivo, and J. P. Pekola, 1999, Appl. Phys. Lett. **74**, 3020. (cited on pages 66 and 67)

Meirav, U., and E. B. Foxman, 1995, Semicond. Sci. Technol. **11**, 255. (cited on p. 6)

Moskalets, M., and M. Büttiker, 2004, Phys. Rev. B **70**, 245305. (cited on p. 56)

Nitzan, A., and M. A. Ratner, 2003, Science **300**, 1384. (cited on pages 8 and 9)

Niu, Q., 1990, Phys. Rev. Lett. **64**, 1812. (cited on p. 44)

Ohno, K., K. Esfarjani, and Y. Kawazoe (eds.), 1999, *Computational Material Science: from Ab Initio to Montecarlo Methods*, volume 129 of *Solid-State Sciences* (Springer, Berlin). (cited on p. 26)

Parrondo, J. M. R., and B. J. de Cisneros, 2002, Appl. Phys. A **75**, 179. (cited on pages 43 and 67)

Pedersen, M. H., and M. Büttiker, 1998, Phys. Rev. B **58**, 12993. (cited on p. 56)

Pekola, J., 2005, Nature **435**, 889. (cited on pages 67, 79, and 88)

de Picciotto, R., H. L. Stormer, L. N. Pfeiffer, K. W. Baldwin, and K. W. West, 2001, Nature **411**, 51. (cited on pages 12 and 61)

Platero, G., and R. Aguado, 2004, Phys. Rep. **395**, 1. (cited on pages 2 and 45)

Polianski, M. L., and P. W. Brouwer, 2001, Phys. Rev. B **64**, 075304. (cited on p. 55)

Rabi, I. I., 1937, Phys. Rev. **51**, 652. (cited on p. 33)

Reichert, J., R. Ochs, D. Beckmann, H. B. Weber, M. Mayor, and H. v. Löhneysen, 2002, Phis. Rev. Lett. **88**, 176804. (cited on pages 8 and 9)

Rey, M., and F. Sols, 2004, Phys. Rev. B **70**, 125315. (cited on p. 53)

Rey, M., M. Strass, S. Kohler, F. Sols, and P. Hänggi, 2005, Chem. Phys. **319**, 360. (cited on p. 36)

Sambe, H., 1973, Phys. Rev. A **7**, 2203. (cited on pages 16 and 17)

Schwab, K., E. A. Henriksen, J. M. Worlock, and M. L. Roukes, 2000, Nature **404**, 974. (cited on p. 68)

Segal, D., and A. Nitzan, 2006, Phys. Rev. E **73**, 026109. (cited on p. 67)

Shirley, J. H., 1965, Phys. Rev. **138**, B979. (cited on p. 28)

Sivan, U., and Y. Imry, 1986, Phys. Rev. B **33**, 551. (cited on pages 67 and 68)

Sols, F., 1991, Ann. Phys. (N. Y.) **214**, 386. (cited on p. 22)

Sols, F., 1992, in *NATO ASI Series, vol. 236* (Kluwer Academic Publishers, Dordrecht), p. 479. (cited on p. 22)

Sols, F., and J. Sánchez-Cañizares, 1999, Superlatt. Microstruct. **25**, 627. (cited on pages 13 and 57)

Sols, F., and M. Wagner, 2000, Ann. Phys. (Leipzig) **9**, 776. (cited on p. 84)

Stafford, C. A., and N. S. Wingreen, 1996, Phys. Rev. Lett. **76**, 1916. (cited on pages 2, 45, 48, and 88)

Staring, A. A. M., H. van Houten, C. W. J. Beenakker, and C. T. Foxon, 1992, Phys. Rev. B **45**, 9222. (cited on p. 4)

Stern, A., Y. Aharonov, and Y. Imry, 1990, Phys. Rev. A **41**, 3436. (cited on p. 55)

Stone, A. D., 1995, in *Les Houches Summer School Proceedings, Session LXI, Mesoscopic quantum physics* (North Holland, Amsterdam). (cited on p. 4)

Stone, A. D., and A. Szafer, 1988, IBM J. Res. Develop. **32**, 384. (cited on pages 12 and 13)

Strass, M., P. Hänggi, and S. Kohler, 2005, Phys. Rev. Lett. **95**, 130601. (cited on pages 44, 46, 47, and 50)

Switkes, M., C. M. Marcus, K. Campman, and A. C. Gossard, 1999, Science **283**, 1905. (cited on pages 7, 44, 54, 60, and 61)

Talyanskii, V. I., J. M. Shilton, M. Pepper, C. G. Smith, C. J. B. Ford, E. H. Linfield, D. A. Ritchie, and G. A. C. Jones, 1997, Phys. Rev. B **56**, 15180. (cited on p. 44)

Thouless, D. J., 1983, Phys. Rev. B **27**, 6083. (cited on p. 43)

Tien, P. K., and J. P. Gordon, 1963, Phys. Rev. **129**, 647. (cited on pages 15 and 44)

Truscott, W. S., 1993, Phys. Rev. Lett. **70**, 1900. (cited on pages 22 and 35)

Tsu, R., and L. Esaki, 1973, Appl. Phys. Lett. **22**, 562. (cited on p. 21)

Tucker, J. R., and M. J. Feldman, 1985, Rev. Mod. Phys. **57**, 1055. (cited on p. 15)

Wacker, A., 2002, Phys. Rep. **357**, 1. (cited on p. 32)

Wagner, M., 1994, Phys. Rev. B **49**, 16544. (cited on pages 20, 34, 35, and 96)

Wagner, M., 1995, Phys. Rev. A **51**, 798.
(cited on pages xvi, 14, 24, 31, 34, 35, 94, and 96)

Wagner, M., 1996, Phys. Rev. Lett. **76**, 4010. (cited on pages 22, 34, and 35)

Wagner, M., and H. Mizuta, 1993, Phys. Rev. B **48**, 14393. (cited on p. 24)

Wagner, M., and F. Sols, 1999, Phys. Rev. Lett. **83**, 4377.
(cited on pages 14, 18, 44, 54, 59, 60, 61, and 84)

van der Wiel, W. G., S. De Franceschi, J. M. Elzerman, T. Fujisawa,
S. Tarucha, and L. P. Kouwenhoven, 2003, Rev. Mod. Phys. **75**, 1.
(cited on pages 7, 8, and 33)

Zeller, H. R., and I. Giaever, 1969, Phys. Rev. **181**, 789. (cited on p. 4)